ORNL TM 5042

Oak Ridge Tokamak Experimental Power Reactor Study Reference Design

OAK RIDGE NATIONAL LABORATORY
OPERATED BY UNION CARBIDE CORPORATION FOR THE U.S. ATOMIC ENERGY COMMISSION

BLANK PAGE

Printed in the United States of America. Available from
National Technical Information Service
U.S. Department of Commerce
5285 Port Royal Road, Springfield, Virginia 22161
Price: Printed Copy $7.60; Microfiche $2.25

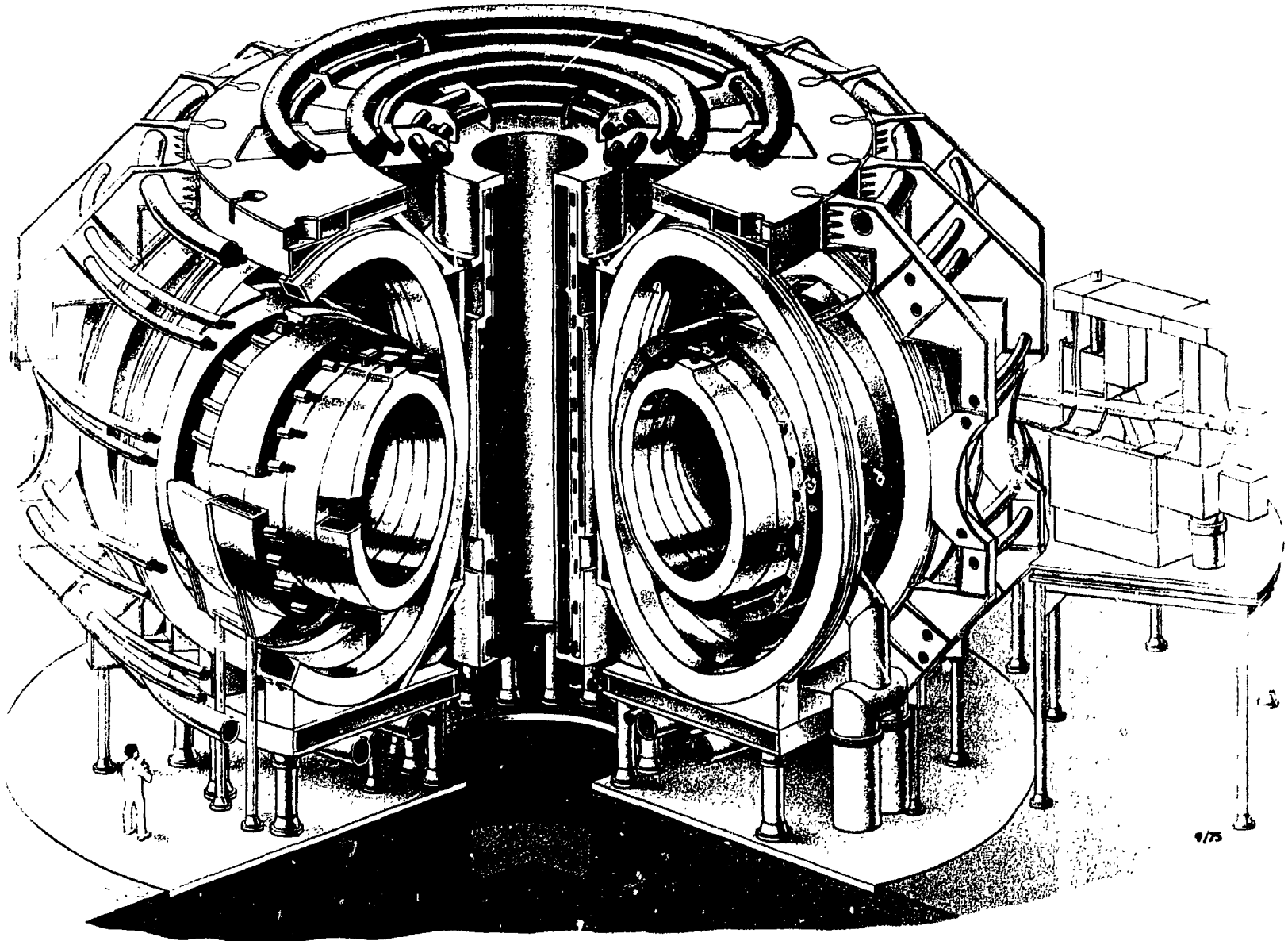

OAK RIDGE EPR REFERENCE DESIGN

ORNL-TM-5042
UC-20

Contract No. W-7405-eng-26

OAK RIDGE TOKAMAK EXPERIMENTAL POWER REACTOR STUDY
REFERENCE DESIGN

M. Roberts, Project Manager
E. S. Bettis,* Design Coordinator

NOVEMBER 1975

*Consultant

THERMONUCLEAR DIVISION
OAK RIDGE NATIONAL LABORATORY
Oak Ridge, Tennessee 37830
operated by
UNION CARBIDE CORPORATION
for the
U.S. ENERGY RESEARCH AND DEVELOPMENT ADMINISTRATION

TABLE OF CONTENTS

Table of Contents

(continued)

FOREWORD

The ERDA Division of Controlled Thermonuclear Research Program for fusion development of tokamak power reactors identifies progressively larger confinement systems leading to a Demonstration Reactor Plant of $\geq$ 500-MWe size by approximately the year 2000. The associated research and technology development would provide the requisite support for proceeding with the confinement systems necessary to the eventual establishment of a commercial power industry. In this sequence, the next logical step after the Tokamak Fusion Test Reactor (TFTR), which is scheduled to begin operation in 1980, is an Experimental Power Reactor (EPR), scheduled for operation in 1985.

For the past year (FY-1975), an EPR scoping study supported by ERDA has been in progress at Oak Ridge National Laboratory (ORNL). Similar studies are in progress at Argonne National Laboratory (ANL), supported by ERDA, and at General Atomic Company with support from the Electric Power Research Institute.

Based on the scoping effort conducted at ORNL, an initial EPR design was identified which, with continued updating, will serve as the focal point of continuing effort aimed at establishment of the EPR conceptual design.

ACKNOWLEDGEMENTS

This reference design document is the product of the focussed efforts of the considerable number of persons associated with the Oak Ridge EPR Project Team. The Project Team is composed of staff members from Departments within the Thermonuclear Division, from the Fusion Reactor Technology Program and other Divisions in the Oak Ridge National Laboratory, and from Departments in the Union Carbide Corporation Nuclear Division Engineering Organization. There are also participants from industry. In particular, the Advanced Systems, Engineering Sciences, Plasma Heating, and Plasma Theory Departments in the Thermonuclear Division are strongly involved, as well as ORNL's Chemical Technology, Instrumentation and Controls, Metals and Ceramics, and Neutron Physics Divisions. The Experimental, Mechanical, Electrical, and General Design Engineering and Project Engineering Departments of the Engineering Organization are centrally involved. Participants from Exxon Nuclear Company and Burns & Roe, Inc. are key members of the team. Preparation of the document directly benefitted from the encouragement of J. F. Clarke and O. B. Morgan, from the critical review of G. G. Kelley, from discussions with and the active participation of H. C. McCurdy, T. E. Shannon, and C. A. Flanagan (industrial participant from Westinghouse) and from the continuing efforts of P. N. Haubenreich who served as manager of the EPR scoping study for the first half of the year. R. E. Marcus assisted in the technical editing. The document was prepared by the information processing of A. M. Legg, C. Bates, and L. B. Dockery, and by the services of the graphic arts and reproduction staffs of ORNL's Information Division and of the Y-12 Plant.

PRINCIPAL CONTRIBUTORS TO EPR REFERENCE DESIGN

Plasma Engineering

D. G. McAlees[1,2]
F. B. Marcus[2]
S. E. Attenberger[3]

Nuclear Systems

E. S. Bettis[4]
R. T. Santoro[5]
T. J. Huxford[6]
D. G. McAlees[1,2]
H. L. Watts[6]

First Wall and Materials Engineering

J. L. Scott[7]
R. J. Colchin[8]
F. W. Wiffen[7]

Electromagnetics

M. S. Lubell[9]
W. C. T. Stoddart[6,9]
J. K. Ballou[9]
P. B. Burn[6]
C. G. Lawson[9]
C. J. Long[9]
J. N. Luton[9]
H. T. Yeh[9]
N. E. Johnson[10]
J. W. Lue[9]

Poloidal Magnetic Field Concept

F. B. Marcus[2]
D. G. McAlees[1,2]
J. R. Moore[6]
Y.-K. M. Peng[2]

Electrical Power Requirements

R. B. Easter[6]

Neutral Beam Injection

G. Schilling[11]

Tritium Handling

R. N. Cherdack[12]
J. S. Watson[13]

System Integration

E. S. Bettis[4]

Project Engineering

E. H. Bryant[6]
R. M. Clark[6]

[1]Exxon Nuclear Company
[2]Plasma Theory Department
[3]Computer Sciences Division
[4]Consultant
[5]Neutron Physics Division
[6]Engineering Organization
[7]Metals and Ceramics Division
[8]Low Beta Plasma Department
[9]Engineering Science Department
[10]Mechanics Research Incorporated
[11]Plasma Heating Department
[12]Burns and Roe, Inc.
[13]Chemical Technology Division

ABSTRACT

A Tokamak EPR Reference Design is presented as a basis for further design study leading to a Conceptual Design. The set of basic plasma parameters selected — minor radius of 2.25 m, major radius of 6.75 m, magnetic field on axis of 4.8 T and plasma current of 7.2 MA — should produce a reactor-grade plasma with a significant neutron flux, even with the great uncertainty in plasma physics scaling from present experience to large sizes. Neutronics and heat transfer calculations coupled with mechanical design and materials considerations were used to develop a blanket and shield capable of operating at high temperature, protecting the surrounding coils, being maintained remotely and, in a few experimental modules, breeding tritium. Nb_3Sn and NbTi superconductors are used in the toroidal field coil design. The coil system was developed for a maximum field of 11 T at the winding (to give a field on axis of 4.8 T), and combines multifilamentary superconducting cable with forced flow of supercritical helium enclosed in a steel conduit. The structural system uses a stainless steel center bucking ring and intercoil box beam bracing to provide rigid support for coils against the centering force, overturning moments from poloidal fields and faults, other external forces, and thermal stresses. The poloidal magnetics system is specially designed both to reduce the total volt-second energy requirements and to reduce the magnitude of the rate of field change at the toroidal field coils. The rate of field change imposed upon the toroidal field coils is reduced by at least a factor of 3.3 compared to that due to the plasma alone. Tritium processing, tritium containment and vacuum systems employ double containment and atmospheric cleanup to minimize releases. The document also contains discussions of systems integration and assembly, key research and development needs, and schedule considerations.

1. INTRODUCTION

The Tokamak Experimental Power Reactor Reference Design presented here was developed by a project team at the Oak Ridge National Laboratory at the conclusion of a scoping study conducted for ERDA-DCTR. The principal aims of the scoping study were:

- a clearer definition of the magnitude, complexities and uncertainties associated with an EPR to be operational in 1985,
- a technical base from which conceptual design studies could proceed in FY-1976, and
- an assembly of the requirements for supporting research and development programs aimed at the EPR.

These three aims have been met, and a summary of the required information with a description of the underlying work appears in the EPR Scoping Study Report, ORNL-TM-5038. The possible alternative goals, technologies and techniques compatible with the EPR objectives and 1985 time scale were examined in each major area.

The reference design was synthesized from the information developed and evaluated in the scoping study. This reference design, which stands as one of the principal results of the study, is shown graphically in the frontispiece and is the dominant subject of the present document. The reference design provides

- a common focus for the EPR design study now in progress, and
- a guide to the supporting development programs required.

The reference design is a dynamic one. As significant data become available, their impact will be assessed and changes will be made in the design. Section 2 contains both a summary of key features and a tabular and graphic description of the principal parts of the design.

Further description in each subsystem area and explanations of the parameters chosen are contained in the next five sections, i.e., Plasma, Section 3; Nuclear, Section 4; Electromagnetics, Section 5; Neutral Beam Injection, Section 6; and Tritium Handling, Section 7. The topics of systems integration, assembly, disassembly and remote maintenance are covered in Section 8.

From the basic scoping study and development of the reference design has come a closer interaction between the various supporting research and development programs and the EPR studies. EPR needs are being used as direct guidance in these programs.[1,2] A list of R&D requirements is summarized in this document as Section 9.

Section 10 is a summary of the steps necessary to achieve a 1985 schedule.

REFERENCES

1. *Superconducting Magnet Development Program Annual Report*, ORNL-TM-5019, Oak Ridge National Laboratory (1975).

2. TTA(P) Program Outline, ORNL-TM-4819, Oak Ridge National Laboratory (1975).

2. SUMMARY

2.1 Key Features and Requirements of the Reference Design

This discussion is intended to highlight those critical topics having the greatest impact on the future design effort or on the future development work related to EPR. A more complete account of the technical features and requirements of each topic is contained in the sections on individual systems. The scoping study considered a wide range of alternatives with varying depths of detailed evaluation. In each major system, some alternatives were noted for probable acceptance and others rejected for specific reasons; in each case one approach has been selected for use in the reference design.

Plasma

- Performance analyses and sensitivity investigations using the current plasma model have resulted in a set of parameters describing a tokamak device that is considered capable of producing a reactor-grade plasma.
- For other fixed parameters, the plasma current, I, decreases rapidly with a decrease in plasma radius. As a result of the scoping studies, the radial distance from the surface of the plasma to the toroidal field coil winding, Δ, is found to be $\sim$ 1.55 m. This, as discussed later in this report, suggests a minimum plasma radius, a, of $\sim$ 2 m.
- The probability of successful plasma performance increases with increasing toroidal field strength. Accordingly, the highest possible toroidal field was chosen consistent with a feasible but aggressive magnet development program. This field value is B = 4.8T on the plasma axis corresponding to a maximum B at the superconductor of 11 T.
- The plasma parameters selected will provide a high neutron flux even in the case of unfavorable scaling with size.

- The scoping study evaluation has emphasized the need for serious study of the questions related to the operating cycle, i.e., startup, fueling, impurities, burn, control, shutdown, etc.

Nuclear

- Analysis of the energy conversion system (first wall, blanket, shield) indicates that a heat removal system can be designed to operate at high temperatures and satisfy the requirements of the EPR.
- This same design, with the substitution of lithium absorber in a few modules instead of potassium, would permit a tritium breeding demonstration.
- The use of a separate material layer as the first radiation wall, with no load bearing requirements, appears mechanically feasible.
- Helium under pressure can provide the desired cooling and heat transfer.

Electromagnetic

- Information relating to toroidal field coil design, including reactions to centering forces, overturning moments, and inter-coil structure, can be produced using a three-dimensional, finite-element structural analysis program.
- The toroidal field superconducting coil design has combined the features of high current density at high field by using multi-filamentary Nb_3Sn cable supported and cryostabilized in a low loss structural configuration using a sturdy steel case and helium coolant under forced-flow conditions.
- The promise of the recent developments in multifilamentary Nb_3Sn wire conductor must now be fulfilled by increased emphasis on this superconductor in the tokamak magnet development program.
- Use of an electromagnetic shielding scheme has provided a solution to the earlier dilemma of obtaining the required volt-second capability without imposing either high rates of

field change at the TF coil or incurring high costs for inefficient production of volt-seconds.

- In the areas of high-energy storage devices and associated switching gear, development is required to ensure the feasibility of the large homopolar generators and high current switches.

Neutral Beam Injection

- Extensions of current neutral beam injection technology are needed to provide high efficiency delivery of beams at levels of many tens of MW into the plasma.

Tritium Handling

- In-plant recycling of tritium from plasma exhaust is a practical necessity requiring significant process development.
- Methods for recovering tritium produced in the blanket are essentially undeveloped.
- Cryosorption pumping has attractive advantages for EPR vacuum systems but requires development for EPR conditions.

System Integration

- An assembly procedure including coolant piping and manifolding, assembly tools and clearance has been examined. The procedure is feasible for the reference design.
- A system power balance indicates that significant output power can be achieved.

Schedule

- Consideration has been given to the technical and administrative requirements for a 1985 operation date for the EPR. A schedule was developed using projections from light-water reactor experience; this schedule includes the expected information from research, results from testing in existing and planned confinement devices, and progress expected in development programs. This schedule requires FY-1979 funding authorization and considerable overlap of various EPR design and fabrication

phases with the design, fabrication and testing phases of the critical magnet development steps: Compact Torus, TTA, and the EPR prototypic coils.

2.2 Reference Design

A set of basic machine parameters for the EPR Reference Design (minor radius of 2.25 m, major radius of 6.75 m, magnetic field on axis of 4.8 T and plasma current of 7.2 MA) was chosen to produce a reactor-grade plasma with significant neutron flux. Despite uncertainties in plasma scaling, it is possible to predict that this flux will be produced under both beam-driven and ignition conditions. The neutral beam power needed is 100 MW with an accelerating voltage of 200 keV. The safety factor, q(a), is 2.5. The burn time is 100 sec with a duty cycle $\geq$ 50%. The overall height of the reactor device is 15 m, and the overall diameter is 22 m. The output power for a driven system is $\sim$ 400 MW(th) and under ignition conditions is $\sim$ 200 MW(th), for the particular operating modes discussed herein.

Neutronics and heat transfer calculations coupled with mechanical design and materials considerations were used to develop a blanket and shield capable of

1) operating at high temperature,
2) protecting the surrounding coils,
3) being maintained remotely, and
4) in a few experimental modules, breeding tritium.

The structural material selected for the blanket is type 316 stainless steel. The blanket consists of 60 autonomous segments which are clamped and welded together to form the torus. The absorber in the non-breeding modules is potassium. Provision has been made to include experimental modules containing lithium metal instead of potassium to demonstrate tritium breeding. The breeding ratio in these modules is $\sim$ 1.2. The coolant is helium at 70 atmospheres. The coolant outlet temperature is $\sim$ 370°C. The limiting constraint on blanket operation is dictated by the thermal loading on the first wall which must be less than 160 MW in the present design.

The requisite of high field strength and the criteria for volume, obtained from considerations of the plasma, blanket, shield and access geometry, resulted in the selection of Nb_3Sn in addition to NbTi superconductors. The toroidal field coil design developed for a maximum field of 11 T at the winding combines multifilamentary superconducting cable with forced flow of supercritical helium enclosed in a steel conduit. There are 20 toroidal field coils of oval shape in the design. The horizontal opening is 7.4 m and the vertical opening is 10.2 m. The total number of ampere turns per coil is $\sim$ 8.1 MA and the stored energy is 34.2 GJ. By using a stainless steel center bucking ring and intercoil box beam bracing, the structural system provides rigid support for coils against the centering force, overturning moments from poloidal fields and faults, thermal stresses, and other external forces. The poloidal magnetics system is specially designed both to reduce the total volt-second energy requirements and to reduce the magnitude of the rate of field change at the toroidal field coils. The rate of field change imposed upon the toroidal field coils is reduced by at least a factor of 3.3 compared to that due to the plasma alone. The total volt-seconds requirement is 185 Wb.

Tritium processing and vacuum systems employ double containment to minimize releases. Cryosorption pumps are used for both plasma vessel and injector vacuum systems. Uranium beds and cryogenic distillation are used for purification of plasma exhaust; storage is accomplished using solid uranium tritide.

Figure 2.1 is an elevation view of the reference design. Figure 2.2 is a plan view. Selected parameters associated with this design are contained in Table 2.1.

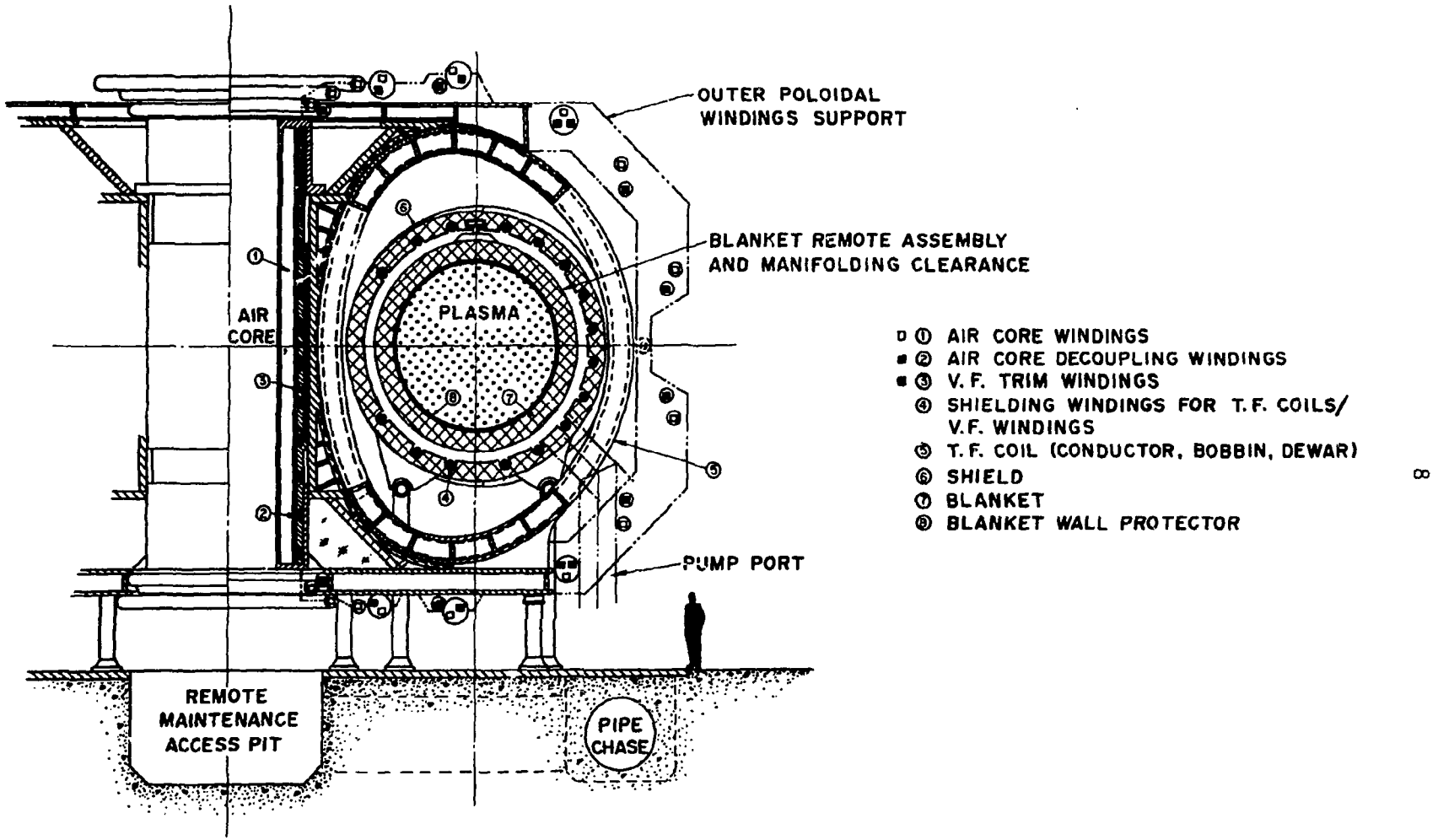

Fig. 2.1 EPR Reference Design Elevation

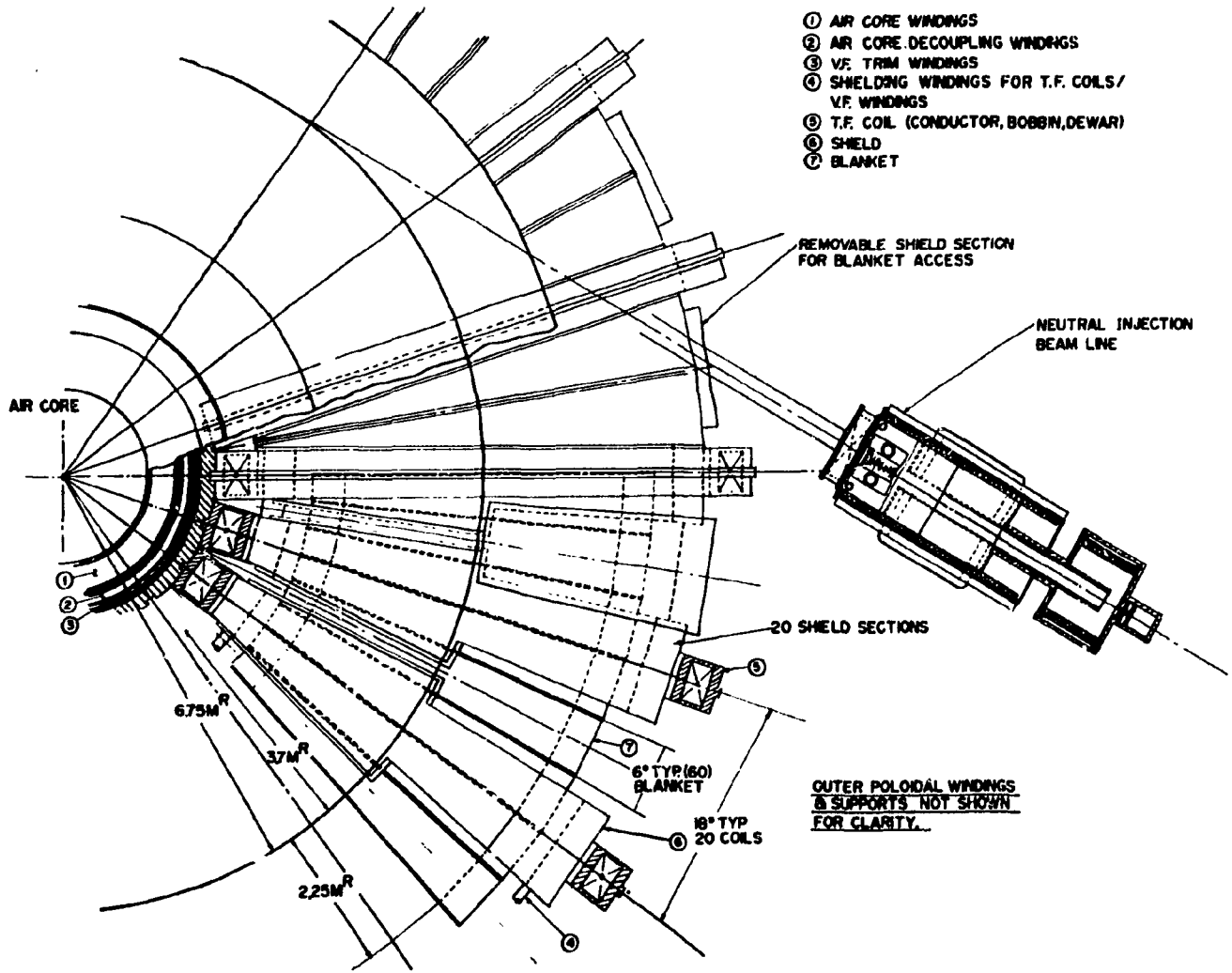

Fig. 2.2 EPR Reference Design Plan.

Table 2.1 Principal Parameters of the Oak Ridge Tokamak EPR Reference Design

(August 1975)

Plasma	
Cross section	Circular
Minor radius, meters	2.25
Major radius, meters	6.75
Aspect ratio	3.0
Toroidal current, MA	7.2
Field at centerline, Tesla	4.8
Neutral beam power, MW	100
Beam energy, keV	200
Safety factor q(a)	2.5
Burn time, seconds	100
Ripple at plasma edge	2.2%
Nuclear	
Blanket	
Maximum power rating, MW(th)	450
Coolant outlet temperature, °C	∿ 370
Coolant	helium
Coolant pressure, atmospheres	70
Thickness, meters	0.515
Breeding ratio (experimental modules only)	1.213
Breeding material	natural lithium metal
Absorber in non-breeding module	potassium
Structural material	316 S.S.
Shield	
Thickness, meters	0.485
Composition	stainless steel spheres, lead slab, borated water
Electromagnetic	
Toroidal field coils	
Number	20
Shape	oval
Horizontal opening, meters	7.4
Vertical opening, meters	10.2
B_{max} at inner winding, Tesla	11
Total amp turns per coil, MA turns	8.088
Stored energy per coil, GJ	1.71

Table 2.1 (continued)

Electromagnetic (continued)	
Conductor configuration	composite cable in a square, stainless steel conduit
Superconductor	
in the high field region	Nb_3Sn
in the moderate and low field region	NbTi in Cu and CuNi mixed matrix conductor
Total weight per coil, 1000 lbs	238
Maximum centering force, 10^6N	250
Structure	stainless steel center bucking ring and intercoil box beam bracing
Poloidal field coils	
Conductors	
in the air core, decoupling, and V.F. trim coils	NbTi in Cu and CuNi mixed matrix conductor
in the shielding/V.F. coils	normal Cu
Configuration	air core with minimum field at TF coils
Volt-seconds, total, Wb	185
in the air core, Wb	130
in the vertical field coil, Wb	55
Tritium Handling	
Tritium	
Containment	double
Purification	uranium beds
Isotope separation	cryogenic distillation
Storage	solid uranium tritide
Vacuum	
Torus pumping	40 1-m diam. ports 40 cryosorption pumps pumping speed - 1,500,000 ℓ/s

Table 2.1 (continued)

General	
Overall height, meters	15
Overall diameter, meters	22
Duty Cycle, %	$\geq$ 50
Output power level	
driven system, MW(th)	$\sim$ 400
ignited system, MW(th)	$\sim$ 200
Electric load, peak, MW	$\sim$ 300
MVAR	$\sim$ 100

3. THE PLASMA

3.1 Introduction

There are many ways to arrive at a set of reference parameters for a future tokamak system. The same difficulty is encountered in most of the procedures, that is, a proven relationship between attainable plasma parameters and system size does not exist at present for the type of device under consideration. Results have been obtained from present day devices and theoretical predictions, but the connection between these and the operating parameters to be attained in an EPR-size system involves much uncertainty.

The theoretical basis used here to arrive at a reference design is straightforward and provides a machine size which should produce reactor-grade plasma in terms of presently accepted[1] reactor modeling calculations. The steps taken in determining the reference design are described below.

3.2 Parametric Considerations
(Current, Magnetic Field, Volt-seconds, Cost)

The first step is a recognition of the critical parameters and the development of their interrelationships. Figure 3.1 shows a diagram of the tokamak geometry. The safety factor, q, is given by

$$q = (1/A)\, B_T/B_p \,. \qquad (1)$$

The toroidal magnetic field strength at the center of the plasma is given by

$$B_T = B_{max}\,(1 - 1/A - \Delta/R_o) \,, \qquad (2)$$

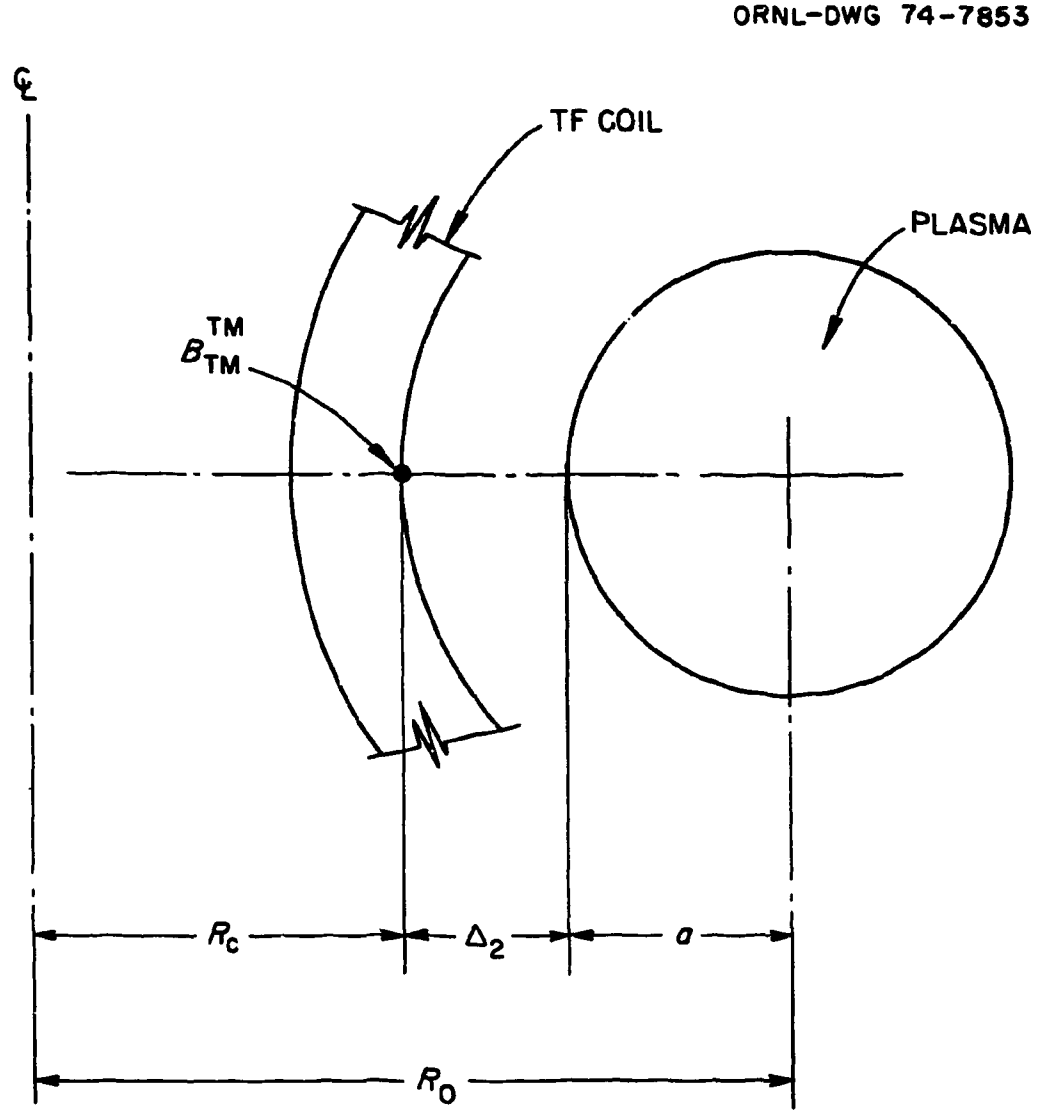

Fig. 3.1 Diagram of tokamak geometry.

where B_{max} is the field strength at the coil winding and Δ is the radial distance from the surface of the plasma to the winding. Combining these equations yields an expression for the plasma current, as follows,

$$I = \frac{2\pi B_{max}}{\mu_o q} \, 1/A^2 \, [(A - 1)a - \Delta] \, . \qquad (3)$$

The current is considered to be an important measure of plasma quality. Alternative quantities involving other variables, such as the aspect ratio, probably could be used as the quality measure, but their detailed functional dependencies are not known at present. Increasing the value of B_{max} or $\underline{a}$ and decreasing the value of Δ or q permits an increased plasma current. These sensitivities to B_{max}, $\underline{a}$, Δ and q are well known and plausible values depend on magnet technology, allowable physical size, blanket and shield requirements, and stability. The variation of I with changes in the aspect ratio, A, is, however, not as simple. Consideration of the variation of I with A yields results that can be summarized in the following points:

- for a given plasma radius, I is relatively insensitive to A,
- for a fixed aspect ratio, I decreases rapidly with a decrease in plasma radius.

This second point can be understood by rewriting equation (3) with all parameters fixed except $\underline{a}$:

$$I \propto a \, [(A - 1) - \Delta/a] \qquad (4)$$

The reason for strong effect of $\underline{a}$ on the value of attainable current is now clear from equation (4). In reactors $\Delta \ll \underline{a}$ is possible and the effect of Δ is of little importance. In the EPR, however, $\Delta \sim 1.55$ suggests a minimum $\underline{a} \sim 2.0$ m so that efficient use can be made of the volume within the toroidal coils.

A high aspect ratio and a given plasma radius implies a large major radius and, typically, increased cost. For example, if, for a fixed $\underline{a}$, A is increased from 3 to 4 and one assumes that the cost of the device is

proportional to R_o^2, the corresponding cost increase is 78%. Even if cost is proportional to R_o, the cost would increase by 33%. In either case, the increase is considerable. This argument favors a low aspect ratio, as does the consideration of stored toroidal field energy. As a result, the aspect ratio is chosen to be as small as is compatible with the space requirements in the center of the torus. A support structure and part of the ohmic heating coil system must be located in this region.

After having considered the sensitivity of $\underline{I}$ to various quantities in equation (3), one can draw the following conclusions:

- An increase in $\underline{I}$ through appropriate variations in A, Δ, or $\underline{a}$ depends on funds available and engineering design.
- An increase in $\underline{I}$ through a variation in q depends on research efforts and ultimate plasma stability.
- Further improvements in $\underline{I}$ through increases in B depend on the magnet development effort.

It is also necessary to discuss the size of the EPR plasma in the context of the overall CTR program. The EPR, in addition to its other objectives, should provide the next logical step beyond the TFTR. Thus, the plasma (or chamber) should be 4–5 meters in diameter.

3.3 EPR Reference Parameters

On the basis of the framework presented above and interactions with the relevant research, development and engineering personnel, the reference parameters have been chosen as shown in Table 3.1 and are discussed below.

Table 3.1. EPR-1 Reference Parameters
Plasma Subsystem Requirements

Plasma radius, a (m)	2.25
Major radius, R_o (m)	6.75
Safety factor, q (a)	2.5
Maximum toroidal field, B_{max} (T)	11.0
Toroidal field on axis, B_T (T)	4.8
Plasma current, I (MA)	7.2
Plasma edge to winding distance, Δ (m)	1.55
Volt-second, (V•s, Wb)	185
Injection power capability, P_b (MW)	100
Deuteron energy, E_b (keV)	200
Number of injectors, N_I	12
Number of toroidal coils, N_c	20
Toroidal field ripple, $\delta(\theta=0;\ r=a)$	<2.2%

Because of the uncertainty in scaling laws for an EPR-size plasma, the critical plasma parameters must be recognized, fundamental relationships between them used and choices made consistent with expected results from ongoing experimental, theoretical and developmental programs. Parameters for the reference design have been selected as follows (Fig. 3.2 shows the geometric relationships of several key parameters):

a) the plasma radius, $\underline{a}$ = 2.25 m. For the present it may be assumed that the plasma fills virtually the entire chamber bore. This size is compatible with reactor-grade plasma operation and is suitable for a post-TFTR device.

b) The distance between the plasma edge and the inner surface of the toroidal coils, where B_{max} occurs, is given by Δ = 1.55 meters.

ORNL-DWG 75-11174

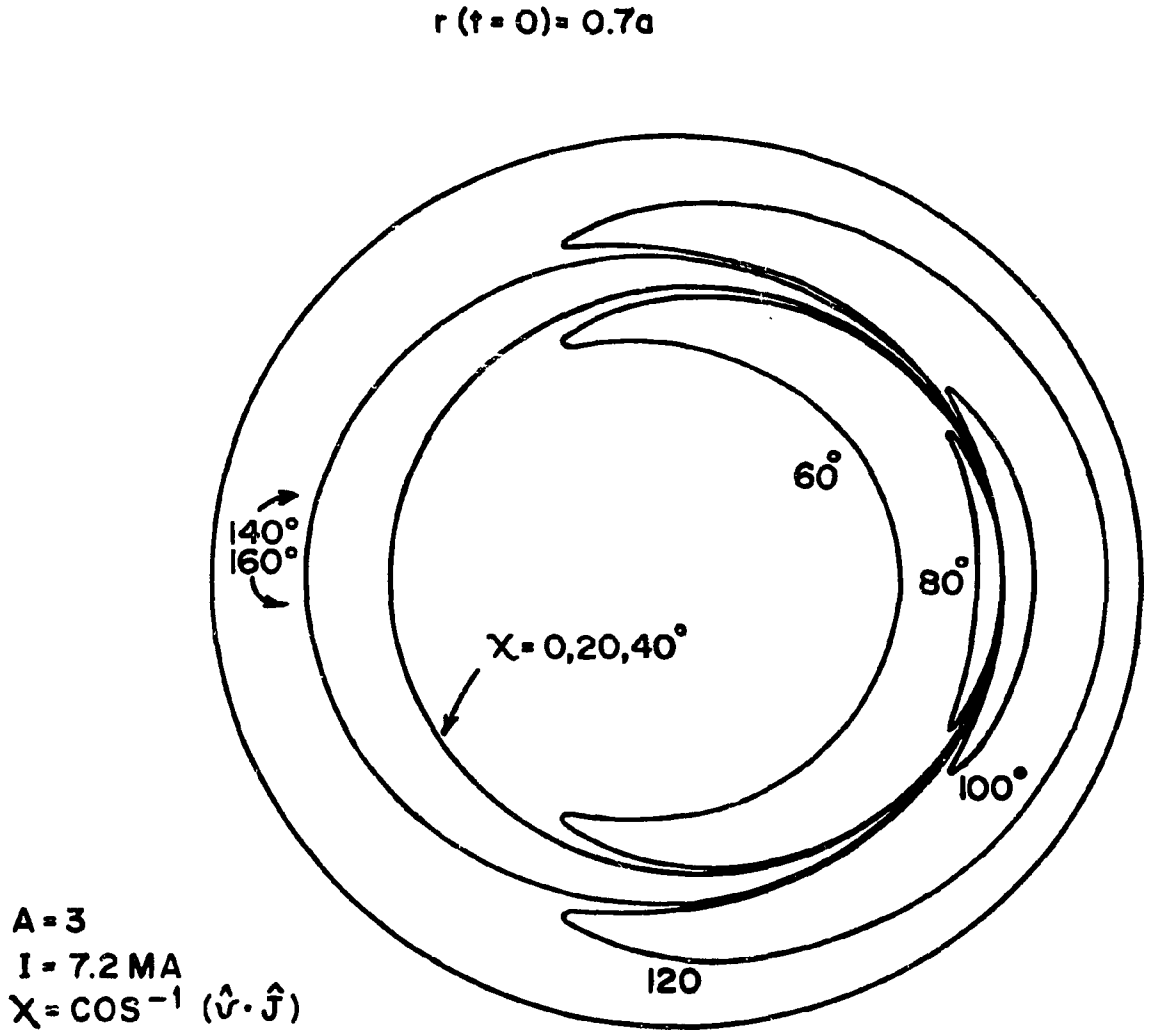

Fig. 3.2 Alpha particle (3.5 MeV) orbits in EPR.

This dimension is a combination of shield and blanket thicknesses and engineering tolerances, and is approximately constant for the range of device sizes analyzed.

c) The aspect ratio A is 3. This choice is based primarily on the consequences of the increased volume and cost associated with $A > 3$ and the construction difficulties imposed upon all the elements of the design with $A < 3$.

d) The safety factor, $q(\underline{a})$, is greater than or equal to 2.5. The minimum value, $q(o)$, depends on the radial distribution of the current. The value $q(\underline{a}) = 2.5$ requires improvements in steady-state behavior over present devices.

e) The machine will be designed for a maximum toroidal field B_{max} = 11 T. Magnets compatible with these requirements for size and field-strength are being developed.

f) The total volt-second capability of the device will be about 185. This includes a margin of a factor of 2 relative to known flux needs.

g) The injection system will have the maximum capability of providing about 100 MW of 200-keV deuterons to the plasma.

3.4 Energetic Particle Containment

One of the objectives of EPR is to attain a reactor grade plasma implying significant thermonuclear alpha-particle production. The device must, therefore, be large enough to contain the drift orbits followed by the alpha particles.[2] A typical family of such orbits is shown in Fig. 3.2. These particles all pass through $r/a = 0.7$ at a minor azimuthal angle of $\theta = 0$. The pitch angles $\chi = \cos^{-1}(\hat{v}\cdot\hat{J})$ range from 0° to 160° at the common point. Examples of both costreaming and counterstreaming orbits are shown. The gross containment of the 3.5 MeV orbits is good, although a more detailed analysis is required to determine the importance of the finite gyroradius effects which lead to the large banana widths shown. The containment property of the system for alphas is shown more generally in Fig. 3.3. In this figure the particle energies perpendicular and parallel to the magnetic

ORNL-DWG 75-11167

A=3
ALPHA (3.5 MeV)
I= 7.2 MA
$J(r)=1-(r/a)^2$

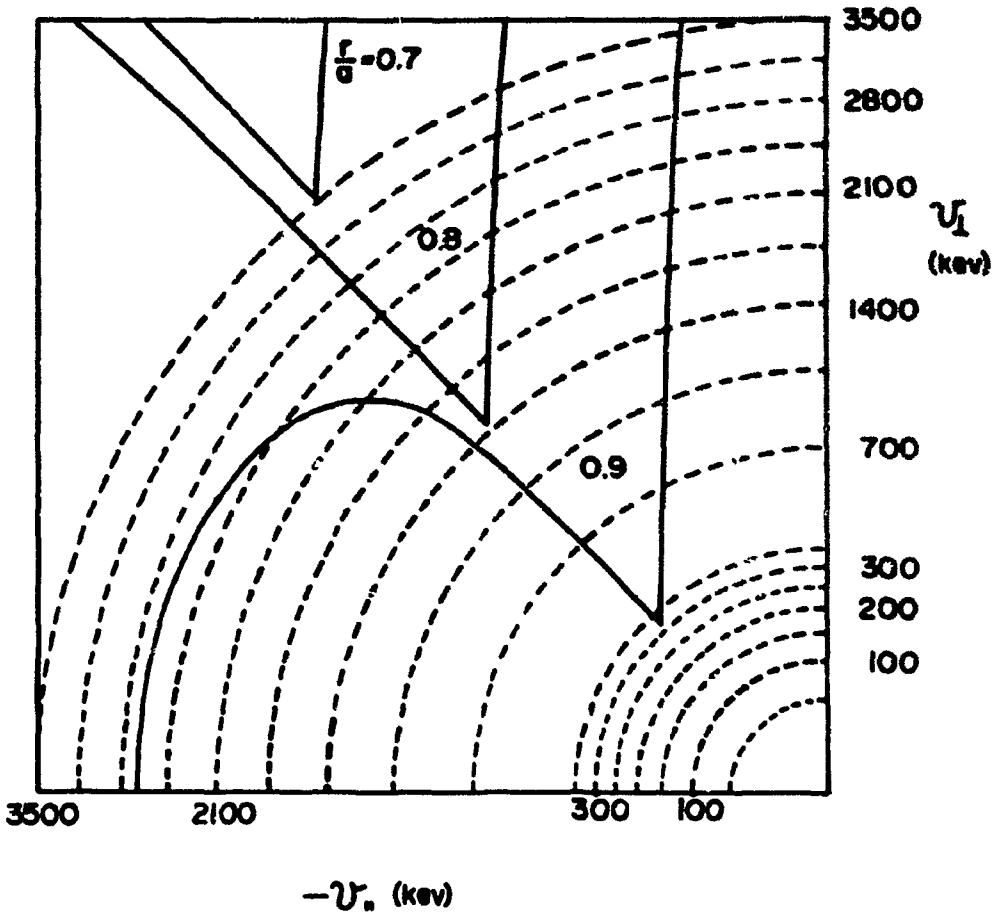

Fig. 3.3 Loss regions for alpha particles in EPR. Pitch-angle space for counterstreaming particles is shown; coordinate values are given in terms of the corresponding particle energy.

field are represented by y and x coordinates respectively.[3] Thus the 3500-keV arc represents the alpha-particle initial energy and pitch angles between 90° and 180°. When the energy arc and pitch angle are such that the particle's position in the pitch-angle space is within a loss region, the particle orbit is not contained within the plasma boundary and the particle is considered lost. For example, all alpha particles produced at $r < 0.7a$ follow contained orbits. Alpha particles with energy (E_α) less than 1400 keV and $r < 0.8a$ follow contained orbits, but, when $1400 \leq E_\alpha \leq 3500$ and $0.7 \leq r/a \leq 0.8$, the loss region indicates that particles from a finite portion of pitch angle space will escape. Note that for 3500 keV and $r/a = 0.7$ no alpha particle orbits should intersect the plasma boundary, since the loss region lies at $E_\alpha > 3500$. These observations are in accord with the orbits shown on Fig. 3.2. Figure 3.4 shows similar information on fast-ion orbits using 200-keV deuterons. Finally, note that deuterons below 160 keV are contained regardless of their pitch angle and that a negligible fraction of deuterons, existing at $r > 0.9a$ and $E_d > 160$ keV, follows uncontained orbits.

In summary, the reference system will provide adequate containment of both 200-keV deuterons and 3.5 MeV alpha particles from the heating point of view. Additional analyses are required to determine the finite gyroradius effects to be expected and the plasma response to them.

3.5 Neutral Injection System Energy and Power Requirements

The energy of the fast neutral particles injected into the plasma must be high enough for adequate penetration into the system and low enough to ensure acceptable attenuation. Initial calculations of the deposition characteristics of 150–200 keV deuterons injected tangentially into the plasma suggest that $E_b = 200$ keV is adequate to provide a desirable energy deposition profile.[4] However, additional analyses are required to include impurity effects, possible neutral gas blanket limitations, etc., before the final energy can be determined. With the densities anticipated ($N_e \approx 7.5 \times 10^{13}$ cm^{-3}) for the EPR, attenuation is no problem at $E_b \approx 200$ keV.

ORNL-DWG 75-11166

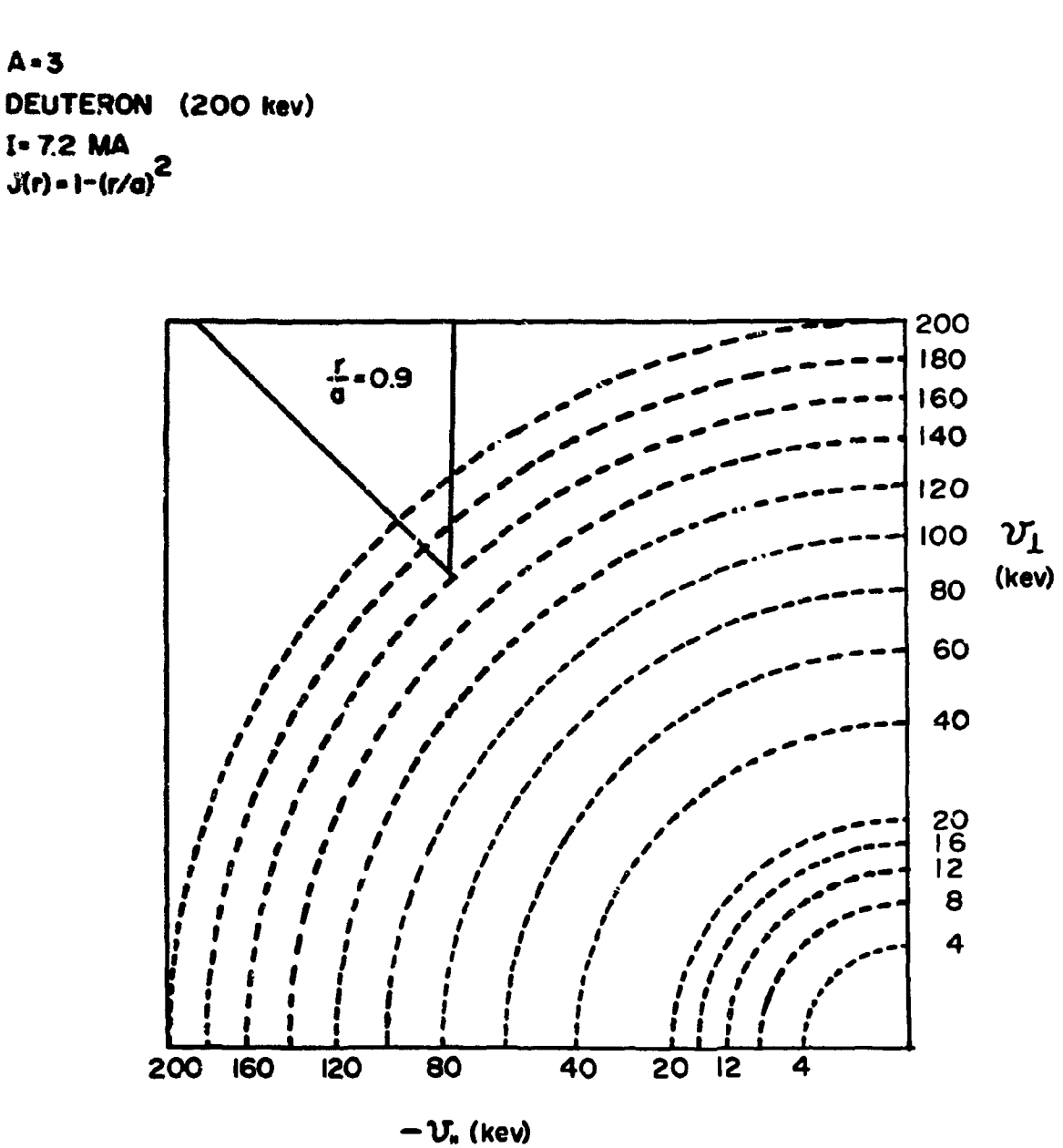

Fig. 3.4 Loss regions for deuterons in EPR. Pitch-angle space for counterstreaming particles is shown; coordinate values are given in terms of the corresponding particle energy.

The power requirements depend directly on confinement scaling and thus are uncertain. On the basis of models to be discussed below, 75—100 MW of injection power could be required. At this time the reference design device is capable of handling the mechanical and electrical requirements of a 100-MW injection system (access, power, etc.).

3.6 Plasma Modeling

Two models have been used to simulate the plasma. The first, a time-independent point model, was used to determine the sensitivity of various machine and plasma characteristics to changes in specific parameters. The model represents a plasma operating at steady state with losses balanced by injection and alpha particles, or alphas only in ignition cases. The second, a time-dependent point model, was used to analyze the dynamic phase of system operation during heating and the burn.

The scaling laws used are uncertain. This fact is well known and the results shown here are meant to provide an indication of power levels, operating modes, parameter sensitivities, etc., using the presently presumably conservative model. The model assumed includes the effects of the nonlinear limit of the dissipative drift instability at low collision frequencies. It seems unlikely that losses due to these instabilities will be more severe than the model indicates. The model is similar to those used in other reactor design work and thus serves as a basis for comparison. In addition to the dissipative trapped-particle diffusion terms, the scaling model includes pseudoclassical and neoclassical diffusion terms, conduction and convection, impurity effects and radiation. Fueling is provided not only by neutral beams, but also by zero energy particles to maintain the plasma density. Beam-plasma as well as Maxwellian or bulk fusion events are included.

Figure 3.5 shows beta poloidal and plasma radius versus $N\tau$ for several toroidal field strengths on the plasma axis. The following assumptions are made: $A = 3$, $N_D = 0.25\ N_i$, $Z_{EFF} = 2.0$ or 3% C, $T_e = T_i = 8$ keV, $E_b = 150$ keV, and $\beta_{pe} = 1$. The important points are as follows. The total β_p including thermal ions and fast ion pressures is shown. At low $N\tau$ values

ORNL-DWG 75-11168

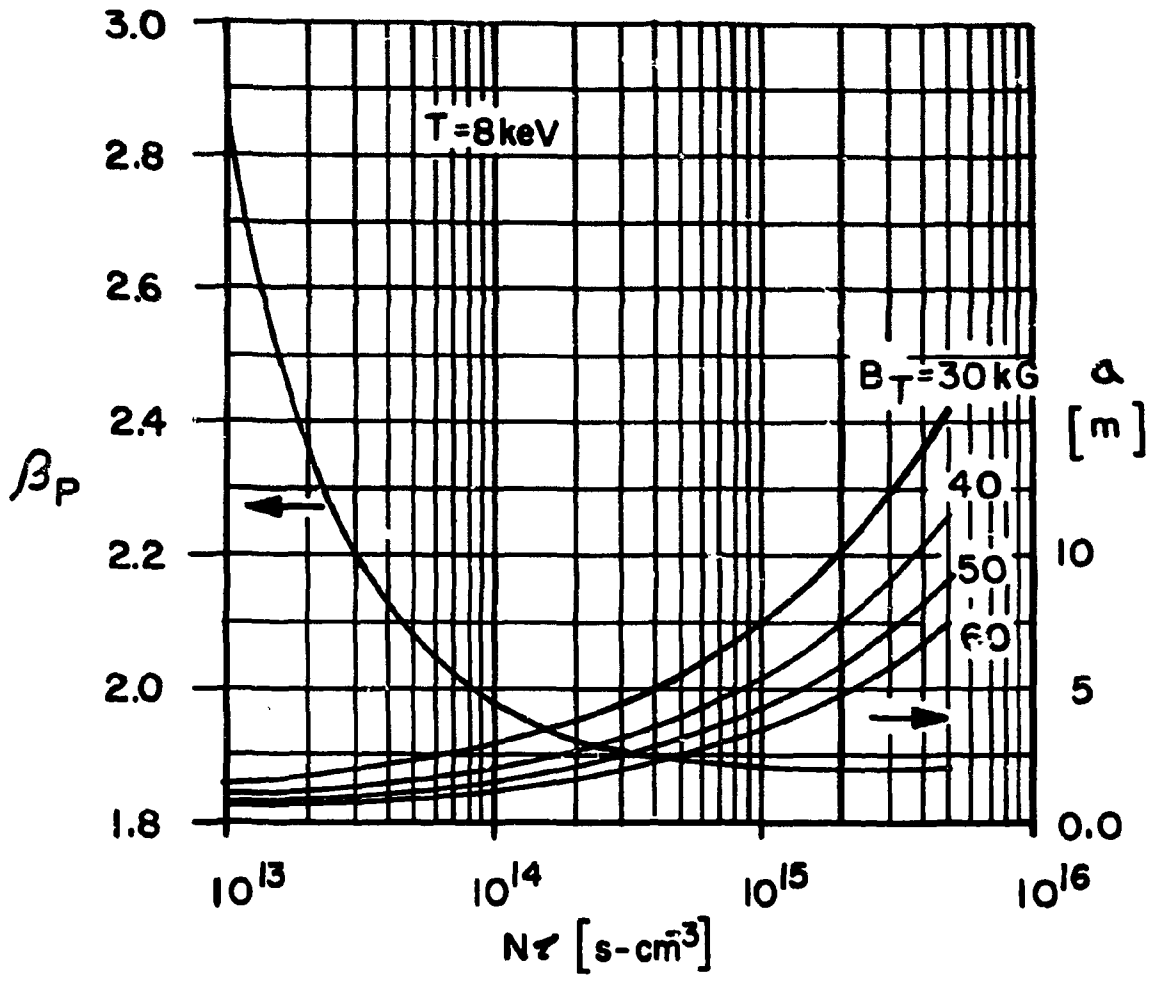

Fig. 3.5 Beta poloidal and plasma radius as a function of $N\tau$ for different toroidal magnetic field strengths.

($\sim 10^{13}$ cm^{-3}-s) the contribution of the fast ions (primarily due to injection) to the total pressure is significant, but $\beta_p < A$. In these circumstances, the system would be beam driven.[5,6] For $N\tau > 10^{14}$, $\beta_p \gtrsim 2\beta_{pe}$, since the system size has increased, confinement has improved and beam power per unit volume has decreased. The EPR system typically will operate under conditions such that $\beta_p \gtrsim 2\beta_{pe}$. The figure also shows the sensitivity of the size required to achieve a particular $N\tau$ to the toroidal field strength. For example, at $N\tau = 5 \times 10^{14}$ cm^{-3}-s, under the assumed conditions, doubling B_T from 3 T to 6 T permits a decrease in plasma radius from $\sim$ 5m to 2.5m. The precise sensitivity is dependent on the exact conditions considered, but the benefits of high magnetic fields, from the plasma point of view, are numerous.

Figure 3.6 shows an example of the plasma radius required to achieve various $N\tau$'s as a function of scaling uncertainty, in this case, in the trapped-particle mode loss coefficient. Here the continuation of the dissipative trapped-particle mode to the overall confinement time is varied by a factor of 10 as a somewhat arbitrary measure of the range of uncertainty. This example is for 4T on axis and shows that the size required to attain $N\tau = 5 \times 10^{14}$ cm^{-3}-s could range from 2–4m. On the other hand, a system with a plasma radius of 2m and a 4 T field could operate between $N\tau = 8 \times 10^{13}$ cm^{-3}-s and 6×10^{14} cm^{-3}-s. In actual fact, of course, we do not know even the functional dependence of the scaling, let alone the coefficients. Therefore, this sensitivity illustrates only one facet of the problem. Herein lies the difficulty in sizing the EPR.

The second time-dependent model has been used to analyze the reference system given in Table 3-1. Recall that $B_T = 4.8$ T, a = 2.25 m, I = 7.2 MA, $N_D \gtrsim 0.25\ N_i$, $Z_{EFF} = 2$ (3% C), and $N_e = 8 \times 10^{13}$ cm^{-3} with the injection power given on the curve. Figure 3.7 shows these results. For 50 MW of injection pow and 10% of the theoretically predicted trapped-particle losses, the plasma ignites in about 4.8 seconds. The fusion power would be 225 MW immediately before ignition and 175 MW after the beams are terminated at ignition. The neutron wall loading is $\sim$ .2 MW/m^2, the ion temperature is $\sim$ 9 keV, and $N_e\tau_E = 6 \times 10^{14}$ cm^{-3}-s.

ORNL-DWG 75-11170

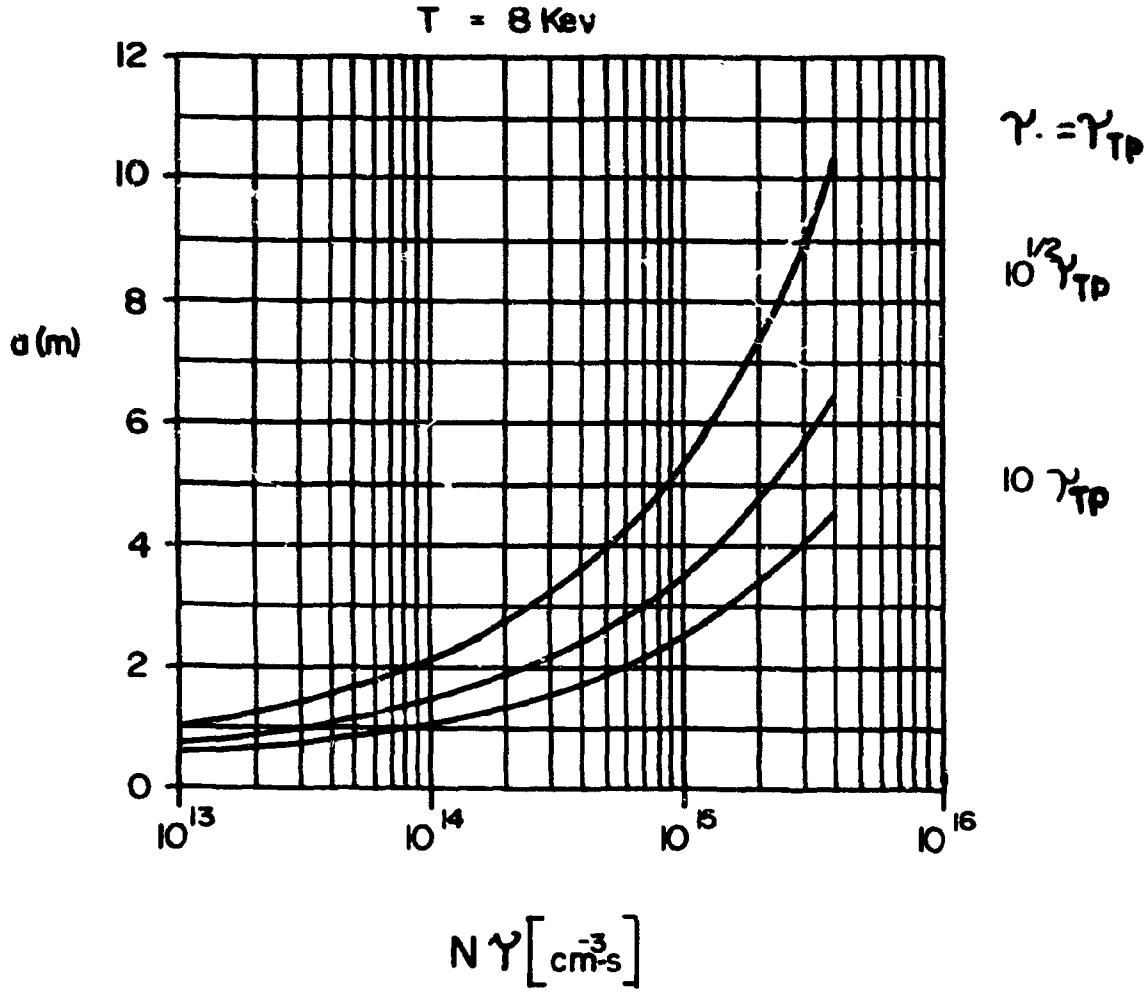

Fig. 3.6 Plasma radius required to attain temperature of 8 keV for different trapped particle loss coefficients.

ORNL-DWG 75-11172

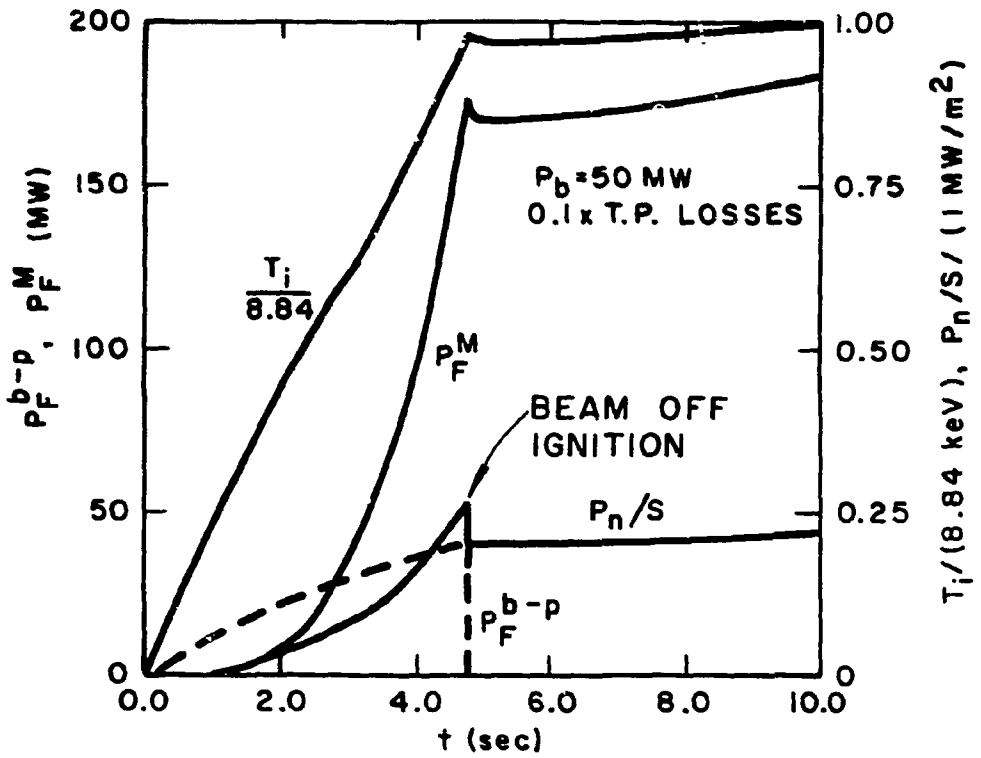

Fig. 3.7 Fusion power outputs as a function of time for 50 MW of injection power and 0.1 times trapped-particle losses. Superscript M refers to Maxwellian or bulk plasma reactions and superscript b-p refers to beam-plasma reactions.

Figure 3.8 shows the results for the same system with 100 MW of injection and the full trapped-particle mode contribution. The plasma does not ignite. Under the steady-state conditions achieved, the beam-plasma fusion power is 90 MW, and Maxwellian fusion power is 210 MW. The neutron wall loading is 0.4 MW/m^2. The total recoverable heat from this system is about 400 MW. It is important to note that, even when the system is beam driven with full losses, the reference system produces about 70% of the total fusion power in the background plasma.

Figure 3.9 shows the β_{pe} attained under the same conditions for the reference system. $\beta_{pe} = 0.75$ both in the case of ignition and when driven with 100-MW system. With 50 MW of injection power and full losses, β_{pe} of about 0.4 would be obtained. The current-rise phase of operation occurs during the first second. This explains the oscillations, since the confinement time is dominated first by pseudoclassical and then by diffusion dominated by the trapped-particle mode.

Figure 3.10 shows the ratio of alpha power production to the total instantaneous energy loss rate from the plasma, P_α/P_{loss}, as a function of time. The ratio P_α/P_{loss} can be considered a measure of the degree to which a particular operating mode represents reactor-grade performance. In the ignition case, $P_\alpha/P_{loss} > 1.0$ immediately before ignition, due to beam-plasma produced alpha particles. After the beams are terminated, $P_\alpha/P_{loss} \approx 1$, which is the definition of ignition. In the beam-driven cases, the ratios are 0.4 for 100 MW injected and 0.2 for 50 MW injected. In the 100-MW driven case, 400 MW of recoverable heat is produced.

Figures 3.11 and 3.12 show the P_α/P_{loss} ratio versus time for 3 toroidal field values, 100 MW of injection, and for full and reduced trapped-particle losses, respectively. In the full loss cases, the benefit of increased field strength is clear. Confinement is improved by operation at higher plasma currents permitted by the increased central field. Thus the alpha particles provide a successively larger fraction of the total plasma losses as B_T increases. In the reduced loss cases ignition occurs at both 4.8 and 4.4 T. Plasma conditions at both field levels are very similar at ignition. The 3.7-T case does not ignite and the beam power is reduced after 2 seconds to prevent β_{pe} from exceeding 1. The benefit of increased B_T is obvious.

ORNL-DWG 75-17025

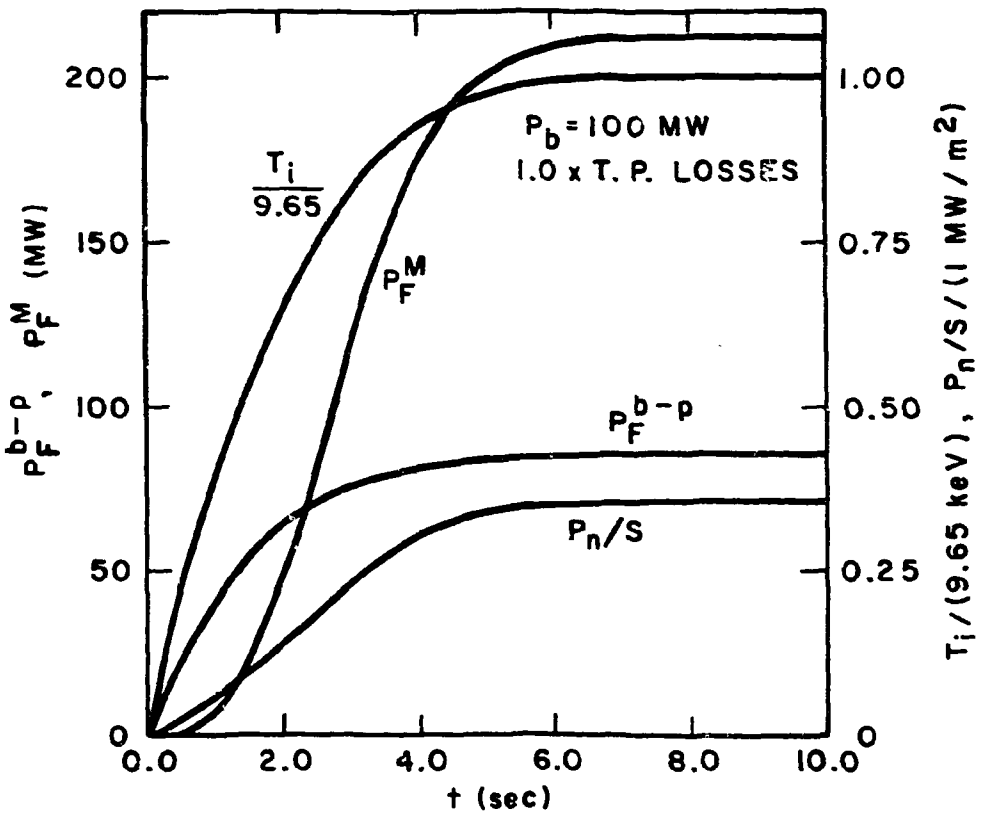

Fig. 3.8 Fusion power outputs as a function of time for 100 MW of injection power and full trapped-particle losses. Superscript M refers to Maxwellian or bulk plasma reactions, and superscript b-p refers to beam-plasma reactions.

ORNL-DWG 75-11173

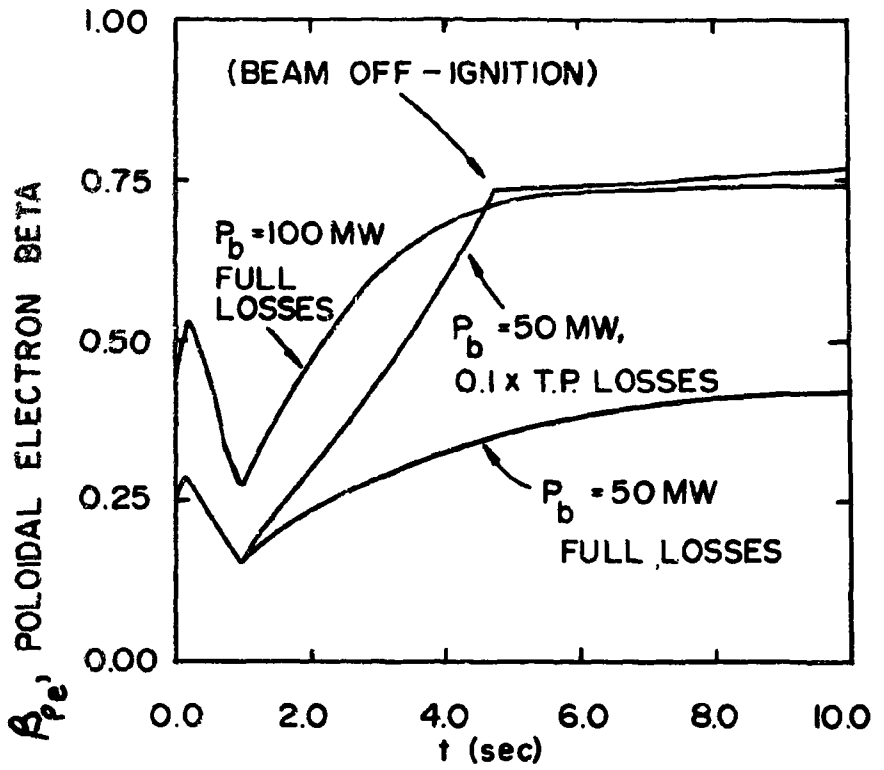

Fig. 3.9 Poloidal electron beta as a function of time for different injection powers.

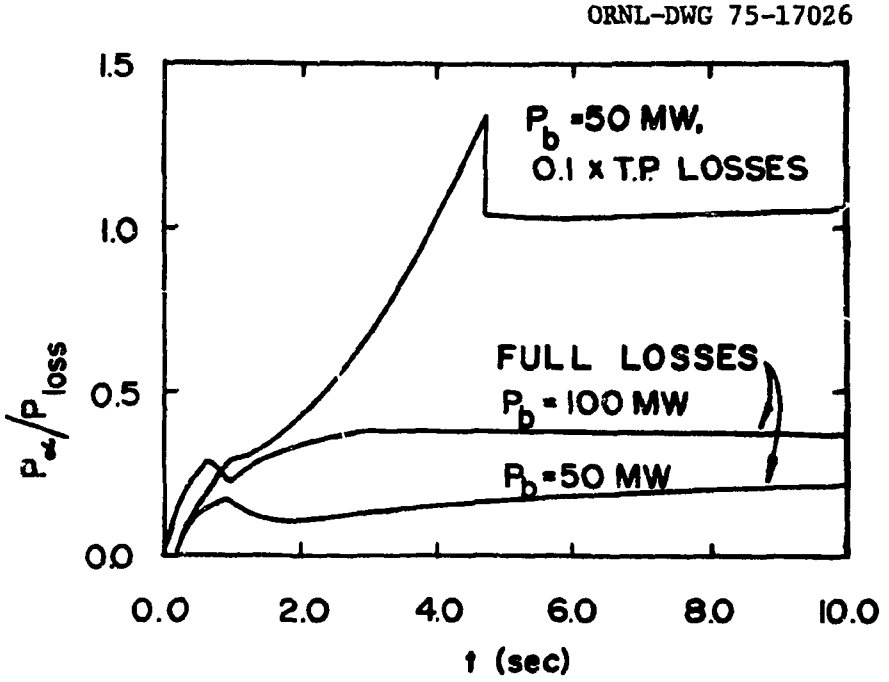

Fig. 3.10 P_α/P_{loss} as a function of time for different trapped-particle losses and injection power.

ORNL-DWG 75-11171

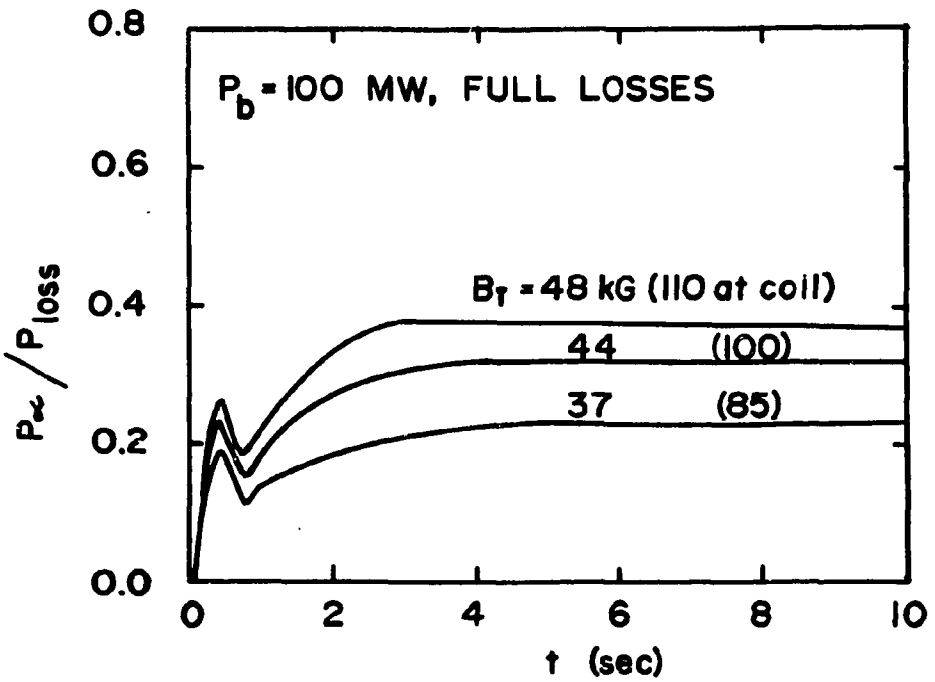

Fig. 3.11 P_α/P_{loss} ratio for full trapped-particle losses as a function of time for three values of toroidal field.

ORNL-DWG 75-17027

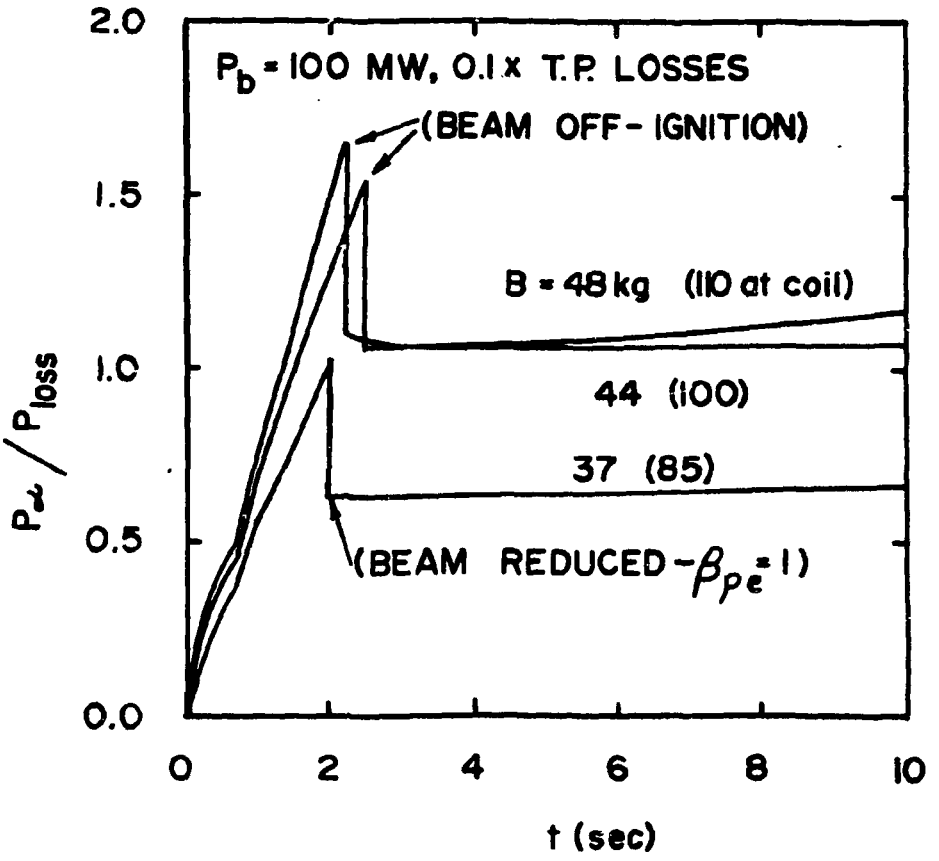

Fig. 3.12 P_α/P_{loss} ratio for reduced trapped-particle losses as a function of time for three values of toroidal field.

In summary, a reference set of parameters has been chosen. The plasma size, current and toroidal magnetic field on axis are consistent with the operation of a reactor-grade plasma even under the assumptions used. That is, the particular scaling model used to analyze the operation of the plasma is believed to represent the unfavorable limit of the expected behavior based on present knowledge. The uncertainty in the scaling laws used suggests a range of eventualities.

At the one end ignition occurs and the system produces $\sim$ 200 MW of fusion power; 50 MW of injection is required for heating. Even in this case, higher power operation is possible and depends on detailed assumptions.

At the other end, with less favorable containment properties the system can be injection driven using 100 MW of 200-keV beams to produce 300 MW of fusion power (of which 210 MW comes from background fusion events, 90 MW from beam fusion events) and 400 MW of recoverable heat.

In either the ignition or driven case the reference system provides reactor-grade plasma operation and significant neutron wall loadings, and represents a suitable post TFTR step in the program.

3.7 The EPR as an Irradiation Test Facility

The main objectives of the EPR are related to fusion physics, post-TFTR plasma operation and long-pulse, power-producing operation in general. Scenarios including beam-driven and ignition-system dynamics have been discussed. Preliminary consideration has been given to the potential of the EPR facility in filling a further role, namely, that of an irradiation test facility. Present and planned 14 MeV neutron irradiation facilities can provide high flux, but the available test volume is limited. It is possible that the EPR, operated in the irradiation mode, could contribute to the solution of this problem by providing considerably larger test volumes.

The present reference design includes a plasma chamber 4.5 m in diameter and a central field of 4.8T. The neutron wall loading, computed using the time-dependent model described in Section 3.6, with 100 MW of injection producing $\sim$ 300 MW, is $\sim$ 0.4 MW/m^2. By injection of 230 MW into the system

(which requires 130 MW of beam beyond the reference design), the neutron wall loading achieved increases to 1 MW/m^2.

Alternatively, a smaller plasma system can be operated in the device. For example, with R_o = 5.7 m, a = 1.2 m, B_T = 5.7 T, A = 4.75 and 200 MW of injection power, the source neutrons will pass through the plasma surface area at a rate equivalent to $\sim$ 1 MW/m^2. The physics of a smaller driven system is uncertain in several ways. In this case β_{pe} = 1.6, but A = 4.75, so that higher β_p operation may be tolerable. The particle confinement time is $\sim$ 800 msec, which is a small fraction of long pulse time. Therefore, long pulse operation represents many particle containment times. In this case, the impurity and fueling burdens could be great.

The primary role of the EPR is not that of an irradiation facility. Consideration, however, has been given and will continue to be given to the possibility of operating the EPR facility in such a mode. It appears that the desired wall loading can be achieved in more than one way, ranging from full-bore large volume operation to smaller volume operation, with the added possibility of in-situ testing.

REFERENCES

1. S. O. Dean et al., Status and Objectives of Tokamak Systems for Fusion Research, WASH-1295, Washington D. C. 1974.

2. D. G. McAlees, ORNL-TM-4661, Oak Ridge National Laboratory, (November 1974).

3. J. A. Rome, D. G. McAlees, J. D. Callen, and R. H. Fowler, ORNL-TM-4855, Oak Ridge National Laboratory (April 1975).

4. J. A. Rome, J. D. Callen, and J. F. Clarke, *Nucl. Fusion* 14, p. 141 (1974).

5. J. M. Dawson, H. P. Furth, and F. H. Tenney, *Phys. Rev. Lett* 26, p. 1156 (1971).

6. R. W. Conn, W. A. Houlberg, and J. Kessner, UWFDM-106, University of Wisconsin (1974).

4. NUCLEAR SYSTEMS
(Blanket, Shield, Neutronics and Materials)

4.1 Introduction

The blanket for the EPR was designed to perform three functions:

1) absorb at least 90% of the plasma energy at the level of a few hundred MW, and convert it to heat at a temperature of 370°C,
2) (with the shield) attenuate the plasma neutrons and radiation to protect the winding of the toroidal field coils, and
3) provide some experimental modules where breeding of tritium could be demonstrated.

Several types of blankets were evaluated in the Scoping Study and one successfully fulfilled these three requirements. This was chosen for the reference design and is shown in Fig. 4.1. Neutronic and heat transfer calculations for blanket and shield were done initially by simple one-dimensional methods. More sophisticated multi-dimensional computer calculations, including effects at penetrations, edges, and joints, will be performed in these areas.

4.2 Blanket Description

The blanket is composed of sixty autonomous segments which, when clamped and welded together, make up the torus. In addition to the three primary functions performed by the blanket it also constitutes the vacuum enclosure for the plasma.

Each blanket segment is composed of three compartments. The first compartment is the main absorber. All the blanket segments are identical except for the substitution of lithium for potassium in the experimental breeding segments. Potassium and lithium were selected as the absorbers because liquid metal absorbers are easily cooled themselves and good thermal conductivity is required to conduct heat from the first wall to the coolant tubes. Lithium is used in the experimental breeding module to produce tritium.

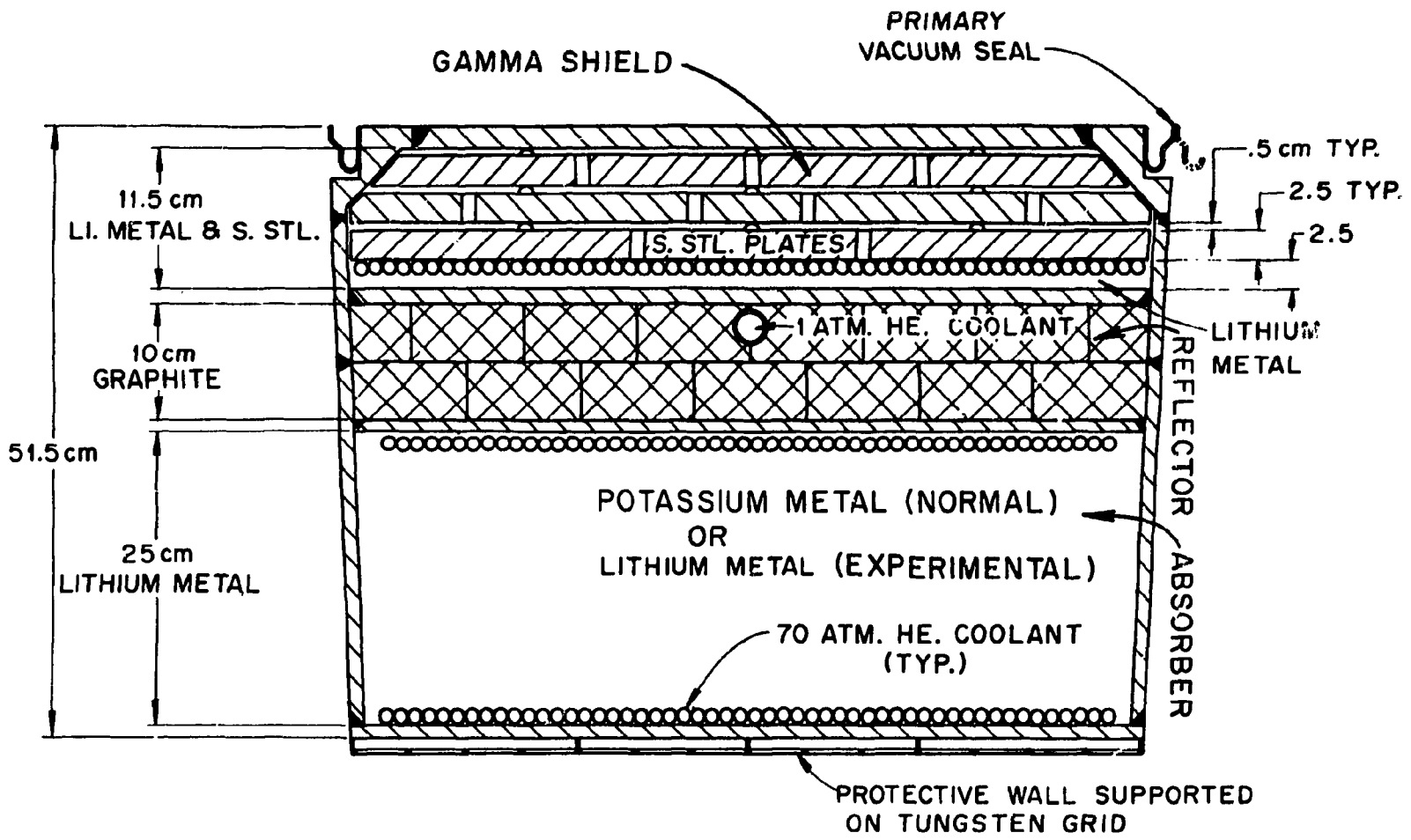

Fig. 4.1 EPR reference design blanket segment.

The second compartment is the reflector. A fraction of the relatively high energy neutrons which have passed through the liquid metal absorber is reflected back into the metal. This is not important for the non-breeding modules but it is an essential feature of the tritium breeding test module. The breeding performance is discussed in the paragraphs dealing with neutronic analysis. Graphite was selected for the reflector because the reflected moderated neutrons reentering the absorber region are more effectively captured by the lithium-6 when reflected by graphite.

The third blanket compartment is a gamma shield composed of three concentric cylinders of stainless steel. In the annuli between these cylinders is liquid metal. The purpose of the liquid metal is to conduct and convect the heat from the stainless steel cylinders to the cooling tubes. Liquid potassium or lithium was selected as the heat transfer medium because the heat from the stainless steel gamma absorber is easily conducted through the liquid metal to the coolant tubes.

As shown in Fig. 4.1, the inner liquid metal compartment has two rows of coolant tubes. Helium at a pressure of 70 atmospheres is circulated through these tubes to remove the heat. One row of tubes is adjacent to the inner wall but not attached to it. Heat from the inner wall is transferred by conduction to the helium coolant tubes. The second row of tubes is adjacent to the rear wall of the liquid metal compartment but is not attached to it. This placement is for the purpose of removing the heat from the liquid metal together with the heat that is radiated from the graphite reflector.

A simple bellows is located on the outer diameter and at both sides of the blanket segment. A seal weld is made at this point circumferentially around the segment to make the vacuum-tight compartment for the plasma. Although not shown in this figure, a mechanical connection is also made between segments for structural strength of the complete torus.

Using the energy deposition values determined from the neutronic calculations, the necessary forced convection coolant conditions were calculated and are summarized in Table 4.1. The design criteria were that the temperature of the blanket structure be held to approximately 550°C and that the helium coolant enter the module at a temperature of 260°C and exit at a temperature of 370°C.

Table 4.1 Results of Thermal-Hydraulic Calculations for Blanket EPR Reference Design

(Driven System)

Total Reactor Power, MW(th)			400
Neutral Beam Power to Plasma, MW(th)			100
Heat Flux on First Wall, MW(th)/m^2			0.27
First Wall Neutron Loading, MW(th)/m^2			0.40
Helium Flow Rate, Kg/sec			658
Helium Inlet Temperature, °C			260
Helium Outlet Temperature, °C			371
Helium Pressure, atm			70
Helium Pumping Power, MW: %			22; 5.5
Max. Temp. in Graphite Curtain, °C			1779
Max. Temp. in Blanket Structure, °C			604
Max. Temp. in Lithium, °C			502
Max. Temp. in Graphite Reflector, °C			789
Helium Tube Bank	1	2	3
Surface Area, m^2	1523	1673	1772
Average Gas Velocity, m/sec	76	83.15	22
Surface Heat Flux, W/cm^2	16	5	3

Temperatures through the blanket were calculated using a one-dimensional conduction model, evaluated at various azimuthal locations around the blanket poloidal perimeter. The results of three such calculations are shown in Fig. 4.2. This figure is representative of the temperatures to be expected in this blanket design.

These calculations were performed for each of the modes of operation examined in section 3, i.e., a driven system using neutral beam power, and a system that ignites. The data presented in Fig. 4.2 and Table 4.1 are for a driven case with 100 MW of injection. Under steady-state conditions, the beam-plasma fusion power is 90 MW, and the Maxwellian fusion power is 210 MW. The neutron-wall loading is $\sim$ 0.4 MW/m^2. The total recoverable power from this system is $\sim$ 400 MW(th).

The first structural wall of the blanket is to be protected from the plasma by a separate first radiation wall. The heat from this wall will be radiated to the first structural wall of the blanket. The blanket cooling has been designed to remove this heat as well as that produced by particle absorption in the blanket structure and absorber metal. The temperature of the first radiation wall will be about 1400°C.

Helium inlet and outlet headers are brought to each blanket module. The cooling tubes are connected to these headers by means of a gas manifold inside the blanket modules. These coolant headers enter the blanket below the equatorial plane of the torus.

4.3 Shield

The blanket does not attenuate the neutrons and gamma rays sufficiently to protect the superconducting toroidal field coils from radiation damage. A thermal barrier between the high temperature blanket and the cryogenic TF coils is also needed. For these two reasons, a water-cooled shield 48.5-cm thick is installed around the blanket in the annular space between the blanket and the TF coils. This shield, like the blanket, is made of 316 S.S. cans. There are 20 of these shield segments fitting underneath the TF coils plus twenty 180° segments and forty 90° segments making up another 20 segments which are placed between the TF coils to

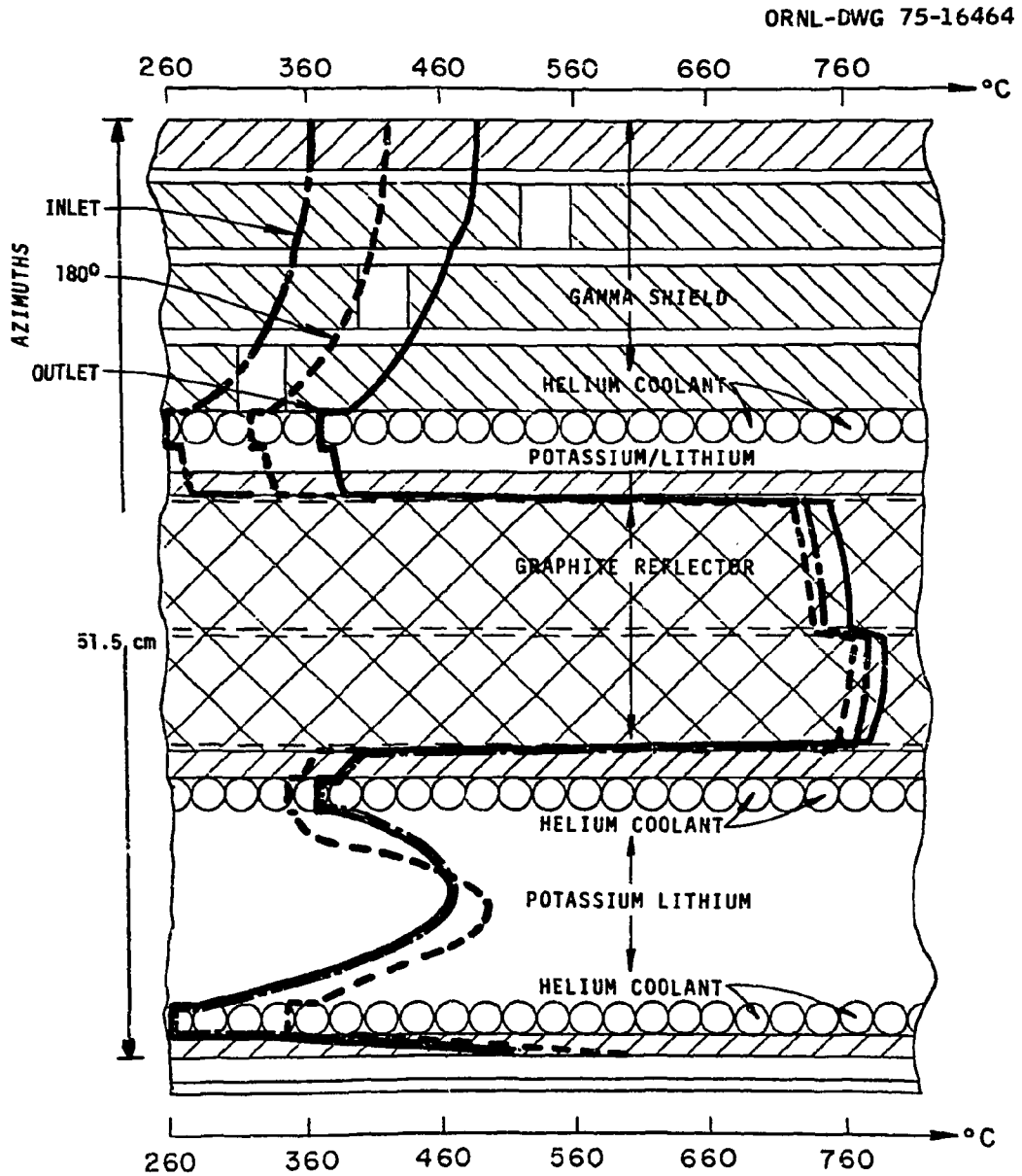

Fig. 4.2 Blanket Concept—Component Arrangement and Temperature Profile.

complete the shield. In addition to the absorption in the wall structure, the absorber materials in the shield are stainless steel spheres cooled with borated water. Adjacent and bolted to the outside container wall of the shield is a 6.2-cm layer of lead. The attenuation of neutrons and gammas in this shield is given in Section 4.5. The power produced in the shield is lost, since the cooling water temperature is too low for it to be utilized.

4.4 Materials Selection for the Blanket

Materials for use in CTR systems must be chosen to provide maximum reliability of the reactor while providing minimum restriction on the reactor design and operation. For the EPR, these requirements and the tentative project schedule dictate that, where possible, materials must be chosen from those that are available now and have well-understood properties under the proposed operation conditions. Although there are a large number of material selections to be made before detailed design can begin, only the two critical choices of the first structural wall and the plasma-structure interface (first radiation wall) have been considered in detail when establishing a reference design for the EPR.

The first structural wall of the reference design is type-316 stainless steel. This material is available, economical, and will be adequate to meet the needs of EPR.

The first radiation wall presents a more difficult material choice. While it appears likely that bare type-316 stainless steel is not the optimum plasma-structure interface, the properties required by the interface material are not well defined. A very tentative choice has been made for the reference design, that is, a "shingle" wall, with the shingles held in place by a refractory metal lattice attached to the first structural wall. Possible shingle materials include W, Nb, C, refractory carbides and refractory oxides. Further design work will be required to verify the concept and additional materials work will be necessary before a choice of shingle material can be made.

First Structural Wall for the EPR Reference Design

The reference design material choice for the EPR first structural wall is type-316 stainless steel. This material is readily available, is economical, has a history of use and testing under conditions similar to those required for EPR, and will permit design, construction and operation of EPR without unduly limiting the project goals.

Type-316 stainless steel is a readily available commercial product manufactured in a variety of forms needed for EPR construction. There is extensive experience in fabricating and welding this material, although procedures for this particular application may require some development. Design methods have been developed and most of the data for design are available; however, we require more extensive experience in the higher temperature (creep-controlled) regime.

Requirements unique to CTR application of structural materials are resistance to the neutron flux originating from the D-T fusion, and compatibility with blanket and coolant fluids. Non-neutronic radiation effects (surface radiation of photons, ions and neutrals) are limited to surfaces facing the plasma and are borne in the reference design by the first radiation wall, which protects the first structural wall. Swelling from the neutron-produced displacement damage and helium will not be a problem for the modest effective full-power lifetime required of the EPR. There is, however, a more important effect of the neutron irradiation that will set a limit on the lifetime of the type-316 stainless steel structure. Helium produced by (n,α) reactions will accumulate at the rate of 40 appm per year of operation at a neutronic wall loading of 0.2 MW/m^2 and a plant factor of 100%. Helium in this concentration, or higher, will embrittle stainless steel in tensile loading at 600°C or higher[1], and dictates that the structure service temperature be held to no greater than 550°C.

Requirements of compatibility between the structural wall and lithium contained in blanket modules for tritium production necessitate temperatures below 600°C. For a rapidly circulating lithium stream the required upper temperature limit would be approximately 500°C, but for the slow lithium circulation in the reference design a temperature limit of 550° C will probably be acceptable. In blanket segments designed only for heat

generation (90% of the EPR blanket modules) the Li will be replaced by K (Na or NaK could also be used), and higher temperature limits could be tolerated owing to compatibility considerations with these liquid metals. The limitation imposed by radiation embrittlement of 550°C will, of course, still prevail.

Coolant tubes circulating helium through the blanket are subject to the same consideration on the Li or K side. However, there are no problems anticipated at the steel-He boundary inside the tube.

In summary, type-316 stainless steel will be an acceptable and adequate first structural wall material for the EPR, if temperatures are restricted to $\lesssim$ 550°C. This choice allows some optimism for extrapolation to higher power reactor systems (such as the Demonstration Plant and beyond). Improvements in the performance of this alloy can probably be expected. Two approaches currently being examined are use of the material in the cold-worked state and use of the alloy with slight chemistry modification. Both these options promise improvement in the problem area of controlling helium embrittlement.

The First Radiation Wall for the EPR Reference Design

The Plasma Contamination Problem. A first radiation wall is specified for the EPR, between the plasma and the first structural wall, because it is uncertain that bare type-316 stainless steel is sufficiently resistant to the plasma environment. This environment of x-rays, photons, ions and neutral particles (with an aggregate energy deposition rate on the first wall of about 10 watts/cm^2), and possibly the neutron flux, will sputter the wall material into the plasma. The introduction of such impurities leads to radiation losses which cool the plasma. Therefore, it is imperative that these impurities be kept to a minimum. Since the energy losses are proportional to Z^n, where Z is the atomic number and n is between 2 and 4, the first radiation wall should preferably consist of a low-Z material with a low sputtering rate.

Reference Design Choice. The reference liner consists of a refractory metal lattice supported from the first structural wall containing "shingles"

of liner material. Because cooling occurs by radiation alone, temperatures well above 1000°C limit the materials selection to nonvolatile materials with a high melting point.

The choice of shingle materials cannot yet be made, but some important materials considerations limit the choice. Sputtering coefficients for various elements exposed to helium ions with energies up to 600 eV are available.[2] The components of stainless steel, Fe, Ni, and Cr have relatively high sputtering coefficients and relatively high Z's. The higher Z refractory metals have lower sputtering coefficients. Of the three low-Z solids — Be, B, and C — beryllium, boron and their compounds have poor radiation stability because of high gas production rates; a great deal of attention was therefore focused on carbon. Until recently, it was thought that carbon was not susceptible to neutron radiation damage above 1200°C. However, data of Van Den Berg et al.[4] showed that graphites are more susceptible to neutron damage at higher temperatures, and undergo rapid densification followed by expansion at fluences to be experienced in the EPR. With any form of carbon, one is also concerned about chemical reactions between energetic deuterium or tritium ions resulting in the formation of methane or acetylene.

A possible alternative to carbon, SiC, has been proposed by Hopkins.[5] Silicon carbide has a relatively low Z and has better radiation stability than carbon. Not enough is known about hot-ion chemistry to know whether or not SiC will react with energetic deuterium or tritium ions.

The sputtering coefficients for various elements[2] suggest that some high-Z materials such as tungsten may not sputter enough to create problems. It is also possible that compounds such as WC, NbC, or ZrC might be better than any elemental material.

The spectrum of shingle materials, then, includes at least W, Nb, SiC, ZrC, NbC, WC, or some other refractory ceramic. Perhaps an oxide such as Al_2O_3 might be used. The final selection will be made on the basis of results of an experimental program which assesses sputtering rates, neutron radiation effects, thermal-shock resistance, chemical sputtering, and other relevant properties at the temperatures to be experienced in EPR.

Alternative Radiation Walls. One possible alternative is to coat the structural wall. Perhaps a coating would be preferable to "shingles". While extensive work has not been done on coatings, main potential problem areas are fabrication difficulties, mismatch in thermal-expansion coefficients, lack of compatibility with the structural wall, and thermal-shock resistance.

Another alternative we rejected is the thin carbon curtain or the thick carbon liner proposed by Conn et al.[3] The potential problem areas with carbon were discussed above.

An alternative geometry that we considered was a honeycomb structure, brazed or otherwise attached to the structural wall. At present, not enough is known about honeycomb designs or materials to allow one to choose them for a reference design.

It is clear that a great deal of work remains to be done before a definitive and defensible choice of a first radiation wall can be made. Information relevant to this problem area will be forthcoming from the surface studies program sponsored by DCTR and from the ISX research program.

4.5 Neutronic Analyses

The results of the neutronic analyses[6] were obtained under the constraints of several broad assumptions concerning the material composition of the structure and shield, the various dimensions, and operating conditions in the reactor. While a more detailed analysis that includes more realistic constraints is essential, the present data should illuminate some of the more salient characteristics of the reference design performance.

A schematic representation of the configuration used in carrying out the one-dimensional neutronics calculations is shown in Fig. 4.3. The model of the toroidal field coils differs in detail from the design shown in Fig. 5.1, but the differences should not significantly affect the neutronics results.

The omnidirectional neutron flux per unit energy in the first structural iron wall of the reactor is shown in Fig. 4.4. In this spectrum,

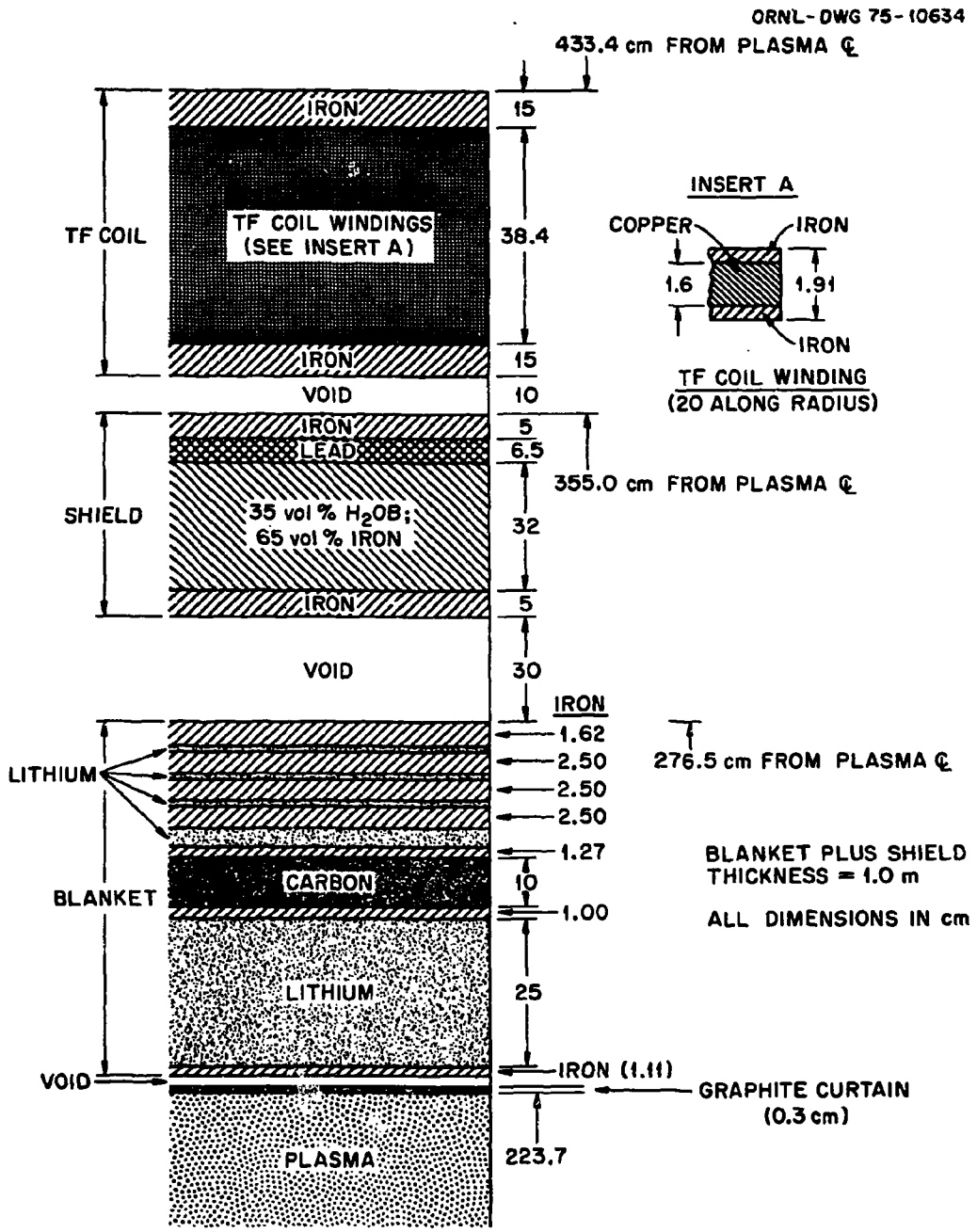

Fig. 4.3 Model of blanket and shield used in neutronic analysis.

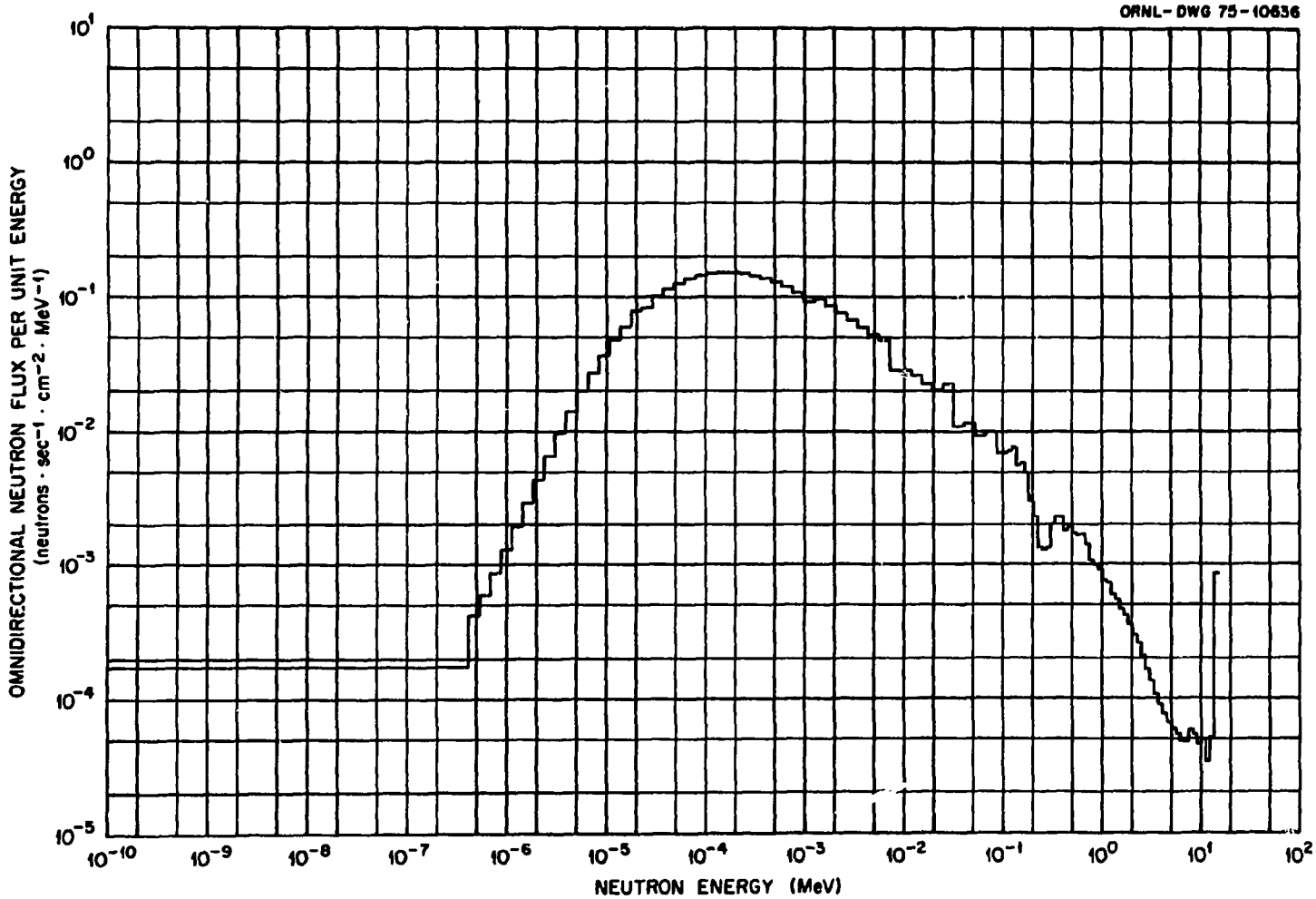

Fig. 4.4 Omnidirectional neutron flux per unit energy in the first structural iron wall of EPR. (Flux values are normalized to one incident neutron per second per unit length.)

approximately 75% of the neutrons have energies > 100 keV and approximately 80% of the neutrons are neutrons below the highest neutron energy group from 13.5 — 14.9 MeV.

Since a one-dimensional model was used in estimating nuclear performance, a radius vector from the center of the plasma passes through all components of the reactor, and it is not possible to model the TF coils accurately or to predict radiation-induced effects on their lateral surfaces.

The TF coil assembly was approximated by alternating iron and copper layers 0.6 and 1.61 cm thick, respectively. Modeling the coil in this manner gives an approximate representation of the conductors and their supports. No attempt was made to include NbTi or Nb_3Sn superconducting wire, insulation, and helium-cooling plenum. The conductors of the TF coil were surrounded by 15-cm-thick iron supports at the inner and outer radii.

In these calculations, iron was taken to be the structural material for computational simplicity. Nuclear performance was estimated for this element only, though it was recognized that a stainless-steel alloy or refractory metal alloy will actually be used.

All the neutronics calculations were carried out by applying the one-dimensional discrete-ordinates code ANISN,[7] which uses a P_3 scattering expansion, an S_{12} quadrature, and the coupled neutron-gamma-ray cross-section library (100 n - 21 γ) of Plaster, Santoro, and Ford.[8] Energy deposition in the reactor was estimated using coupled neutron-photon kerma factors obtained from MACKLIB[9] and SMUGG.[10] Radiation damage was calculated using the displacement cross sections of Gabriel, Amburgey, and Greene,[11] and (n,p) and (n,α) reaction cross sections from ENDF/B-4.

The nuclear performance of the EPR reference design was estimated using the reference plasma sizes and the power parameters summarized in Table 4.2.

The neutron flux is reduced by a factor of 7 in passing through the blanket and is further reduced by a factor of 700 in passing through the shield. The blanket and the shield combine to produce a neutron attenuation of approximately 4900.

Table 4.2. EPR-1 Reference Parameters used for Neutronics Calculations

Plasma Dimensions	
Major radius, m	6.75
Minor radius, m	2.237
Plasma volume, cm^3	6.67×10^8
Plasma surface area, cm^2	5.96×10^6
Toroidal length, cm	4.24×10^3
Reactor Power Parameters	
Assumed neutron power (basis for calculations), MW	100
Neutron wall loading, MW/m^2	0.168
Neutron wall loading (flux), $n/cm^2/sec$	7.43×10^{12}

Although tritium breeding has not been considered a major requirement for the EPR, tritium breeding must be demonstrated in a few breeding blanket modules. The total breeding ratio in the reference design is 1.213 tritium nuclei per incident neutron. The contributions to the total breeding from ^{6}Li and ^{7}Li are summarized in Table 4.3.

The blanket must absorb a sufficient fraction of the fusion neutrons and secondary gamma rays to allow the blanket coolant temperature to be raised high enough to permit efficient recovery of this energy. The energy-deposition rate as a function of radial distance from the plasma center is shown in Fig. 4.5. Note that the abscissa is offset by 200 cm. The solid curve shows the radial dependence of the heating due to neutrons and gamma rays. The curve bearing the tick marks shows the radial dependence of the heating from neutrons only. The heat deposition occurs predominantly in the blanket, followed by a somewhat rapid reduction in the heating through the shield. The effectiveness of the iron and the lead layers in the shield, in attenuating gamma rays generated in both the blanket and the shield, and converting these to heat in the shield rather than in the cryogenic TF coil, is shown clearly by the large differences between the two curves for these materials. The structure in the two curves in the TF-coil region shows the contributions to local heating from the copper coil windings and their iron enclosures.

The integral heat depositions from the neutrons and gamma rays in the various components of the reactor are given in Table 4.4. The total fraction of energy deposited in the blanket assembly (zones 4 through 16) is 89.8%, which is consistent with the design specification for 90% energy deposition in the blanket.[12] The graphite layer and the shield absorb 10.1% of the total heat and the remainder ($<<$ 0.1%) is absorbed in the TF-coil assembly.

Estimates of the radiation damage in the first iron wall and in the first copper winding in the TF coil are given in Table 4.5. These results are for one year's continuous operation at a wall loading of 0.168 MW/m^2. The displacement cross sections used in arriving at these values have thresholds of 40 eV for iron and 30 eV for copper.

Table 4.3. Tritium Breeding Ratio

Zone[a]	Description	Tritium Nuclei, Incident Neutron		
		$R_{^6Li}$	$R_{^7Li}$	R[b]
5	25-cm Absorber	0.619	0.434	1.053
9	2.5-cm Absorber	0.111	0.007	0.118
11	0.5-cm Absorber	0.016	0.001	0.017
13	0.5-cm Absorber	0.013	0.0005	0.014
15	0.5-cm Absorber	0.012	0.0003	0.012
	Total	0.771	0.443	1.214

[a]Zones are identified in Table 4.4 and Fig. 4.3.

[b]$R = R_{^6Li} + R_{^7Li}$ = total breeding.

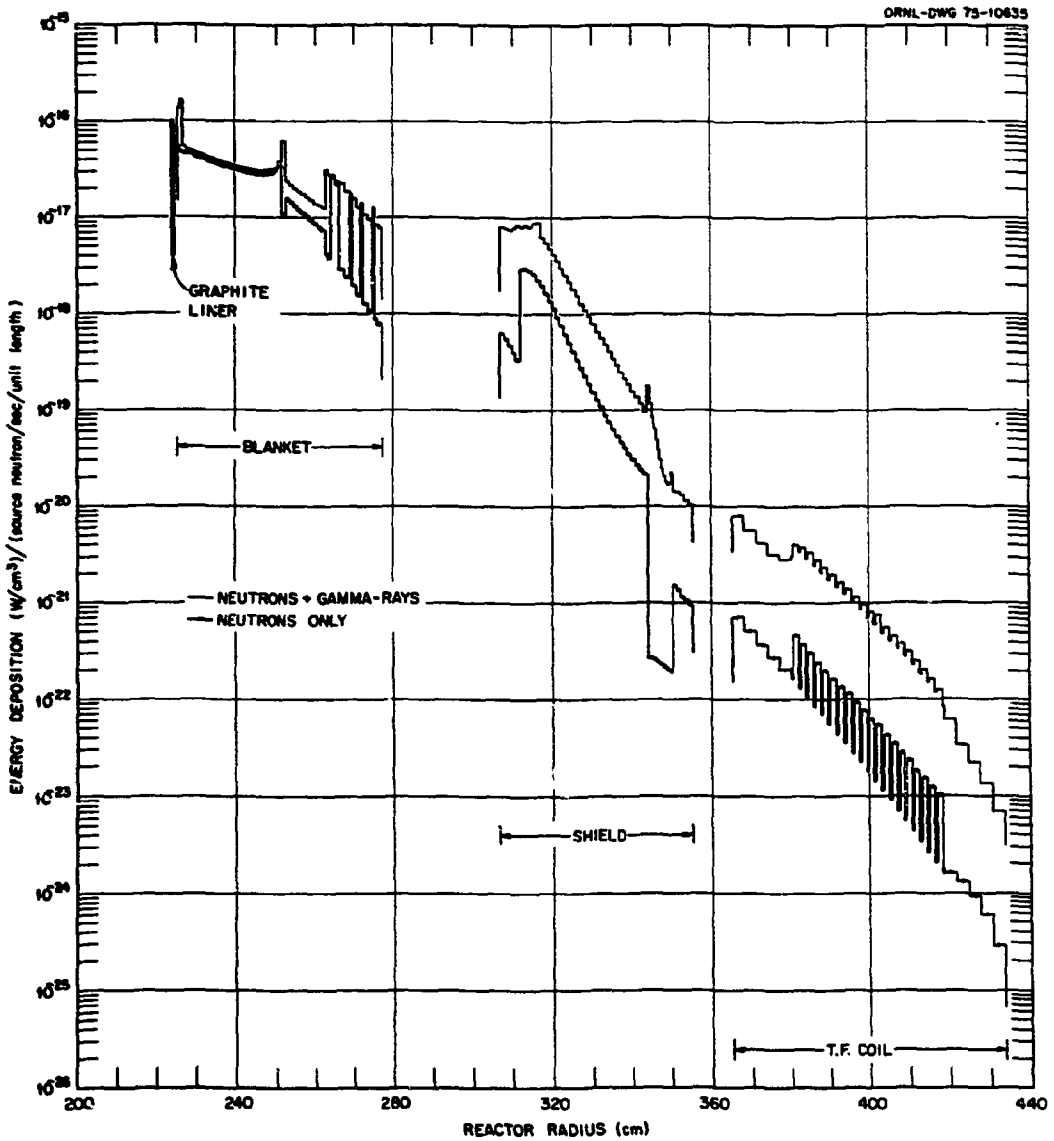

Fig. 4.5 Energy-deposition rate as a function of radial distance from plasma center.

Table 4.4. Volume-Integrated Neutron and Gamma-Ray Contributions to the Energy Deposition

Zone	Material	Outer Radius (cm)	Neutron Heating	Gamma-Ray Heating	Total Heating	Heat Fraction (%)
			[W/(neutron/sec/unit length)]			
1	Plasma	223.70	--	--	--	--
2	Graphite	224.0	3.58×10^{-14}	7.27×10^{-15}	4.31×10^{-14}	1.61
3	Void	225.0	--	--	--	--
4[a]	Iron	226.10	9.08×10^{-14}	1.32×10^{-13}	2.23×10^{-13}	8.32
5	Lithium	251.11	1.29×10^{-12}	1.07×10^{-13}	1.40×10^{-12}	52.22[c]
6	Iron	252.11	1.89×10^{-14}	7.32×10^{-14}	9.21×10^{-14}	3.44
7	Carbon	262.11	1.77×10^{-13}	9.81×10^{-14}	2.75×10^{-13}	10.26
8	Iron	263.38	8.32×10^{-15}	5.27×10^{-14}	6.10×10^{-14}	2.28
9	Lithium	265.88	1.01×10^{-13}	4.51×10^{-15}	1.06×10^{-13}	3.95[c]
10	Iron	268.38	1.11×10^{-14}	7.64×10^{-14}	8.75×10^{-14}	3.26
11	Lithium	268.88	1.44×10^{-14}	6.15×10^{-16}	1.50×10^{-14}	0.56[c]
12	Iron	271.38	7.41×10^{-15}	5.31×10^{-14}	6.05×10^{-14}	2.26
13	Lithium	271.88	1.15×10^{-14}	4.31×10^{-16}	1.19×10^{-14}	0.44[c]
14	Iron	274.38	5.01×10^{-15}	3.83×10^{-14}	4.33×10^{-14}	1.62
15	Lithium	274.88	1.04×10^{-14}	3.17×10^{-16}	1.07×10^{-14}	0.40[c]
16	Iron	276.50	2.33×10^{-15}	2.00×10^{-14}	2.23×10^{-14}	0.83
17	Void	306.50	--	--	--	--
18[b]	Iron	311.50	4.56×10^{-15}	6.18×10^{-14}	6.64×10^{-14}	2.47
19	Shield	343.50	4.90×10^{-14}	1.13×10^{-13}	1.62×10^{-13}	6.04
20	Lead	350.0	3.32×10^{-18}	7.37×10^{-16}	7.40×10^{-16}	0.02
21	Iron	355.0	1.33×10^{-17}	1.27×10^{-16}	1.40×10^{-16}	5.2×10^{-3}
22	Void	364.0	--	--	--	--
23[b]	Iron	380.0	1.46×10^{-17}	1.55×10^{-16}	1.70×10^{-16}	6.0×10^{-3}
24–64	TF Coil	418.40	1.05×10^{-17}	1.16×10^{-16}	1.27×10^{-16}	4.7×10^{-3}
65	Iron	433.40	3.83×10^{-20}	1.06×10^{-18}	1.10×10^{-18}	4.1×10^{-5}

[a] Zones 4 through 16 comprise the blanket assembly.

[b] Zones 23 through 65 comprise the TF-coil assembly.

[c] Non-breeding blanket modules will contain potassium instead of lithium. Neutronics calculations of the blanket with potassium are in progress; the composition of Zone 5 may be changed, if needed, to improve the nuclear performance.

Table 4.5. Estimates of Radiation Damage in First Iron Wall and in Toroidal Field Coil[a]

	Gas Production Rate	
	Hydrogen Atoms	Helium Atoms
dpa/year	atoms/year	atoms/year
	First Iron Wall	
1.89	4.73×10^{18}	1.47×10^{18}
	First Copper Winding in TF Coil	
4.20×10^{-5}	3.75×10^{12}	8.71×10^{11}

[a]For assumed wall loading of 0.168 MW/m^2 (see Table 4.2).

If the radiation damage data for 0.168 MW/m^2 wall loading are extrapolated to a wall loading of 1.0 MW/m^2, the atomic-displacement rate is 11.25 dpa/y, a value that is consistent with the rates predicted by Kulcinski, Doran, and Abdou[13] and by Williams, Santoro, and Gabriel.[14] It should be noted that in both Refs. 13 and 14 stainless-steel alloys rather than just iron were used in calculating the dpa rates. Correspondingly, if the gas-production data are extrapolated to 1 MW/m^2, the hydrogen- and helium-production rates in the first iron wall increase to 2.82×10^{19} hydrogen and 8.80×10^{18} helium atoms per year. These values correspond to 334 appm hydrogen and 104 appm helium per year, and are consistent with values obtained by Abdou and Conn[15] in their comparison of radiation damage in several first-wall materials. At the higher wall loading, the displacements-per-atom and gas-production rates are still low in the TF-coil windings.

REFERENCES

1. E. E. Bloom and F. W. Wiffen, The Effects of Large Concentrations of Helium on the Mechanical Properties of Neutron-Irradiated Stainless Steel, ORNL-TM-4861, Oak Ridge National Laboratory (May 1975).

2. G. K. Wehner, R. V. Stuart, and D. Rosenberg, *Annual Report on Sputtering Yields*, General Mills Report No. 2243 (November 1961).

3. Robert W. Conn, Gerald L. Kulcinski, Halil Avci, and Mohamed El-Maghrabi, "New Concepts for Controlled Fusion Reactor Blanket Design," *Nucl. Technol.* 16(2), pp. 125–45 (June 1975).

4. M. Van Den Berg, M. R. Everett, and A. Kingsbury, "The Relationship Between Irradiation Temperature and Dimensional Changes of Nuclear Graphites," *12th Biennial Conference on Carbon Extended Abstracts and Program*, American Carbon Society, pp. 307–10 (July 28 — August 1, 1975).

5. G. R. Hopkins, "Fusion Reactor Applications of Silicon Carbide and Carbon," CONF-740402-P (NTIS), *Proc. First Topical Meeting on the Technology of Controlled Nuclear Fusion*, San Diego, pp. 437–47 (April 16–18, 1974).

6. R. T. Santoro, E. S. Bettis, D. G. McAlees, H. L. Watts, and M. L. Williams, Neutronic Scoping Studies for a Tokamak Experimental Power Reactor, ORNL-TM-5035, Oak Ridge National Laboratory (in preparation).

7. W. W. Engle, Jr., A Users Manual for ANISN, a One-Dimensional Discrete Ordinates Transport Code with Anisotropic Scattering, Report K-1693, Computing Technology Center, Union Carbide Corporation (1967).

8. D. M. Plaster, R. T. Santoro, and W. E. Ford, III, Coupled 100-Group Neutron and 21-Group Gamma-Ray Cross Sections for EPR Calculations, ORNL-TM-4872, Oak Ridge National Laboratory (1975).

9. M. A. Abdou and R. W. Roussin, MACKLIB — 100-Group Neutron Fluence-to-Kerma Factors and Reactor Cross Sections Generated by the MACK Computer Program from Data in ENDF Format, ORNL-TM-3995, Oak Ridge National Laboratory (1974).

10. N. M. Green et al., AMPX: A Modular Code System for Generating Coupled Multigroup Neutron-Gamma Libraries from ENDF/B, ORNL-TM-3706, Oak Ridge National Laboratory (to be published).

11. T. A. Gabriel, J. E. Amburgey, and N. M. Green, *Trans. Am. Nucl. Soc.* 21, 67 (1975).

12. P. N. Haubenreich (Ed.), Tokamak Experimental Power Reactor: Basic Considerations and Initiation of Studies at Oak Ridge, ORNL-TM-4853, Oak Ridge National Laboratory (1975).

13. G. L. Kulcinski, D. G. Doran and M. A. Abdou, "Comparison of the Displacement and Gas Production Rates in Current Fission and Future Fusion Reactors," preprint (1974).

14. M. L. Williams, R. T. Santoro, and T. A. Gabriel, The Performance of Various Structural Materials in Fusion-Reactor Blankets, ORNL-TM-5036, Oak Ridge National Laboratory (in preparation).

15. M. A. Abdou and Robert W. Conn, "A Comparative Study of Several Fusion Reactor Blanket Designs," to be published in *Nucl. Sci. Eng.*

5. ELECTROMAGNETIC SYSTEMS

The electromagnetic systems include the toroidal field coils, the poloidal field coils, and the associated refrigeration and power supply systems.

5.1 Toroidal Field Coil Design

There are several constraints on the Toroidal Field coils which dictate rather specifically some of the design choices.

- For example, the field at the windings of the toroidal field coils will be 11T to provide the reference design field of 4.8T at the plasma centerline. Therefore, the design uses Nb_3Sn as superconductor in the higher field regions in addition to the more ductile NbTi for those parts of the coil at 7T or less.
- Even though the TF coils are in principle shielded from pulsed fields, it is likely that imperfections in the shielding current arrangement will result in variations of a few tenths of 1 T/sec; therefore, filamentary conductors capable of handling these variations are specified rather than tapes.
- Use of non-superconducting coils is precluded because of the very large power requirements.
- It is required that if a normal region is produced by some transient — conductor slippage, plasma instability, etc. — then the coil should recover, and in a predictable fashion. For the required current density, field strength, and coil dimensions, aluminum is a better choice than copper as the stabilizing material, and forced flow cooling through a well-defined passage is essential. We have therefore chosen to specify a cabled conductor inside a hollow steel tube. The tube walls are substantial and the electrical insulation is placed between the cable and the tube, allowing the tubes to be metallurgically joined to each other and to the case. An integral structure is thus formed in which each turn is separately and securely fixed. This arrangement also

spreads the conductors over a larger cross section of the coil, giving a higher on-axis field for a given maximum field at the conductor. The outer case enveloping the coil provides a secondary leak-tight enclosure and efficient restraint against bending.

- For such a large coil it is desirable to grade the conductor according to the field in which it will be used, and to minimize the number of conductor joints. This leads not to a pancake coil but to a layer winding, wherein the maximum field along a given conductor on any layer is nearly constant. In the layer winding, grading is thus accomplished without internal joints, i.e., all joints occur at the ends of each layer, at the end of the coil. Furthermore, in contrast with large monolithic conductors, the large cable conductors can be supplied in very long lengths, and joints between layers are unnecessary unless it is desired to change the conductor at that point. However, for sufficient cooling each layer must have a helium inlet and outlet.

The considerations listed above indicate a coil whose cross section is shown in Fig. 5.1 and whose parameters are listed in Table 5.1. An attempt has been made to achieve a workable design, although not an optimized one. For example, the current density has been assumed to be uniform from layer to layer; under this condition the design of the inner layer is the most difficult of all layers. The whole coil has been treated as if it were wound of this same conductor. In actual practice there is probably an economic advantage in changing to NbTi part-way through the coil, as well as an advantage to performance in having a higher current density in the outer lower field layers.

Although the coil described herein could not be constructed with today's technology, there appear to be no fundamental obstacles to the development of such technology within a five-year time span if the proper effort is expended. Calculations and experiments on the forced flow bundled-conductor are being done at Francis Bitter National Magnet Laboratory for ORNL, and the initial results are encouraging. However, it remains to be shown that the scheme is suitable for large, high-field coils.

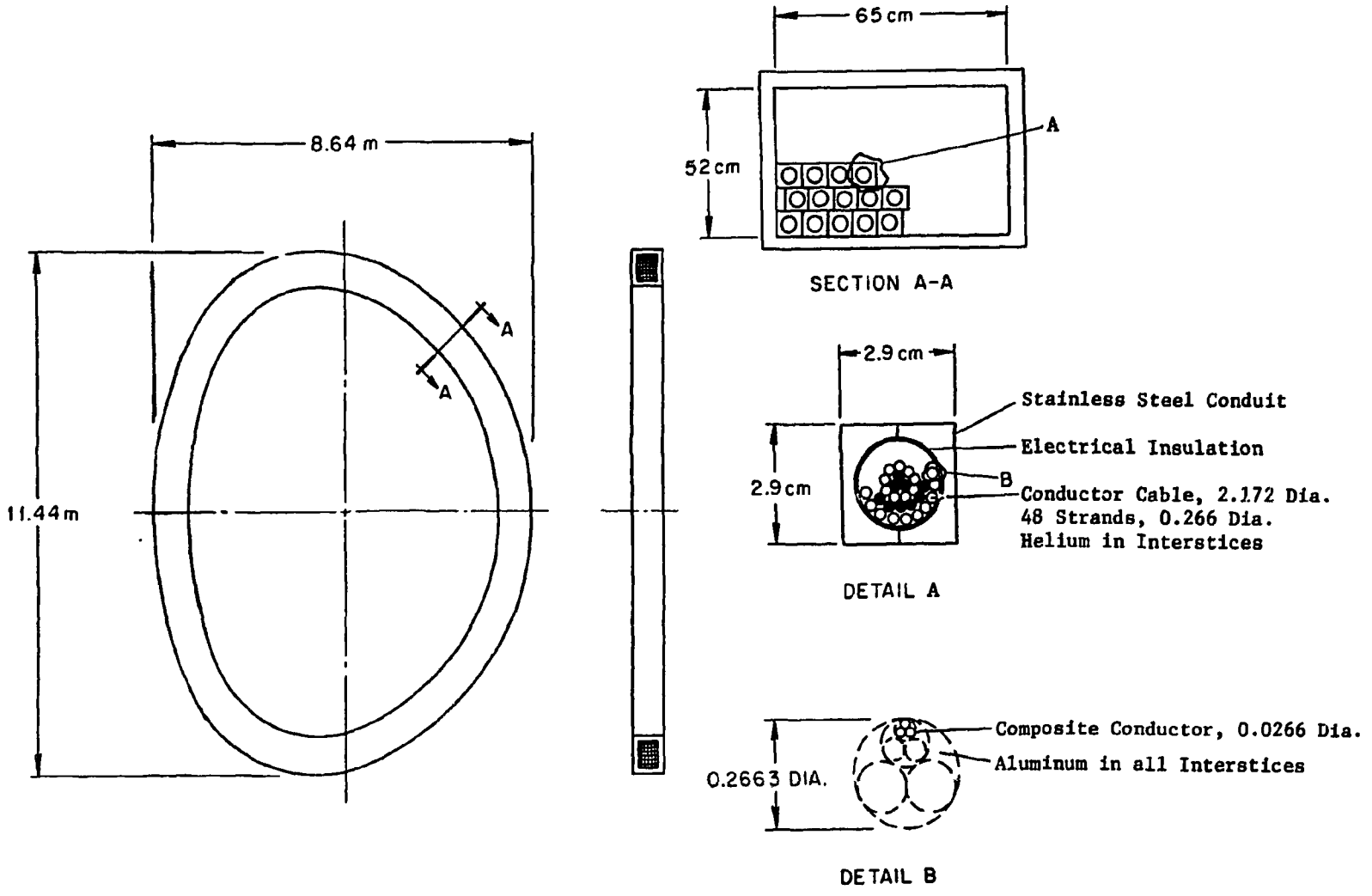

Fig. 5.1 EPR reference design toroidal field coil.

Table 5.1. TF Coil Design

Coil

The coil is oval and layer wound. The insulated conductor cable lies in stainless tubes and is cooled by the forced-flow of supercritical helium. The tubes are structurally welded to each other and to an enclosing coil case.

Symbol	Value	Units	Description
N_c	20	--	No. of coils
	10.85 x 8.0	m	Vertical and horizontal diameters
B_{max}	11.0	T	Maximum field at winding
R_o	6.75	m	Major radius
n_z	21.5	--	Number of turns per layer
n_r	18	--	Number of layers per coil
I	20.9	kA	Conductor current
--	5	cm	Thickness of steel case at coil ID and OD locations
--	4	cm	Thickness of steel case at coil ends
ℓ	635	m	Length of each of 18 coolant paths per coil
	11,500	m	Length of conductor in 1 coil (145 miles in 20 coils)
S/ℓ	40.0	cm^2/cm	Cooling surface per unit conductor length
p_2	2.5	atm.	Outlet helium pressure
p_1	5.7	atm.	Inlet pressure (83 psia)
$\dot{m}$	2,7	g/sec	Helium flow per path
v	30	cm/sec	Helium velocity
t_t	5.4	min	Helium transit time
$20\ P_p$	4.8	hp	Helium pumping power, total for 20 coils
P_n	150	W/coil	Average neutron heating
P_p/ℓ	7.8×10^{-5}	W/cm	Pumping losses per unit length of conductor (steady state)
P_n/ℓ	6.5×10^{-5}	W/cm	Neutron heating per unit length of conductor (steady state)
ΔT_b	0.8	K	Bulk heating of the helium in the steady state

Table 5.1 TF Coil Design
(continued)

Symbol	Value	Units	Description
Coil (continued)			
P_ρ/ℓ	1.04	W/cm	I^2R losses with all current in the aluminum
h_f	0.093	W/cm^2K	Film heat transfer coefficient
ΔT_f	0.28	K	Temperature drop across helium film with all current in the aluminum
T_i	4.5	K	Inlet helium temperature
Conductor (considering only the Nb_3Sn components at this time) Filamentary Nb_3Sn in three times as much CuSn, with Al added after reaction to give a strand which is 73 vol% Al.			
d_s	0.266	cm	Strand diameter
n_s	48	--	Number of strands (triad core plus 3 concentric layers)
A_{He}	1.03	cm^2	Helium flow area (interstitial area)
d_h	0.079	cm	Hydraulic diameter
I/I_c	0.84	--	Operating current divided by critical current at 11 tesla and 6.2K
	0.0266	cm	Diameter of composite wire
	25	lb/coil	Weight of a single composite wire
	27	--	Number of wires in a strand
ρ_{Al}	4.63×10^{-9}	Ω-cm	Resistivity of aluminum 'potting' between wires
	34.4	kA/cm^2	Critical current density in the composite at 11 tesla and 6.2K
	1.78	kA/cm^2	Current density averaged over windings plus coil case
	2.38	kA/cm^2	Current density averaged over windings
	5.65	kA/cm^2	Current density averaged over cable including helium
	29.0	kA/cm^2	Current density averaged over composite wire
	116	kA/cm^2	Current density averaged over Nb_3Sn

Table 5.1 TF Coil Design

(continued)

Symbol	Value	Units	Description
Protection			
			External dump resistors for coil protection will be used in addition to connecting the coils in the toroidal magnet in several parallel loops.
Losses (considering for these calculations an approximation that all conductor is Nb_3Sn in an Al matrix)			
			Losses in 20 coils, with a time history for the spatially averaged pulse field of 2 sec rise at 0.05 T/sec, 98 sec flat, 2 sec at -0.05 T/sec, 98 sec flat.
P_n	3000	*	Neutron heating
P_h	100	*	Hysteresis in 10 μm superconductor filaments
P_{eAl}	22	*	Aluminum matrix eddy current loss
P_{coup}	30	*	CuSn matrix — filament composite coupling loss ($\dot{B}_\perp$ and $\dot{B}_{\|\|}$)
P_{cAl}	50	*	Estimated coupling loss via aluminum
P_{ess}	670	*	Eddy current loss in stainless case and tubes
P_{leads}	840	*	Losses in current leads
$20\ P_p$	3900	*	Helium pumping power
P_{th}	1900	*	Thermal radiation from environment (dewar losses)
--	9550	*	Total excluding leads
--	4.8	†	Refrigeration input power at 500 W/W excluding leads
--	1180	‡	Losses from energized current leads
--	2.8	†	Refrigeration input power for current leads
--	7.6	†	Total refrigeration power

*Average power at 4.5 K, watts.

†Average power at 300 K, MW.

‡Equivalent liquid liters per hour that are required as vapor to cool the leads. The refrigeration requirement assumes that the other losses provide the 840 W required to evaporate the liquid, so that the only refrigeration charged to the leads is that required to reduce the helium gas temperature from 300 K to 4.5 K without liquefaction.

That is, given a conductor cable, one should indeed be able to construct the complete conductor and the coil; it should recover from small disturbances and be undamaged by large ones; bundles carrying large currents should not degrade, etc. The outlook for production of the required conductor cable seems equally promising, but further work is required.

The strand detail design in Fig. 5.1, detail B, assumes filamentary Nb_3Sn in a Cu-Sn matrix so that the developmental work now in progress is applicable. It also assumes the development of a method of providing an aluminum "potting" between the strands of a cable after the Nb-Cu-Sn reaction is complete. If this potting is not accomplished, another method is to use composite wires, indicated by solid circles in Fig. 5.1, detail A. Composite and aluminum wires are laid in alternate layers of the cables, which is assigned for current transfer by induction. Cables of both types must be constructed for testing. Research on NbTi in an aluminum matrix is possibly further advanced, but remains to be proven. In conclusion, there are smaller or peripheral items, some no doubt still to be uncovered, which should be investigated early enough to avoid subsequent delays.

5.2 Toroidal Field Coil Structure

A detailed structural analysis of the EPR reference design was performed as part of the structural work of the ORNL Superconducting Magnet Development Program.

The oval shape of the toroidal field coils for EPR is based on analyses performed at ORNL during the last two years in support of various tokamak systems. Studies have shown that for tokamaks with 20 toroidal field coils, with circular or ideal D shape, and similar distributed support, the stresses due to bending of the coil are as great as those due to tension, although the bending stresses are of opposite sign for the two shapes. This suggests that bending stresses may be minimized by choosing an intermediate or oval shape reducing the structure volume and/or stresses. In addition, for equal horizontal diameters, the oval shape will have less centering force than the ideal D shape and will similarly reduce the stresses or required volume for the hub structure. Preliminary studies

also indicate that fabrication difficulties with oval coils are midway between pure D coils and circular coils.

In order to confirm the choice of coil shape, a detailed finite element analysis has been made of the toroidal field coils and their structural support system. An earlier EPR concept was used in this analysis; the geometry and loads require only a minor extrapolation to the current reference design.

The type and scope of the desired analysis were guided by two basic criteria. First, the analysis would have to be sufficiently complete so as to allow investigation of all significant design loads, i.e., in-plane loads due to the toroidal field, out-of-plane loads caused by both the poloidal field and fault conditions, thermal stresses, and external excitations such as earthquake. This criterion prompted the use of a three-dimensional finite element structural analysis technique. Secondly, the model would have to be simple enough for use in evaluating the effect of numerous design parameters and load conditions without expending excessive amounts of computer time. This second criterion dictated the employment of elementary beam and plate elements for simulation of the structural system.

The finite element model which has been developed is shown in Fig. 5.2. This beam and plate model, which represents a symmetric quarter-section of the toroidal field coil system, has been designed to be used with the NASTRAN finite element computer program. It should be noted that this idealized model stands for the structure shown in Fig. 5.3. The resulting structural model represents a complete system for integrated analysis of toroidal field coils and associated support structure.

Next, the desired set of significant loading conditions were selected. Since the largest source of loads is developed by the field produced by the toroidal field coils, it was decided that the initial analysis effort would be restricted to a consideration of the effect of these loads, at first only under normal operating conditions. This decision was predicated in part by a desire to have some general stress data available during the early portions of the scoping study, in order to accomplish basic sizing of the toroidal field system structure. It should also be noted that,

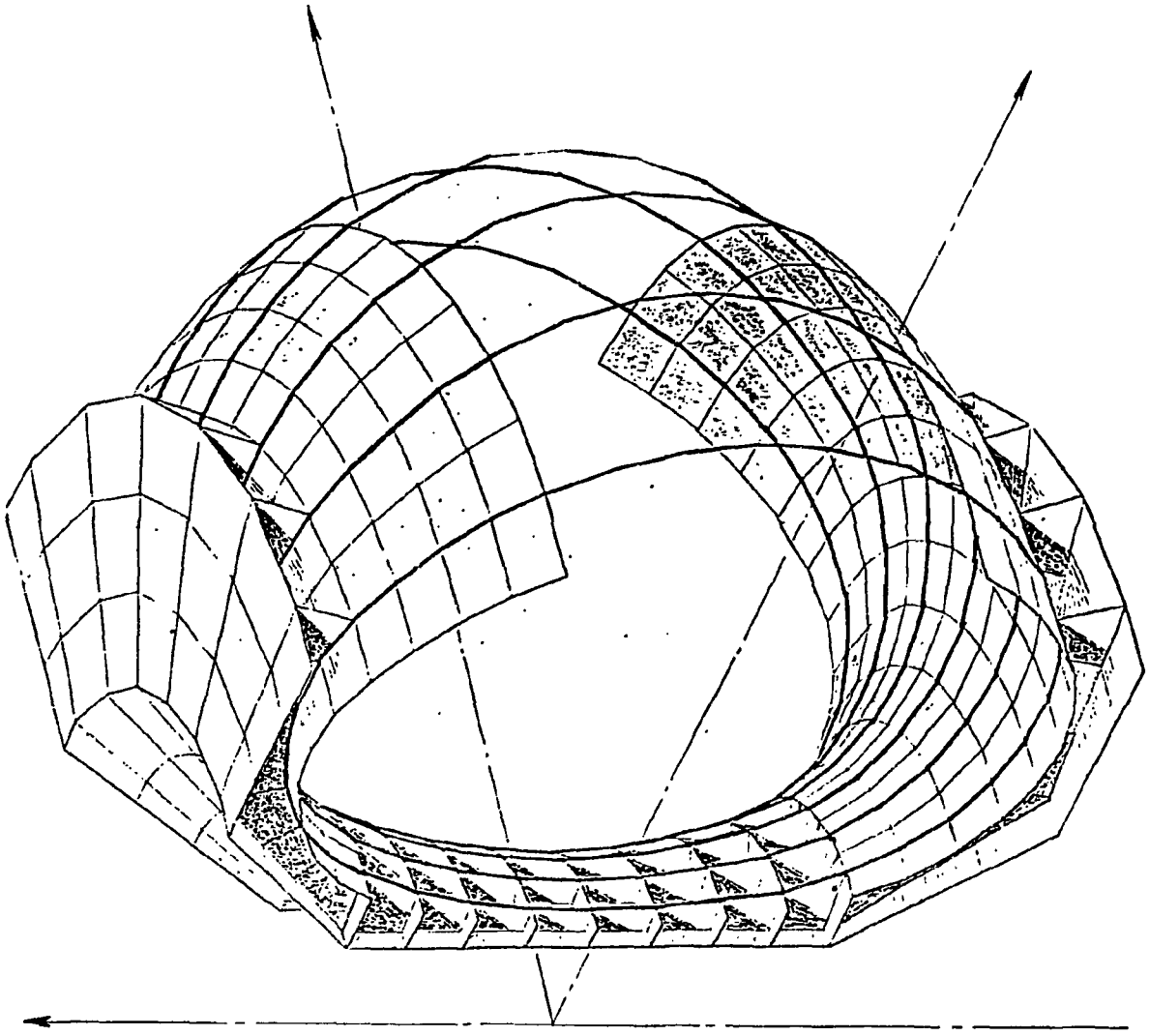

Fig. 5.2 Finite element model of EPR toroidal field coil structural system.

ORNL-DWG 75-17030

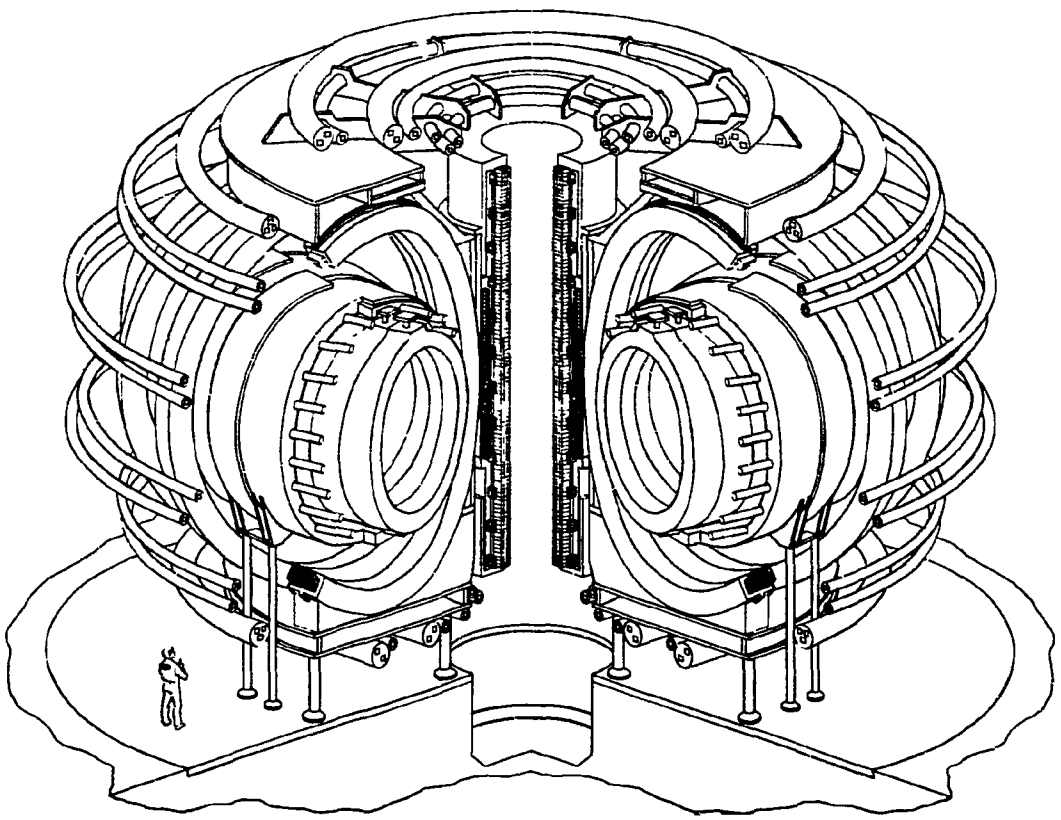

Fig. 5.3 Oak Ridge EPR reference design.

although the symmetric quarter model can be used to determine stresses in the entire structure with proper use of symmetric and anti-symmetric loads and boundary conditions, the loading condition initially considered was completely symmetric.

Several additional studies have been made with the above finite element model, including both in-plane and out-of-plane loading. Particular attention has been given to mean strain in the conductor, detailed stresses in the hub structure, and the interaction of the secondary hub structure with the coil-to-coil interface structure. During these studies, the criterion of less than 0.2% strain in the conductor matrix has been a standard for acceptability. Generally, stresses in all support structures have been limited to less than 60,000 psi. This work is still in progress and final results are not yet available. However, extrapolations indicate that the toroidal field coils and their support structure as described in the reference design represent a reasonable concept.

5.3 TF Magnet Fabrication

The manufacturing processes needed for the coil shown in Fig. 5.1 are composite wire manufacture, cable winding, stainless steel conduit forming, and plate rolling. The fabrication processes are:

1) prewinding, that is, assembly of the cable into the stainless conduit,
2) layer-winding the conduit onto a coil form, and,
3) fixing the position of the conduit by welding the conduit to the coil form and neighboring conduits. The welding will be inspected continuously during winding so that all flaws are detected and corrected before winding continues.

Two dissimilar-wire splice joints are required: one from Nb_3Sn to the high field NbTi and one high field NbTi to the low field NbTi. Each of the 18 layers could begin with a wire splice. Thus, of the maximum of 18 splices, two will be dissimilar wire but the number of strands of wire will always be the same.

Each layer will also begin with either an entrance or an exit coolant port. The splice and coolant port will be built in the same operation in the winding line downstream of the cable tensioning device. The splice must retain permeability to helium flow. The coolant ports must retain high integrity of insulation from ground.

There are two possible orientations for the winding operation: 1) with the coil bore axis vertical, and 2) with the coil bore axis horizontal. Figure 5.4 shows a conceptual arrangement of the equipment which could be used for winding in the horizontal orientation. Note the laser welder which is being advertised by welding equipment manufacturers. Such a machine could be used to make full penetration welds (i.e., 2.9 cm) with depth to width ratios of 5 to 8 in two orthogonal planes simultaneously.

For the vertical orientation a concept was considered in which the coil form would not rotate but would rise and fall vertically to generate the helical pitch angle ($\approx$ 1.1°). The moving platform would be required to carry all the pre-winding preparation equipment. Another trailing platform would follow with a welding head. Weld dressing and inspection would follow on separate platforms.

All the fabrication equipment should be installed at the reactor site to conserve on: 1) transportation of 250,000 lb pieces, 2) multi-industrial capitalization, and 3) maintenance equipment capitalization.

5.4 Refrigeration System Requirements

The liquid helium refrigeration and reliquefier are required to establish and maintain the superconducting state of the coils. Heat leaks into the magnet system come from structural supports and thermal radiation. Additional refrigeration requirements are generated by the absorption of nuclear particles, by resistive power losses in the windings, by the cryosorption equipment of the beam injection devices, and the electrical leads across the cryochamber boundaries.

The hollow conductor magnets will be cooled by circulating liquid helium at 4.2K and supercritical pressure through the windings. Accordingly, heat generated by the hydraulic power for the pumps must also be removed by the refrigerator.

ORNL-DWG 75-10665

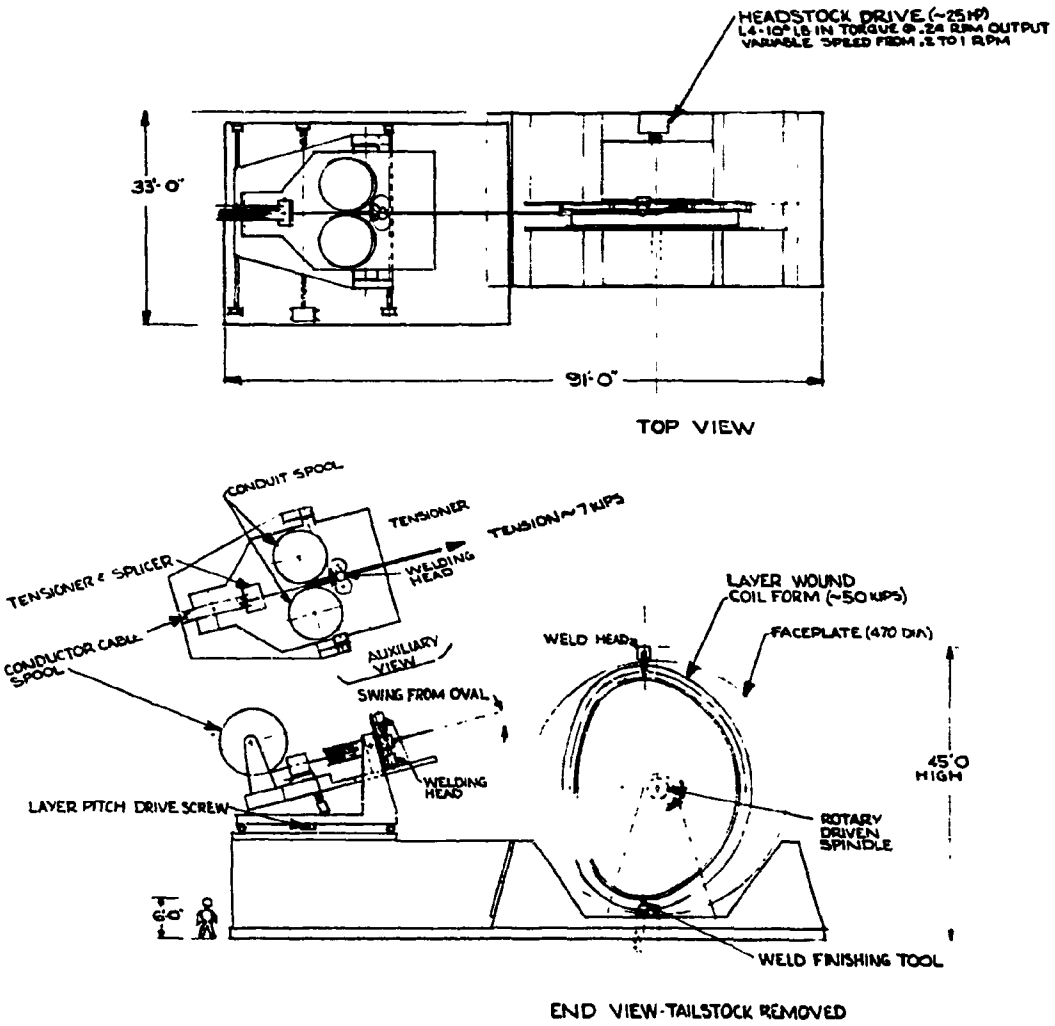

Fig. 5.4 Toroidal field coil winding machine.

The toroidal field magnets have a heat conduction loss through the magnet supports, instrumentation ports etc. of 1.4 kW, and surface radiation losses of 0.5 kW with the use of aluminized super-insulation. Also, the gamma ray and neutron absorption adds 3 kW of total heat to the 20 magnets. A total of 0.8 kW of heat is dissipated in the magnets from hysteresis and eddy current losses associated with the transients fields developed by the poloidal coils. The total heat generation in the magnets, which amounts to 5.7 kW, is removed by a super-critical pressure stream of subcooled helium at 4.5° Kelvin under the conditions listed in Table 5.1. The pressure drop required to circulate this helium through the 18 layers of magnet coils (each 635 m in length) is 2.6 atmospheres.

With a 70% hydraulic efficiency, the pumping power will be 3.9 kW for the 20 magnets, for a total loss of 9.6 kW at 4.5°K. The room temperature compressor power to supply this refrigeration (assuming all of it is supplied at 4.5°K in a 13% efficient machine) is 500 x 9.6 = 4.8 MW.

The magnets are assumed to each have a set of 21 kA electric leads entering at 300°K and delivering at 4.5°K. These loads require 58.8 liter/hr of helium vapor at 4.5°K for each pair. The helium vapor will be supplied by boiloff from the refrigeration cooling and will be heated to 300°K while cooling the loads. This energy loss must be made up by the liquefaction of helium. The power for the lead cooling, therefore, amounts to about 2.8 MW for the 20 toroidal coils. If any of the toroidal field coils are arranged in series electrically, then the power associated with the lead cooling may be reduced proportionately.

The poloidal coils are subject to eddy current heating because of the large transient fields required to drive the plasma. The combined values of the eddy current heating and the nuclear heating are estimated at about 5 kW based on extrapolating the nuclear heating curve (see the discussion on the blanket heat removal system) and the eddy losses (∿2 kW at 4.5°K) presented in the poloidal coil design discussion. The heat conduction losses are estimated at 1.5 kW at 4.5°K and the thermal radiation heat leaks at 0.5 kW. The total refrigeration requirements at 4.5°K are estimated at 15 kW. (These estimates are based on preliminary designs and are subject to change.)

The leads for these coils are 25 kA; seven pairs are needed. The refrigeration required to re-cool the helium flow to 4.5°K is 1.2 MW (based on 13% mechanical efficiency for refrigeration system).

The power requirements have ignored the losses associated with the magnet conductor joints because of the recent success in developing low resistance joints of superconducting windings.

It is anticipated that future optimizations of plasma radiation heating of the coils will reduce the magnet heat loads and that their improvements might be offset by refrigeration losses external to the magnets that are not included in the above estimates. The pump power losses will probably also be reduced as further work is done to decrease the magnet internal heat loads.

The neutral beam injection system (included here for completeness of the refrigeration requirements) requires cryosorption panels to maintain the vacuum in the injector chambers by removing the non-injected deuterium gas from the injection tubes. These cryosorption panels operate at 20°K and the amount of power utilized by these panels is 15 kW at 20°K. At 13% mechanical efficiency and a temperature range to 300°K, the room temperature compressor power requirement is 1.6 MW. The radiation absorption to the walls of the injection device is assumed to be removed by some other means than cryogenic refrigeration.

The summation of the refrigeration requirements is given in Table 5.2.

5.5 Poloidal Magnetic Field Concept

Introduction

The function of the poloidal system is to create the plasma current, and to maintain the plasma column in equilibrium by suitably shaped vertical fields. The design gives special emphasis to reducing stored magnetic energy, and to shielding the superconducting toroidal field coils from pulsed magnetic fields. The electromagnetic shielding is a vital function, since pulsed fields can quench the superconducting windings. Pulsed fields come from both the OH winding and from the plasma current and may be especially important if the plasma exhibits disruptive instabilities, a

Table 5.2 Summary of Refrigeration Requirements

I.	Toroidal Field Coils	
	1. Conduction through supports and instrument leads $\frac{70 \text{ watts}}{\text{coil}} \times \frac{20 \text{ coils}}{1000 \text{ W/kW}}$	= 1.4 kW
	2. Surface heat radiation losses $\frac{25 \text{ watts}}{\text{coil}} \times \frac{20 \text{ coils}}{1000 \text{ W/kW}}$	= 0.5 kW
	3. Hysteresis and eddy losses	= 0.8 kW
	4. Neutron heating of the coil $\frac{150 \text{ watts}}{\text{coil}} \times \frac{20 \text{ coils}}{1000 \text{ W/kW}}$	= 3.0 kW
	5. Pumping power (70% hydraulic efficiency)	= 3.9 kW
	Total refrigeration at 4.5°K	9.6 kW
II.	Poloidal Field Magnets	
	1. Eddy heating and other pulse-related losses	= 2 kW
	2. Neutron heating	= 3 kW
	3. Conduction through support and frame	= 1.5 kW
	4. Thermal radiation losses	= 0.5 kW
	5. Pumping power	= 8.0 kW
	Total refrigeration at 4.5°K	15.0 kW
III.	Vapor Cooling of Leads (liter of LHe/hr/lead)	
	1. Toroidal and poloidal field coils	= 58.8 ℓ/hr
	Total vapor supplied at 4.5°K and warmed to 300°K	58.8 ℓ/hr
IV.	Neutral Beam Injectors	
	1. Cryosorption panels for vacuum chamber	= 15 kW at 20°K
	2. Cooling of vacuum chamber walls*	
	Total	15 kW at 20°K

*Load is sufficiently large to require other than cryogenic heat removal system.

Table 5.2 Summary of Refrigeration Requirements (continued)

V. Room Temperature Power Requirements to Compressor	
1. Refrigeration at 4.5°K, 24.6 kW	12.3 MW
2. Cooldown of helium vapor to 4.5°K (30 lead pairs)	4.0 MW
3. Refrigeration at 20°K, 15 kW	1.6 MW
Total electric power	17.9 MW

universal feature of present tokamaks, which cause rapid current changes and large induced voltages.

The design used here is a version of the "STATIC"* system recently proposed by F. B. Marcus.[1] In the STATIC system, the poloidal magnetics include an air core transformer in a special arrangement. This arrangement requires much less energy than the usual air core transformer, in which a poorly coupled winding is outside the toroidal field coils, and does so in such a way that it shields the toroidal windings from being immersed in poloidal flux. A closely coupled winding provides the shielding function and in addition serves to produce the vertical field. The closeness of this winding to the plasma allows the use of a decay index† of 0.5, which gives good stability against vertical plasma displacements. A further set of external vertical trim coils is provided for extra flexibility. In principle, this system is capable of shielding the toroidal field coils completely, and in practice it can come close to achieving this. First estimates using the reference design geometry indicate a factor of at least 3.3 reduction in the poloidal field level at the toroidal field coils, relative to the plasma field alone. Optimization is under way and further improvement of the shielding effectiveness is expected. Since the rate of field change imposed upon the TF coil might determine the feasibility of the TF coil design, the factor of 3 reduction is already significant.

Primary-OH

A schematic of the coil placement is shown in Fig. 5.5 for the upper half plane of the torus. The principal volt-second capability comes from the set of windings outermost from the plasma, which is an air core transformer with a high central field. A small number of these windings is arranged to prevent the poloidal flux from intersecting the toroidal field

---

*Shielded Tokamak Air Transformer, Iron Core.

†The decay index $n = (R/B_v)\,\partial B_v/\partial R$ characterizes the radial decrease of the vertical field.

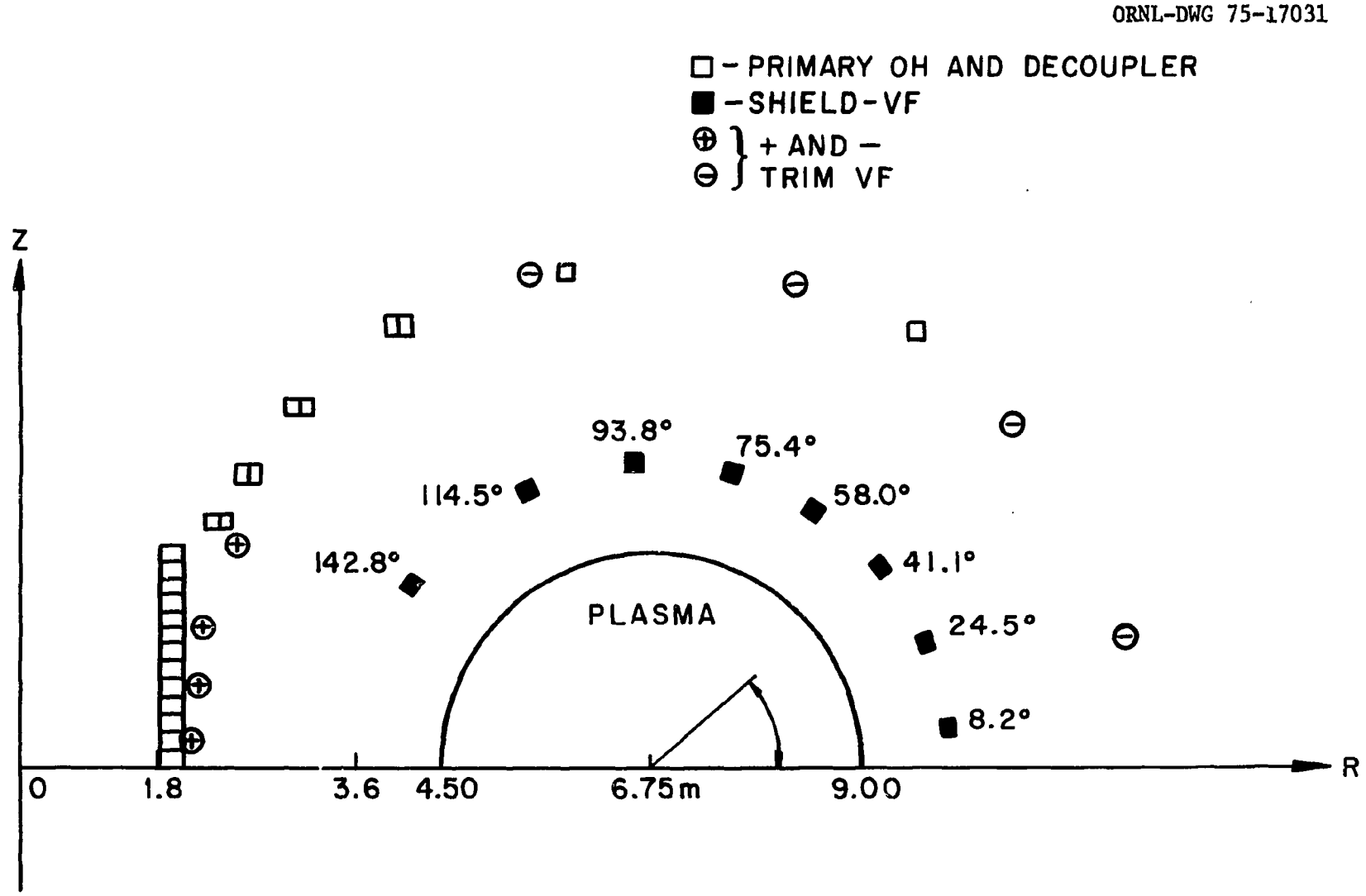

Fig. 5.5 Optimized poloidal coil positions for circular plasma.

coils. This is similar to the present TCT-TFTR design.[2] An optimization program, developed by Y.-K. M. Peng, varies the coil current and placement until the field strength inside the enclosed region is minimized. The optimum coil placement, with equal currents in each conductor, is shown in the figure. The conductor set requires approximately 43×10^6 amp-turns to produce a central field of 6.5 T on axis. In the case of non-circular TF coils, the solenoid on axis becomes extended, and the return flux coils become similar to those of MATT-1050 (Ref. 3). A further improvement is possible by using a two-region saturated-unsaturated iron core, as in the Joint European Tokamak design, to increase the flux swing and to provide an iron core return. Iron was not included in the EPR reference design due to the increased difficulty in control resulting from the changing effect of the iron as it becomes saturated.

Shield-VF Winding

The unique feature of this design is a closely-coupled Shield-VF winding which simultaneously cancels the plasma field at the toroidal field coils and provides the equilibrium vertical field for the plasma. The total current in these windings is arranged to be equal and opposite to the plasma current, and the distribution of the windings creates a vertical field of the correct magnitude and decay index.

The analogy of a closed perfectly-conducting shell gives a good demonstration of the coil's dual function. If a current is generated inside the shell, eddy currents in the shell wall will prevent any field from appearing outside the shell, and if the plasma shifts, eddy currents will generate a compensating vertical field. In practice the winding design is obtained by the superposition of two current distributions, which require: 1) a winding with full plasma current that creates zero field in the plasma region, and 2) a vertical field winding with a total of zero amp turns, with a decay index of 0.5 for vertical and horizontal stability. These windings were combined because the limited room inside the TF coils allowed only one set of windings with series connections to be imbedded in the neutron shield. In order to decouple the closely coupled winding from the Primary-OH driving voltage, a counterwrap winding of equal and opposite turns in series is made at the same location as the Primary-OH winding.

This combination of shield and decoupling coil can be viewed as an open, resistive, conducting shell of large thickness providing a field-free region between its surfaces. A controlled power supply that senses the plasma current is placed in series with the shield and decoupling coils, and is used to maintain equality of the total plasma and Shield-VF coil currents. Simultaneously it supplies inductive power needed for plasma current distribution and position changes, also supplying sufficient power to overcome resistive losses in the two coils. The basic magnetic energy associated with the establishment of the plasma current is supplied by the air core winding system.

Development of the Requirements

In order to determine the proper current distribution in the Shield-VF windings, values for β_p and ℓ_i (both defined below) need to be determined.

The reference parameters are: $R_o = 6.75$ m, $a = 2.25$ m, $b_{shield} = 3.15$ m, $B_o = 4.8$ T, $q = 2.5$, and $I_p = 7.2 \times 10^6$ amp. The required equilibrium vertical field at the plasma is given by Shafranov[4] (units in MKS) as

$$B_v = \frac{I_p}{10^7 R} \left(\ell n\ 8R/a - 3/2 + B_p + \ell_i/2\right) ,$$

where $\beta_p = \Sigma nkT/(B_p^2/8\pi)$ is the ratio of plasma pressure to poloidal field pressure and ℓ_i is the internal inductance per unit length in EMU. $\ell_i = 0.5$ corresponds to a uniform current density and is higher for a more peaked current density. One definition of ℓ_i is

$$\ell_i = \frac{1}{4\pi\ I^2} \int_o^a dr \int_o^{2\pi} B^2\ r\ d\theta, \quad B = 2\ I_p/r ,$$

where I_p is the plasma current.

The ℓ_i and β_p will depend on the plasma parameters and equilibrium. In order to obtain near-ignition conditions, a plasma β_p of order 2 is

required for ion, electron and alpha pressure. This choice is consistent with a stability limit on β of $\sqrt{R/a}$, or an equilibrium limit of A. It is possible to exceed $\beta_p = A$ and maintain equilibrium if reversed currents can be tolerated in the plasma.[5] To study the effect of high β_p, the ORNL MHD 2-D Free Boundary Equilibrium Code was used. This code solves for the poloidal flux function ψ.

$$\Delta^*\psi \equiv \frac{\partial^2\psi}{\partial R^2} - R^{-1}\frac{\partial\psi}{\partial R} + \frac{\partial^2\psi}{\partial Z} = -4\pi R^2 p - FF' ,$$

where p is the pressure and F is RB_T. R is the major radius and B_T is the toroidal field. The prime denotes the derivative with respect to the flux ψ. A case was run for β_p of ≈ 1.8, with a zero slope of pressure on axis. The result is shown in Fig. 5.6. The externally applied vertical field has centered the flux surfaces and pressure profiles, but the current has shifted outwards and is peaked. The internal inductance for this case is found to be 1.8 by subtracting the external flux function and integrating the remaining flux linkages. Current profiles at lower β tend to be flatter and have lower ℓ_i. Also, it is important to keep the safety factor $q \geq 1$ everywhere in the plasma. For an analytic example of the variation of q with a nonuniform current profile, the sample current density $J = J_o(1 - \frac{r^2}{a^2})^{3/2}$ is used. This distribution has internal inductance $\ell_i = 1.1$. A q of 2.5 at the edge results in q of 1 at r = 0.1a.

Given the uncertainties of the model, a reasonable compromise of design choice is $\beta_p = 1$, $\ell_i = 1$. This is also a maximum for a successful superposition of VF and OH windings. Higher β_p and ℓ_i lead to reversed currents in the superposed windings. For a current of 7.2 MA, this requires a vertical field B_v of 0.34 Tesla. This is the design value for the Shield-VF windings in Fig. 5.5 with a decay index of 0.5. This value was chosen to give good stability against vertical plasma drift. Horizontal drift, or variation in β_p or ℓ_i, causes a variation in the required B_v.

ORNL-DWG 75-17032

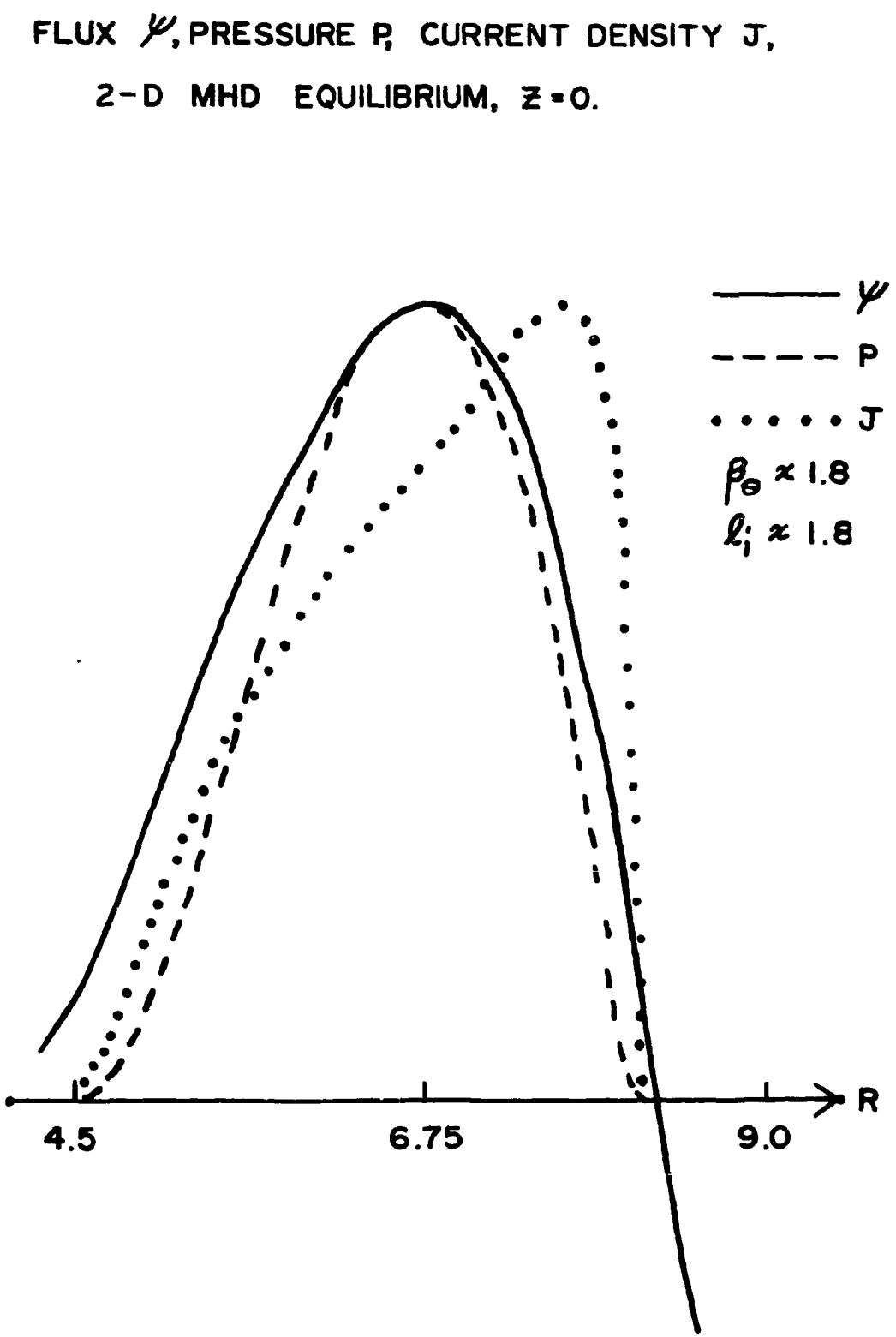

Fig. 5.6 High poloidal beta MHD equilibrium.

For example, the equations $\beta_p = 0.5$ and $\ell_i = 0.5$ imply that $B_v = 0.26T$, whereas the equations $\beta_p = 2$, $\ell_i = 1.8$ imply that $B_v = 0.49$ T. This requirement for a changing B_v may be met either by allowing the Shield-VF current to deviate from the plasma current, thereby reducing the shielding, or by adding an external set of VF coils with the appropriate decay index of 0.5. These coils are shown in Fig. 5.5 at the same radius as the Primary-OH windings. A current of $\pm .28 \times 10^6$ amps in each conductor can provide an extra 0.1 T of vertical field. It seems prudent to include these coils in the design so as to have adequate flexibility for plasma control.

Plasma Driving Requirements

As a basis for the development of the volt-second requirement, the definition of self-inductance L_{pp} is used in the relevant calculations here. The mutual inductance terms, M_{xy}, take account of the flux external to the shield winding.

For plasma radius = a and Shield-VF radius = b, the plasma self-inductance in henries is

$$L_{pp} = \mu_o R(\ell n\ 8R/a - 2 + \ell_i/2) = \mu_o R(\ell n\ 8R/b - 2 + \ell n\ b/a + \ell_i/2) ,$$

where the second expression explicitly shows the component of L_{pp} arising from flux which can link the shield winding. The estimated mutual inductance (single turn) of the Shield-VF coil with the plasma is

$$M_{SP} = \mu_o R(\ell n\ 8R/b - 2) .$$

The self-inductance of the shield can be approximated from the stored VF energy inside the plasma volume, $2\pi R\ \pi b^2\ B_V^2/2\mu_o$, giving

$$L_{SS} = 2\pi^2 R\ b^2\ B_v^2/\mu_o I^2 + M_{SP} .$$

The volt-second requirement for the stored magnetic flux of the plasma is $L_{pp}I_p$ which, for R/a = 3, $\ell_i = 1$, and $I_p = 7.2 \times 10^6$A, is 102.5 VS. Of this, the mutual inductance of the closely coupled winding provides 51.4 VS. The remaining 51 VS must be provided by the central Primary-OH. The total volt-second requirement includes, in addition, setting up losses associated with plasma turbulence and the establishment of the current profile, estimated[6] to be roughly equal to an additional (1–3) LI. Arbitrarily, we allow 51 volt-secs for this loss equal to the plasma inductance requirements for flux inside the closely coupled windings. Furthermore, we wish to maintain a steady-state burn of at least 100 sec to achieve a high duty cycle. The classical single-turn plasma resistance is

$$R_p = \frac{2\pi R}{\pi a^2} \frac{2.8 \times 10^{-8} Z_{eff}}{[T_e ((keV)]^{3/2}} .$$

When $Z_{eff} = 2$ and T = 9 keV, then R_p equals 5.5×10^{-9} Ω and V = IR = .04 volts. Therefore, 100 seconds requires 4 volt-seconds. However, because of the uncertainties in this estimate, an extra 30 volt-seconds will be provided. The total volt-second requirement (ϕ) is 183 VS, of which 51 are provided by the Shield-VF coil and 132 by the Primary-OH winding, for a plasma current of 7.2×10^6 amps.

The field on axis was calculated for a Primary-OH system arranged on a circle. However, structural requirements of the EPR dictate that a long central solenoid be provided with outer coils to return the flux outside the TF coils. The Primary-OH solenoid characteristics may be estimated from an infinite solenoid with $B_{max}/\mu_o = I/h$, where I/h is current per coil length h, the flux is $\pi r_c^2 B_{max}$ and the inductance is, for one turn, $L_{oo} = \mu_o \pi r_c^2/h$. To achieve a given flux swing ϕ from full forward to full reverse current, the average coil radius r_c is obtained from $\pi r_c^2 (2B_{max}) = \phi$.

If ϕ = 132 VS, we obtain $r_c^2 B_{max} = 21$. A maximum reasonable field, especially for a superconducting air core, is of order $B_{max} = 7$ T giving $r_c \approx 1.73$ m.

It should also be noted that the vertical field component of the Shield-VF windings can induce a plasma-loop voltage. However, some of this flux returns inside the plasma radius resulting in cancellation. Detailed mutual inductance calculations are required.

Inductance Calculations

The above inductance formulae are for idealized systems. Exact inductances depend on the existence of finite conductors, leakage flux, etc. A computer program has been developed by P. L. Walstrom which integrates over finite conductors, assuming uniform current density in each conductor. This program was used for the coil configuration shown in Fig. 5.5 with subscripts o = Primary-OH, s = Shield-VF, t = vertical field trim coils, p = Plasma. The plasma was modeled in 3 cases: 1) centered at R = 6.75 m, uniform current to $\underline{a}$ = 2.25 m corresponding to $\ell_i = 0.5$; 2) centered at R = 6.75 m, but current concentrated in $\underline{a}_o$ = 1.125 m, corresponding to $\ell_i = 1.9$; and 3) off center at R = 7.25 m, $\underline{a}$ = 1.125 m. The inductances are for a single turn and are given in microhenries in Table 5.3.

Table 5.3 System Inductances (μH)

	Case 1	2	3
L_{oo}	1.668	1.668	1.668
M_{os}	1.595	1.595	1.595
M_{op}	1.592	1.592	1.593
L_{ss}	12.25	12.23	12.25
M_{sp}	9.096	8.932	10.01
L_{pp}	12.04	17.61	19.55
L_{tt}	16.45	16.45	16.45
M_{ot}	0.015	0.015	0.015
M_{st}	7.63	7.63	7.63
M_{pt}	5.58	5.43	6.38

The L_{pp}, L_{ss}, and M_{sp} terms are in reasonable agreement with the ideal theoretical expressions. The difference between L_{pp} and M_{sp} represents the plasma inductance inside the shielding coils. The nearly identical values of M_{os} and M_{op} indicate that the Shield-VF coils can do a good job of shielding. The large difference between M_{sp} and M_{op} indicates that the plasma coupling to the shield windings is much better than to the decoupling windings, so that the plasma current will couple closely to the current in the Shield-VF coil. It should be noted that minimal energy can be associated with the mutual external flux between the Shield-VF coil and the plasma, since the net ampere-turns is zero. Also, if the Shield-VF current is different from the plasma current, the leakage energy is small, since the energy varies as the square of the ratio of the leakage field to the full, unshielded field. If trim vertical field coils are used, the mutual inductance with the Primary-OH is very small, giving good decoupling.

The inductances and fields of the air core and trimming vertical field windings have been calculated (for the case of these windings) outside an oval TF coil, as in the reference design. The air core winding has a one-turn inductance of 1.05 μH, and a current of 70 MAt creates a field of 6.3 T on axis, with a stored energy of 2.6 GJ. The VF-trim coil requires 310 kA/wire to generate a vertical field of 0.1 T at the plasma. A shielding comparison has been made with a VF coil inside the TF coil, for a decay index n = 0.5. The maximum field at the TF coil with shield winding is .21 T, and with the VF coil is 1.32 T, for a shielding ratio of 6.3.

Operating Cycle

The design parameters associated with the establishment of the plasma current are the breakdown voltage and the plasma current risetime. An important parameter determining breakdown requirements in simple gas discharges is the value of E/p (electric field divided by pressure).[7] Present tokamaks have an initial field of approximately 10 volts/meter. The same electric field in the EPR at a similar filling pressure implies a breakdown voltage of 420 volts. Using the stored reverse current bias of 65 VS, this

voltage could be maintained for 0.15 sec. However, as soon as breakdown is achieved, the voltage may be reduced. Further experimental evidence in large tokamaks is required to determine the time dependence of the loop voltage while the plasma is being established. For the purpose of defining a rate of field change for the superconducting coil design, a one-second interval is taken for the 65 Wb flux change yielding $\dot{B} \sim 7$ T/sec. For the purpose of determining the voltage capability of the coil, the 420 volt number must be multiplied by the number of turns, presently 400. This maximum voltage is exceedingly high and further iteration with both coil number and possible breakdown requirements is necessary.

With superconducting Primary-OH windings, the operating cycle is:

1. Starting from zero current, charge the Primary-OH windings to full reverse current in $\approx$ 50 seconds.
2. Transfer this current to a control circuit consisting of switched resistors and capacitive-like elements. This circuit provides a large loop voltage and a corresponding rapid fall of coil current during breakdown. The plasma current is driven to some fraction of its full value by the time the primary current has fallen to zero. The Shield-VF winding is driven in such a way that its ampere turns are always equal and opposite to the plasma current. With a low-impedance driving circuit, most of the current in this winding is produced by induction. The additional requirement arising from resistive losses and stray inductance is met by a controlled power supply.
3. The Primary-OH winding voltage is maintained at a suitable value by a power supply to bring the plasma current to full value within the next second. During this time, the Primary-OH coil current rises to a fraction of its original value with the opposite sign.
4. The Primary-OH current increases slowly while supplying the plasma resistive losses. The current in the Shield-VF coil is varied by a feedback circuit to keep the plasma centered. Alternatively, the VF-trim coils may be used for this purpose. If the shield and plasma currents differ, stray flux will appear.

5. The Primary-OH voltage is set to zero to allow the plasma to decay with the L/R time constant until plasma performance deteriorates. A negative voltage is applied to the Primary-OH to drive the plasma current to zero.

Other operating methods could include the use of the Shield-VF or trim-VF coils as fast compression coils for adiabatic heating. Further investigation is required.

5.6 Poloidal Field Coil Design

In order to achieve reasonable currents and voltages, reference coil parameters are:

- superconducting Primary-OH system of 400 turns, producing 132 volt-seconds
- resistive Shield-VF winding of 16 turns at cryoresistive temperatures,
- superconducting decoupling coils of 16 turns, and
- superconducting trim-VF coils.

That part of the ohmic heating coil not in the central core is used to guide the flux around the toroidal field coils, and subsequently will not experience the same rate of field change since it is in a lower field; mechanical support, however, will be difficult. The central part of the ohmic heating coils, the solenoid, will have a large field at the conductors and will have a correspondingly large rate of field change. From the point of view of superconducting coil design, the central solenoid is the most difficult coil in the poloidal magnetics system and will consequently be the subject of this report.

Use of a cryoresistive magnet was considered first for this application, but this kind of coil requires considerable power for refrigeration in addition to the power used to overcome resistive losses. For example, one cryoresistive system at 40°K required 5.1 MW to remain in the near steady-state period after the pulse, but required an additional 133 MW (minimum) to refrigerate it; a similar magnet at room temperature required about 170 MW to maintain the magnet under near steady-state conditions.

These power losses clearly indicate that superconducting magnets are needed in the ohmic heating system. The present report discusses a superconducting mmagnet system that will meet the design criteria without incurring substantial losses.

Coil Design Choice

In a design tradeoff with the size of the TF coils and structure, the superconductive central solenoid is constrained to have an outside radius of 1.9 m, and a half-length of 6 meters. The requirements are that it must produce 65 webers in the core, develop up to a 120 Wb flux charge in approximately 2 seconds, and then continue to increase the flux slowly for about 100 seconds more, remaining superconductive throughout this cycle. In addition, the magnet should be cryostable. In order to provide mechanical, electrical, and thermal isolation from the toroidal field coils, while also furnishing ease of maintenance and room for the decoupling voltage coils, the central solenoid should not depend for support on the bucking cylinder for the toroidal field coils. Structure fatigue may also be important, so that the average stress level should be kept low.

A summary of the choices of magnet shape is presented in Fig. 5.7. The curves are for the following fixed parameters: outside radius, 1.9 m; coil length, 12 m; maximum flux, 65 webers. Figure 5.7 clearly indicates that as the coil is made thinner, the maximum field in the winding B_{max} decreases. This makes the steady-state environment of the superconductor more favorable; however, the average hoop stress and overall current density also increase with increasing inside radius. At this time the best compromise appears to be a_i = 1.5 m. The average hoop stress is then 12,500 psi, the overall current density is 1460 A/cm^2 and the maximum field at the windings is 7.0 T. Finally, the coil must make a $\dot{B}$ of 7 T/sec with a 1% duty cycle; this requirement is equal to a drive of 7.0×10^7 amp turns. The number of turns and the connections used (e.g., series sets, series-parallel sets) must satisfy conflicting requirements for voltage breakdown insulation, current switching, construction and cooling. A fully satisfactory arrangement is still being developed.

ORNL-DWG 75-17033

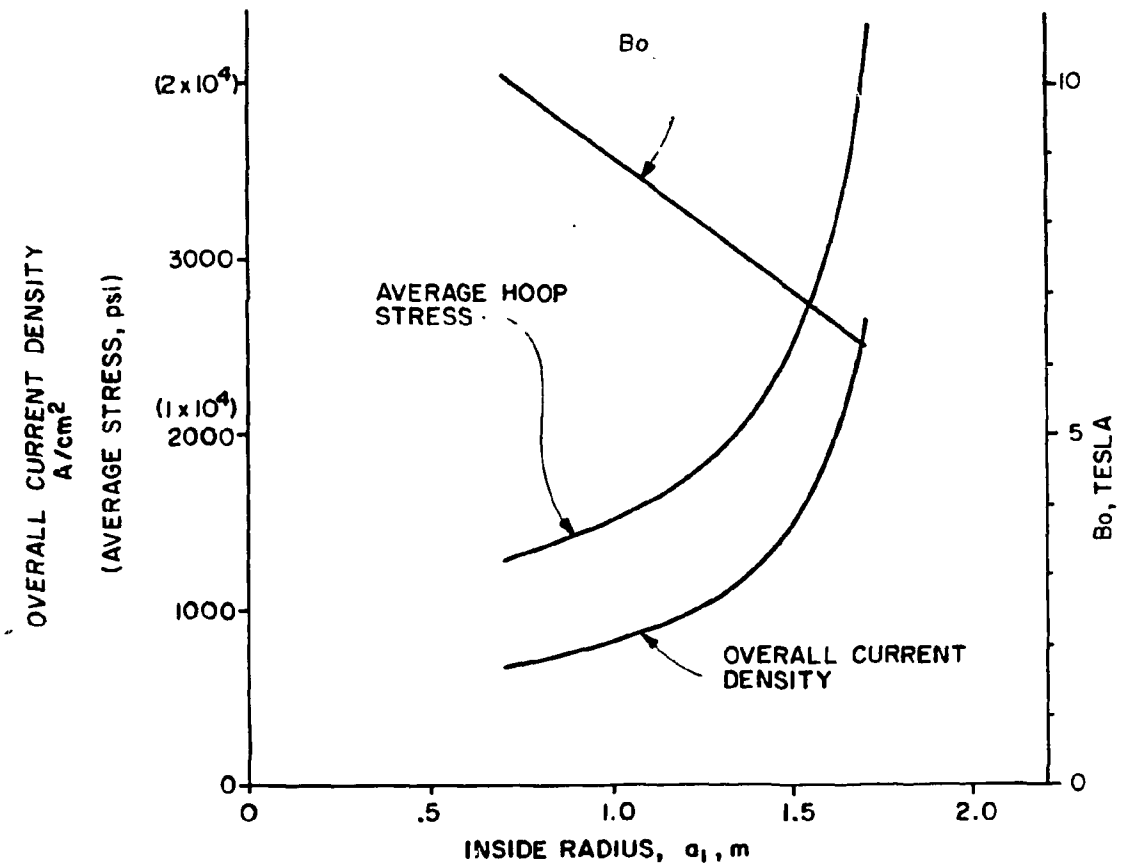

Fig. 5.7 Design curve for 65 weber central solenoid of ohmic heating system (outside radius = 1.9 m, half-length = 6.0 m).

Conductor Design Choices

The large $\dot{B}$ required and the desire to make the coil fully stabilized necessitate careful conductor design. The basic concept is an adaptation of a design developed by Hoenig and Montgomery[8] of MIT under contract to the Superconducting Magnet Development Program at Oak Ridge National Laboratory. The overall conductor is a bundle of mixed-matrix (Cu, CuNi, NbTi) composite conductors in a tube with forced-flow supercritical helium as the coolant. This advanced conductor appears to be a feasible extension of present copper stabilized technology with a vigorous development program. Positive cooling is provided in this case during the pulse. Each tube of conductors is designed to operate at 25 kA. A cross section of the conductor is shown in Fig. 5.8. There are 37 twisted or three-dimensionally transposed strands in the conductor. Each strand is made up of 37 individual wires of twisted Cu-CuNi (matrix) and NbTi (conductor). The entire cable is enclosed in a stainless steel tube with an inner diameter of 3.5 cm and wall of thickness .05 cm. The primary conductor parameters are given in Table 5.4.

The pulsed electromagnetic field losses are given in Table 5.5. The hysteresis losses in the superconductor appear to be irremediable since the filament diameter is already reduced to 4 μm. Eddy current losses can be reduced by 0.9 kW at 4.2°K by the use of a leak-tight fiber-reinforced plastic tube in place of the stainless steel. Both conduction and structure losses are included in the total to illustrate the reduced heat loads when the stainless tube is replaced. The magnet is cryostable even with the stainless steel tube, and the advantage of the fiber-reinforced tube is in refrigeration costs. The extensive analysis by Hoenig and Montgomery[8] demonstrated that conductors of this type were suitable for up to 6000 A/cm^2 in the tube for single heat pulses when there is no continuous heat input. This conductor uses only 3559 A/cm^2. The instantaneous heat flux from the conductor during the pulse is between 64 μw/cm^2 and 344 μw/cm^2. The lower number is optimistic since it assumes that each wire in a strand has equal cooling, but in reality the outer wires in each strand have better helium contact, and consequently better cooling, than wires near the center of the strand. The value 344 μw/cm^2 is pessimistic since it takes the losses over

ORNL-DWG 75-17034

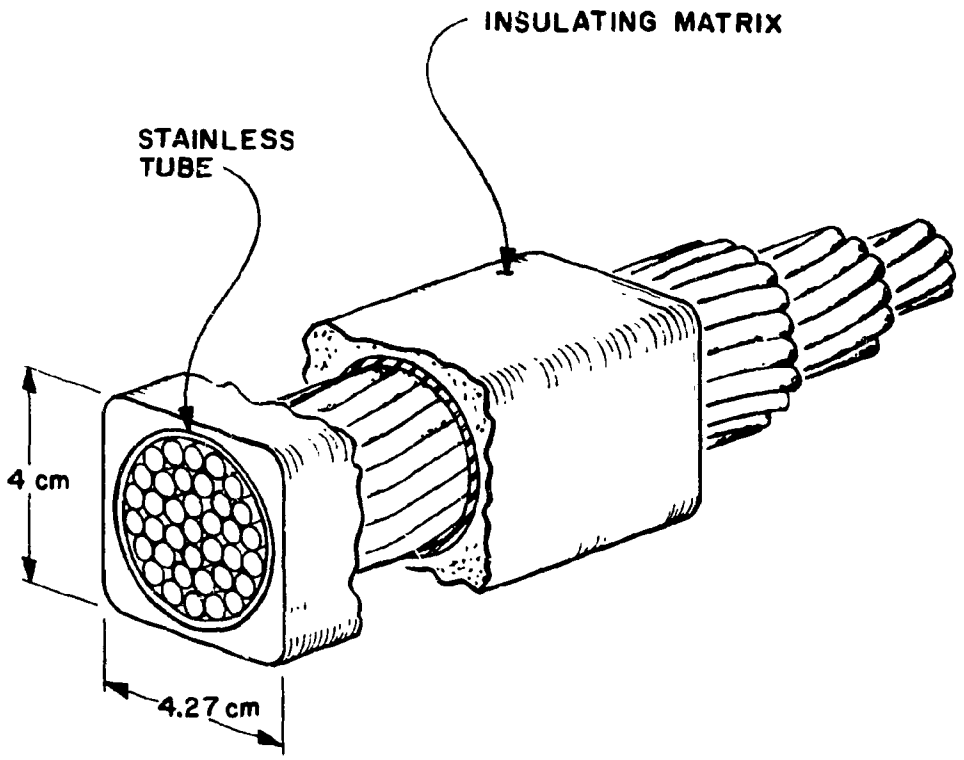

ROUND BUNDLE WITH 37 STRANDS ENCLOSED IN RECTANGULAR CONDUIT SHOWING TRANSPOSITION OF STRANDS

Fig. 5.8 Cross section of poloidal field coil conductor.

Table 5.4 Poloidal Field Coil Conductor Parameters

Symbol	Value	Units	Description
			NbTi
J_c	7×10^8 @ 4.2°K, 7T	A/m^2	Critical current density
J	3.54×10^8	A/m^2	Operating current density
			Matrix
ρ_{Cu}	4×10^{-10} @ 7T	Ω-m	Cu resistivity
ρ_{CuNi}	5×10^{-8} @ 7T	Ω-m	CuNi resistivity
			Structure
ρ_{ss}	5×10^{-7} @ 7T	Ω-m	Stainless steel resistivity
			Wire
I	18.26	A	Current
d_w	5.74×10^{-4}	m	Diameter
--	0.2 : 0.7 : 0.1		Composition NbTi : Cu : Cuni
d_f	4	μm	Filament diameter
n_f	4106		No. of filaments
--	5.15×10^{-3}	m	Twist pitch
			Strand
d_s	3.9×10^{-3}	m	Diameter
n_w	37		No. of wires
			Other
n_s	37		No. of strands
--	3.48×10^{-2}	m	Bundle O.D.
--	1:1		Metal/Helium Area
--	5×10^{-4}	m	S.S. Tube wall thickness
--	3.5×10^{-2}	m	S.S. Tube wall diameter

Table 5.5 Pulsed Electromagnetic Field Losses in the Central Solenoid of the Ohmic Heating System

The heat flux, which is instantaneous during the pulse, is used as input to the refrigeration requirements. The eddy current losses include both the twist losses and the eddy current losses in the Cu Stabilizer. The stainless steel losses are also eddy current losses.

Loss Type	Instantaneous Heat Flux[a] (W/cm^2)		Energy Loss per cycle (joules)	Refrigerator Loss at 4.0°K averaged over one cycle (watts)
	A	B		
Hysteresis	5.37×10^{-5}	2.89×10^{-4}	1.59×10^{5}	794
Eddy (in Conductor)	1×10^{-5}	5.5×10^{-5}	2.9×10^{4}	145
Eddy (in stainless steel)	0.01		1.92×10^{5}	960

[a]The instantaneous heat flux across two different boundary layers is calculated using

A: the wires as a whole, or

B: the strands of wires

a smooth cylinder circumscribed around each strand; however, the cooling area is greater than that since the surface of each strand is not smooth. The eddy current losses in the stainless steel tube result in a 0.01 w/cm^2 heat flux. The heat load will result in a helium temperature rise of approximately 0.1°K from 4°K over the 2-second rise time, if the flow velocity is 1 m/sec at a point on the conductor where the pressure is 5 atmospheres. The total electromagnetic heat load for one cycle is 1.9 kW including the eddy current losses in the structure, but not the pumping losses.

Project Construction

In order to reduce operating current, the coil will be divided into twelve physically separate but magnetically coupled groups. Each of the groups is, in turn, divided into seven parallel segments. Each of the 7 parallel segments will have an operating voltage of 3.5 kV and current of 25 kA. The segments will be layer wound. If required in subsequent iterations with power supply capabilities, the number of axial turns per segment can be reduced and the resultant voltage lowered, at the cost of raising the resultant total current and thereby introducing additional switching problems. The coil mandrel will be a fiber-reinforced plastic cylinder and the turns will be wound with enough tension to hold the coils without an outer coil case. The typical cooling path per coil segment is approximately 400 m. Significant developmental tasks are associated with assuring the feasibility of these design choices. Handling the current distribution among the seven parallel segments and among the twelve groups as well as the pulsed operating voltage will require continued design investigation with concurrent development. Alternative choices are also being considered.

5.7 Electrical Power Requirements

This section describes the power requirements of the electromagnetics systems of the EPR, emphasizing the ohmic heating supply, shielding supply, toroidal field supply, and all solid state supplies. It also includes b am heating and various cooling and auxiliary support functions. A summary of requirements for both resistive and reactive power at various times in the operating cycle is tabulated in Table 5.6. The operational cycle assumed for the EPR is used as the basis for these discussions and is shown in Fig. 5.9. Taking 100 seconds as the nominal burn time and assuming a required duty cycle of $\leq$ 50%, the charge and discharge times were constructed to be 50 seconds each. Further study is needed to determine the minimum times possible in order to maximize the duty cycle and the average fusion power output.

Ohmic Heating Supply

On the basis of a required flux change of 132 volt-seconds using 400 turns in 12 groups, a peak primary current of approximately 2 MA was calculated. If the charge-up of the air core is to be completed in 50 seconds, it requires a power supply voltage of approximately 40 volts, which implies a peak power from the ohmic heating supply of approximately 80 MVAR and an average power of 20 MVAR.

The ohmic heating supply will also be used during the 100-second burn cycle to compensate for the plasma losses. In this period, the primary coil will be driven from about 90% full current to full current over the 100-second burn time. The supply voltage necessary is about 2 volts giving a peak power of around 4 MVA.

Shielding Supply

The purpose of the shielding supply is to maintain a current equal and opposite to the plasma current in the shielding windings. The expected plasma current in the reference design EPR is approximately 7 MA. There will be 16 turns for both shielding and bucking windings requiring a current of about 440 kA. This supply need only provide resistive losses of less than 10 MW if the coils are made cryoresistive. However, a

Table 5.6 Electrical Power Requirements for EPR

System	Power Level		Required during these parts of the operating cycle
	Resistive (MW)	Reactive (MVAR)	
Ohmic Heating	10	100 peak	charge
	5		burn
Shielding	10	100 peak	burn
Toroidal Field		8*	all
Vertical Trim Coils		16	burn
Beam Injectors	200		burn (or start of burn only for ignition ∿ 5 sec.)
Support Functions:			
Building Services	8		all
Refrigeration & Compressors			
Experimental Services			
Maintenance Shops			
Fabrication Shops			
Cryogenic Plant	50		all
Vacuum System	<1		all
Pump House	3		all
Cooling Tower	2		all

*Used only during chargeup.

ORNL-DWG 75-17035

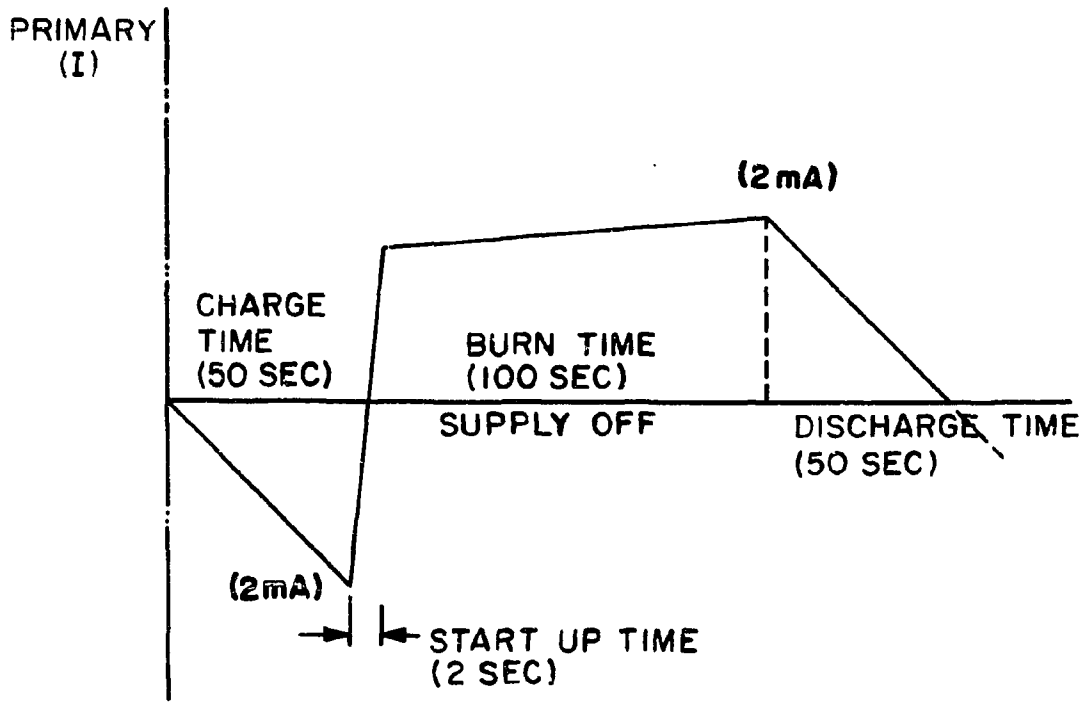

Fig. 5.9 One cycle of operation for EPR ohmic heating power supply.

significant inductive power requirement of about 95 MVAR is introduced by the energy associated with maintaining the plasma current in its centered position in the face of a non-perfect shield. The required power supply voltage is 220 V and the total stored energy at the end of the charge is 120 MJ.

Vertical Trim Coils

Shielding can only be complete when the shield coil current is equal and opposite to the plasma current. In constraining the shielding coils to conduct exactly the plasma current for shielding purposes, some of the stabilizing flexibility is sacrificed. To restore the proper field shape, 16 extra poloidal coils will be wrapped around the torus, carrying a net zero ampere-turns. Both shielding and trim currents will be controlled by a feedback control circuit into which information from a plasma-current sensing coil is sent.

The peak current called for in the trim coils is about 140 kA. This current requires a peak driving power of 16 MW and results in a total stored energy of 16 MJ. The required voltage is 110 volts.

Toroidal Field Supply

Each toroidal coil will be operated by a power supply of 20 kA, 14 V. The power supplies will be built in a modular fashion with the capability of series and parallel operation. The toroidal coils will be series or parallel for the desired performance and protection as determined by the Superconducting Magnet Development Program.

Experiments in the SCMDP's magnet test and fabrication laboratory will be with 6- and possibly 10-meter-bore superconducting magnets. By charging with constant voltage, it will take approximately 4 hours with an available supply of 8 MW to obtain the operating current.

System Requirements

A summary diagram of the various power needs in the EPR is shown in Fig. 5.10 which includes support functions as well as direct coil needs. The power requirements can be tabulated and classified by function and recoverability, i.e., whether the power is resistive and must be charged

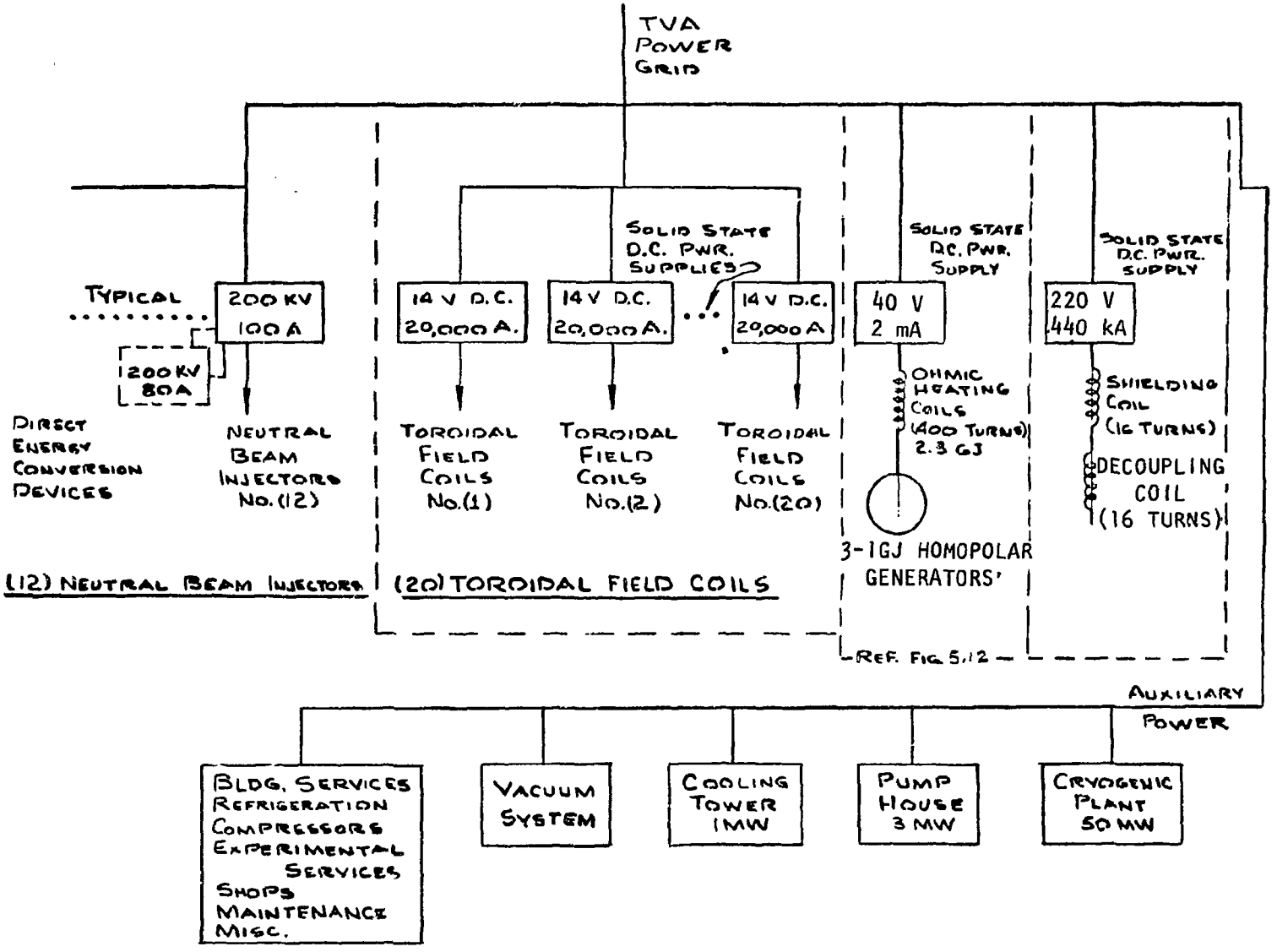

Fig. 5.10 Block diagram of power requirements for EPR.

as a loss in a power balance, or reactive and can be recovered at some efficiency over the operating cycle. This compilation is intended to be indicative of the magnitudes involved rather than a precise expression of the total energy requirements, because many of the numbers will be reduced as the design refinement proceeds.

5.8 Energy Storage and Switching

The toroidal field contains the greatest amount of energy; however, it will not be required to be charged up every cycle. Therefore, it does not represent an energy storage problem.

The shielding and vertical trim power supplies will be SCR bridges which can be operated as inverters simply by advancing the firing angles. In this way they will return the stored energy in these coils to the power grid after each operating cycle. This is illustrated in Fig. 5.11.

The energy in the ohmic heating coils will be handled in the same way at the end of the burn cycle, but the beginning of the ohmic heating cycle must be handled differently. It is currently planned to reverse-bias the ohmic heating coils before firing and to switch the primary current from full negative to full positive in order to achieve a maximum flux change in the plasma. This means that approximately 2.3 GJ must be transferred from the ohmic heating coil to some energy storage device and then back again in a period of about 2 seconds. A homopolar generator can be designed to do this.[9] The largest machine now in operation is the Australian device at Canberra.[10] This generator is rated at about 560 MJ, 900 V and 1.6 MA. The possible application of a similar design to the EPR appears feasible with no major problems foreseen in scaling the present device up by about a factor of 5.[11] Satisfactory resolution of the overall electrical systems questions might well require some other accommodation of energy storage and switching devices with a modified load; these options are being considered.

In order to produce the required flux change in the ohmic heating core, a certain coil shape and size is called for along with a certain current. The height and diameter of the OH coils are specified by various

ORNL-DWG 75-17037

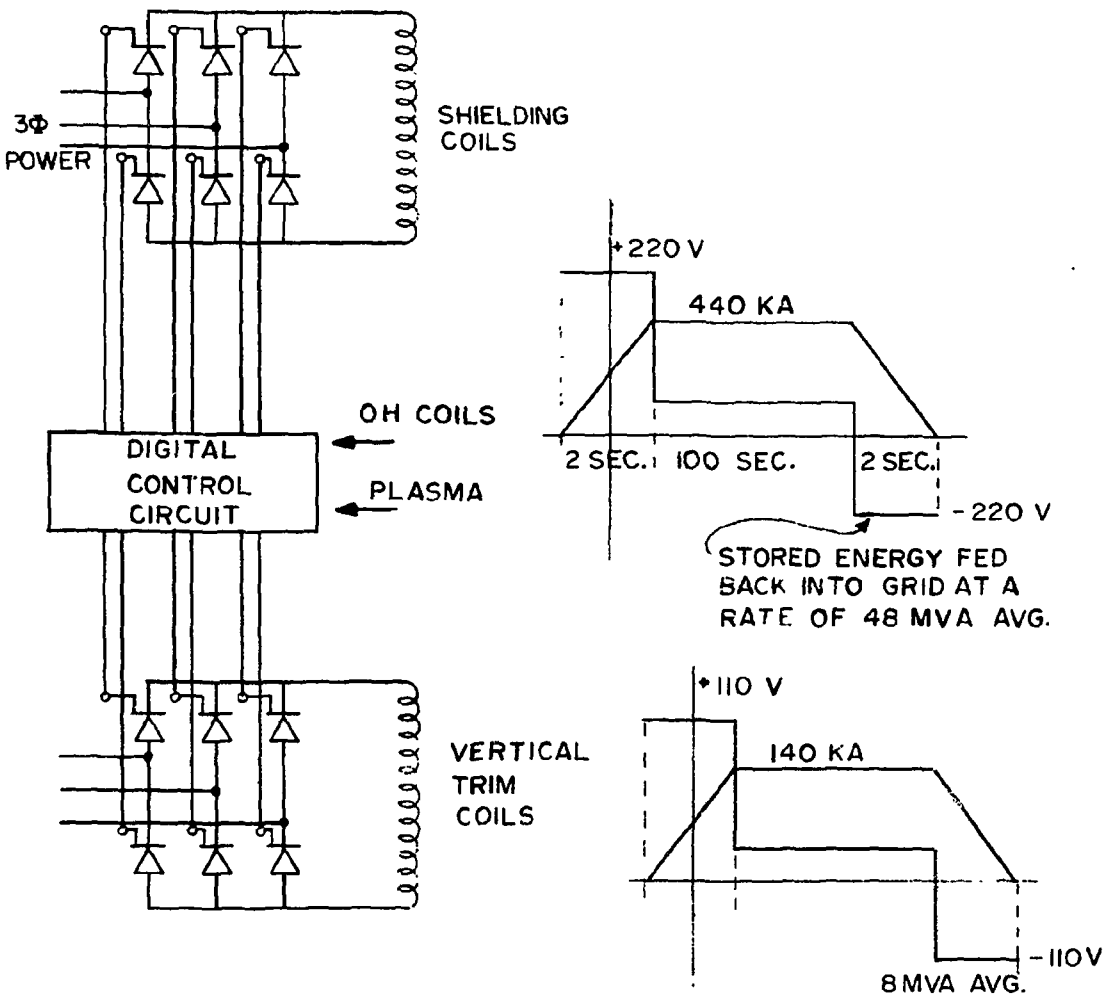

Fig. 5.11 Poloidal Field Power Supplies

practical considerations. A nominal value of 400 turns, based on present superconductor technology and the required smoothness of the field pattern, was initially selected. Having fixed both the volume of the OH coils and the necessary flux, a total stored energy is set. With present dimensions and field requirements, this turns out to be approximately 2.3 GJ. The one remaining parameter in this portion of the circuit is the winding or connection pattern and hence the inductance. If the 400 turns were wound in simple fashion as an ordinary solenoid, the resulting inductance would turn out to be .15 H. This, coupled with the proposed 2-sec reversing interval, calls for a peak voltage of around 42 kV. Such a voltage appears untenable from the viewpoints of the superconducting magnet and also the homopolar generator. Therefore, the OH windings will be divided into 12 groups of 33 turns each. All 12 groups will then be connected in parallel giving a total inductance of around 1 mH, which will require a peak voltage of 3.5 kV and an equivalent capacitance from the homopolar generator of 385 F, both of which are believed to be reasonable numbers. The only disadvantage in this arrangement may be the necessity of producing 2 MA from the solid state power supplies.

To cope with a peak voltage of 3.5 kV, it is currently proposed to regroup the individual superconductor cables into insulated cases such that the insulation problem can be minimized.

The arrangement and ratings of the power supply and generator as well as the coils are shown in Fig. 5.12 along with the operating cycle to which the switching times are keyed.

At the start of the reversal, the OH current is transferred from the power supply to crowbar S_2, so that the power supply can be disconnected at S_1. S_2 will require considerable development; however, S_1, S_3 and the contactors will not, like S_2, be called upon to switch against any voltage. The purpose of the resistor, R, is to provide high voltage at the start of the current reversal. A resistance of approximately 1.75 mΩ will provide an initial voltage of 3.5 kV across the OH coils. In this way an initial 100 volts will be supplied at the plasma, which is necessary to aid plasma breakdown. This resistance will be gradually shorted out by the inductance L' in around 35 mw, during which time approximately 10% of the stored

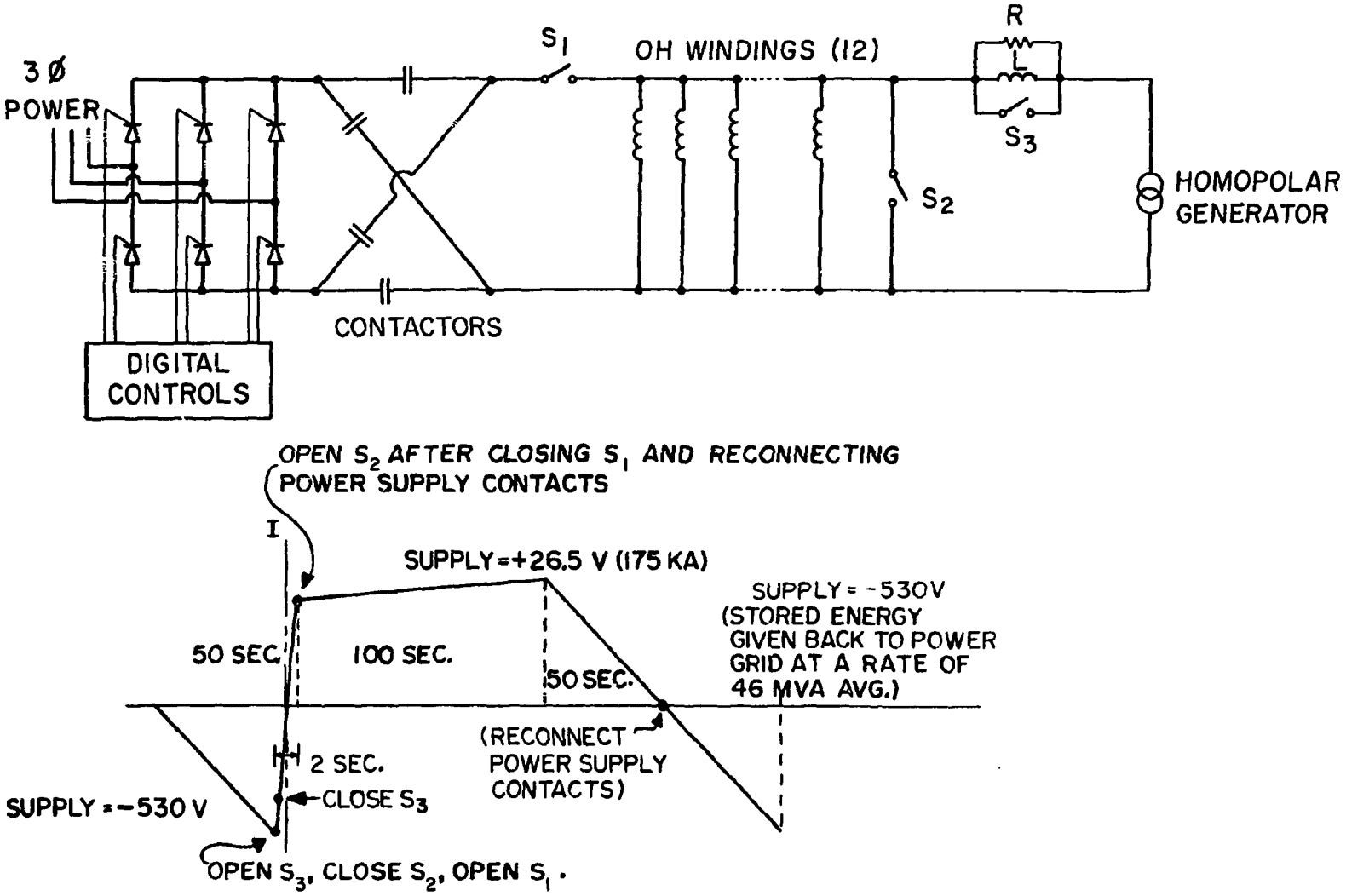

Fig. 5.12 Ohmic Heating Supply and Operating Cycle.

energy will be lost as heat in R. When the OH current passes through zero, S_3 will be closed. The OH voltage waveform is shown in Fig. 5.13.

ORNL-DWG 75-17042

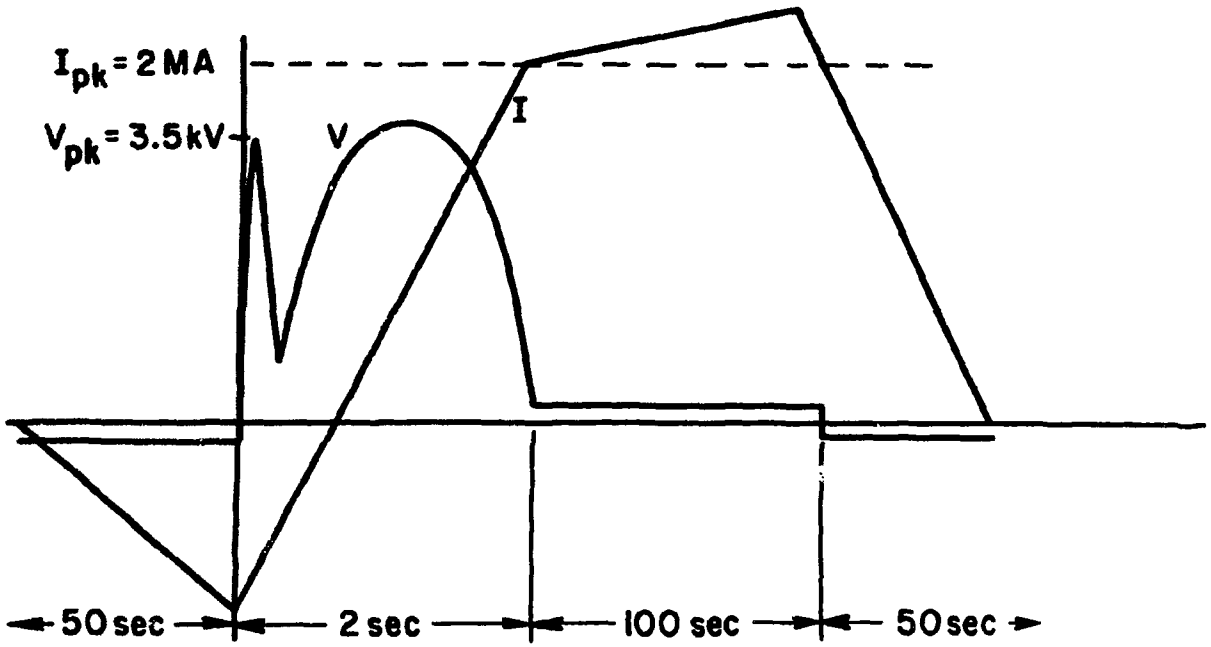

Fig. 5.13 OH Primary Voltage and Current Waveform.

REFERENCES

1. F. B. Marcus, Y.-K. M. Peng, R. A. Dory, and J. R. Moore, "A Magnetic Shielding System for the Tokamak Experimental Power Reactor"; Y.-K. M. Peng, F. B. Marcus, R. A. Dory, and J. R. Moore, "Optimal Poloidal Field Coil Design for Tokamak Experimental Power Reactor (EPR)", papers submitted for publication in the proceedings of IEEE's Sixth Symposium on Engineering Problems of Fusion Research, San Diego, November 1975.

2. TCT-TFTR Conceptual Design, Princeton Plasma Physics Laboratory (February 1975).

3. R. G. Mills, A Fusion Power Plant, Princeton Plasma Physics Laboratory (August 1974).

4. V. S. Mukhovatov and V. D. Shafranov, "Plasma Equilibrium in a Tokamak", *Nucl. Fusion* 11, p. 609 (1971).

5. J. D. Callen and R. A. Dory, "Magnetohydrodynamic Equilibria in Sharply Curved Axisymmetrical Devices", *Phys. Fluids* 15, pp. 1523–8 (1972).

6. H. A. Bodin, "Start Up", *Fifth Conf. Plasma Physics and Controlled Nuclear Fusion Research*, IAEA (Tokyo), Paper S-4 (November 1974).

7. R. Papoular, "The Genesis of Toroidal Discharges", EUR-CEA-FC-769, Foutenay-aux-Roses, France (April 1975).

8. M. O. Hoening and D. B. Montgomery (MIT), private communication.

9. Design Studies of a Reversible Energy Storage and Transfer Systems for the Reference Theta Pinch Reactor, Report EM-4620, Westinghouse Corporation (September 1974).

10. E. K. Inall, *Proc. Inst. Mech. Eng.*, 181, p. 7.7 (1967).

11. E. K. Inall, private communication.

6. NEUTRAL BEAM INJECTION

6.1 Goal

The design goal for neutral beam power delivered to the EPR plasma is 100 MW at 200 keV.

The duration of a beam pulse is determined by

a) the volt-second OH limit if the EPR is capable of purging helium and refueling,

b) the impurity-buildup limit, and

c) whether or not the plasma ignites.

6.2 Beam Model

The model shown in Fig. 6.1 is used to calculate the properties of these two beam systems which appear to be the most favorable and realistic of the four possible systems discussed in the scoping study.

The ion accelerator contains two efficiencies. η_1 represents the fraction of the extracted ion beam which is the useful ion species, $D^+/(D^+ + D_2^+)$ for positive ions, $D^-/(D^- + e^-)$ for direct extraction of negative ions, or the D^- production efficiency (energy efficiency) if use is made of an alkali metal vapor charge exchange of low-energy D^+ to D^- coupled with post-acceleration. η_2 represents $D^\pm$ beam losses to accelerating grids as well as further geometric losses downstream.

The neutralizer is either a D^+ charge exchange neutralizing cell or a D^- stripping cell. The associated efficiency, η_3, represents the actually used fraction of an equilibrium cell, of conversion efficiency $F_{0\infty}$.

The deflection magnet removes the remaining charged particles from the beam leaving the neutralizer, and directs them to the ion dump.

The drift tube transports the D^0 beam from the deflector to the EPR plasma. The associated efficiency η_4 represents primarily ionization losses from collisions with background gas in the drift path.

Associated electric or equivalent neutral particle currents are I_A, the electric current into the ion accelerator first grid, and I_0, the

ORNL-DWG 75-17039

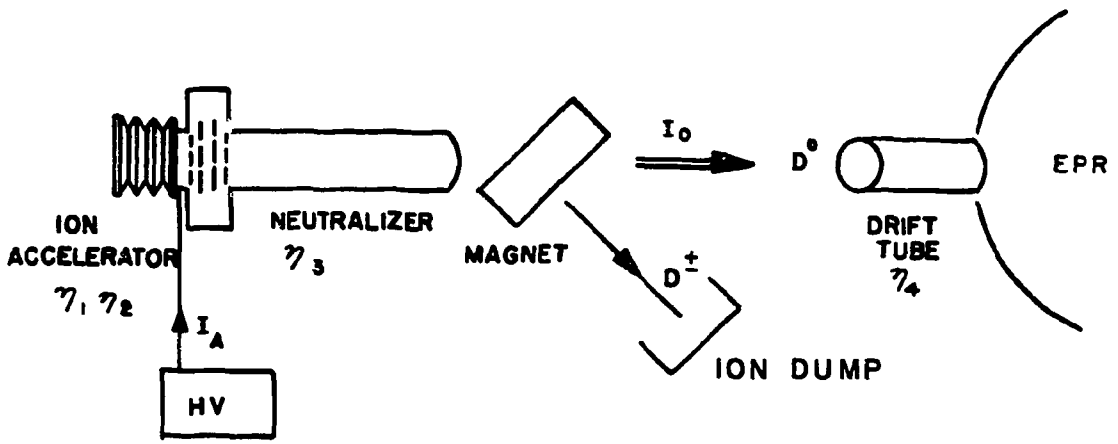

Fig. 6.1 Model of neutral beam injector systems.

neutral 200 keV D^0 current into the EPR plasma. These currents are related by the equation

$$I_o = I_A \eta_1 \eta_2 \eta_3 F_{co} \eta_4 .$$

The associated power is simply taken as P = I•V; the ion production power is assumed to be negligible compared to the acceleration power.

6.3 Beam System Design

The reference design system is taken to be a negative ion source, with no recovery of charged particle fraction energy. This design couples the ORNL beam-handling experience gained from the 150-keV TFTR beams[1] with the development of a suitable negative ion source to give an efficient overall system. The benefits gained from a direct ion energy recoverer do not yet warrant the added complexity of the recovery system.

The backup design system is taken to be a positive ion source with no recovery of the energy in the charged particle fraction. That design is a direct extension of the 150-keV TFTR beams and injectors to slightly higher voltage and to twice the current per injector. All ORNL TFTR experience is directly applicable here.

The more complex negative ion reference scheme requires the development of suitable negative ion sources, but has the advantage of lower input electrical power. That suggests its use for a steady-state, beam-driven EPR. The positive ion backup scheme is a direct extension of the TFTR injectors, requiring less development but more input electrical power. This suggests its use for an igniting EPR with an energy storage system supplying this startup power.

The two systems, reference design and backup design, are compared in Table 6.1. The beam transport efficiencies η_1, η_2 and η_4 represent goals for the beam program to achieve by the time needed for the EPR. The accumulated experience of the ORNL beam program, progressing in a direct line from ORMAK through PLT, DIII, PDX, TTAP and through TFTR to EPR will maximize the probability of achieving these goals.

Table 6.1 Comparison of Reference Design and Backup Design

	Reference Design (D^-)	Backup Design (D^+)
I_o (amps)	500	500
η_1 useful extraction efficiency	0.95	0.95
η_2 grid and geometric efficiency	0.90	0.90
η_3 neutralizer efficiency	0.90	0.90
η_4 drift tube efficiency	0.97	0.97
$F_{o\infty}$ conversion efficiency of equilibrium cell	0.67	0.20
I_A (amps)	1000	3333
P_A (MW)	200	666
Number of sources	12	36
I_A/source	83	93
Beam lines	6	6
Sources/line	2	6
P_o (MW)	100	100
Efficiency, P_o/P_A	0.50	0.15

The reference design beam system is shown in Fig. 6.2. All parts except the negative ion source are taken directly and scaled up in performance where needed from the ORNL beam system design for TFTR. The negative ion sources must still be developed. The backup design beam system, however, may be taken directly from the ORNL TFTR beam system design. The EPR beam system details will be worked out as a logical next step after TFTR by the beam system design group.

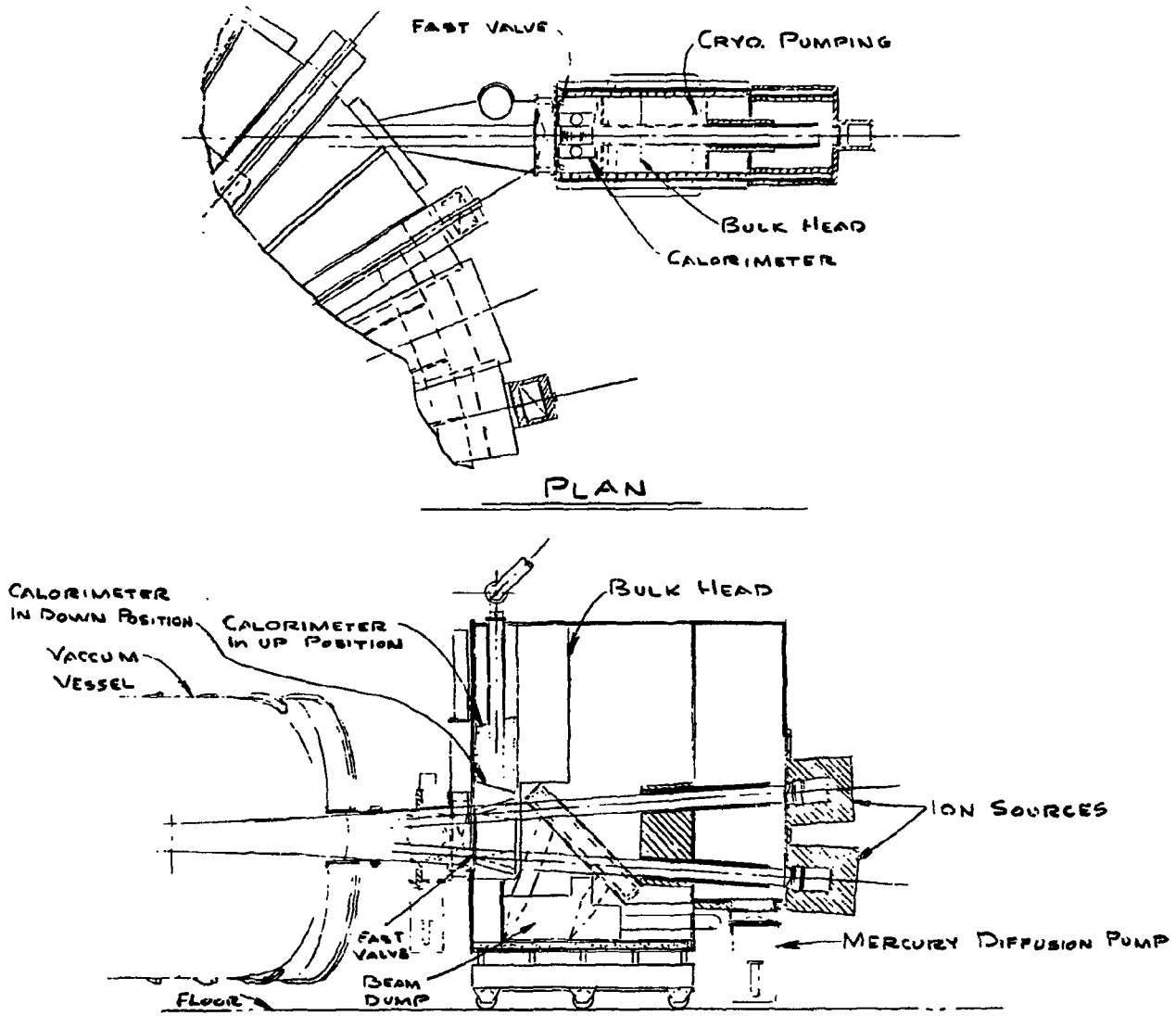

Fig. 6.2 EPR reference design neutral beam injection system.

REFERENCES

1. TFTR Nuclear Beam Systems — Conceptual Design, Parts I—III (SDD-71 Neutral Beam Injection, SDD-72 Neutral Beam Pulsed Energy Conversion, SDD-73 Neutral Beam Control System), Oak Ridge National Laboratory, (September 1975).

7. TRITIUM HANDLING SYSTEMS
(Vacuum, Tritium Process, Tritium Containment)

The tritium handling systems for EPR consist of the main and injector vacuum systems, tritium process systems, and tritium containment and atmosphere cleanup systems.

7.1 Vacuum System

The pumping speed requirements for the main vacuum system have not been determined. The criteria for allowable neutral density outside the plasma are dependent upon energy loss and sputtering problems caused by charge exchange between neutrals and hot ions. For the reference design a nominal pumping speed of 1,500,000 liters per second was chosen based on a gas of mass 5 (DT) at 550°K. This speed can be achieved with 40 vacuum ports of 1-m diam, 5-m length, each being pumped by a 1-m diameter cryosorption pump. If 1.5×10^{22} ions per second leave the plasma, the equilibrium density of neutral gas outside the plasma would be 1×10^{13} atoms/cm^3. The cryosorption pumps have several advantages for this particular application, including the following:

1. Existing concepts can be scaled up to the appropriate speed.
2. Tritium can be recovered easily by thermal regeneration.
3. Helium can be pumped.
4. Very low base pressures can be achieved.
5. Maintenance and reliability appear to be acceptable.

Each of the pumps will be regenerated approximately once every 24 hours. The regeneration will be performed at low temperatures to minimize the time required. The desorbed helium and hydrogen isotopes will then be fed to the tritium processing systems. Mercury diffusion pumps may be used as an alternative to cryosorption pumps if the latter fail to achieve the necessary performance and reliability. All the tritium-bearing streams in the main vacuum system will be doubly enclosed.

The design of the injector vacuum system will follow the refinement of injector designs and the development of operating criteria.

7.2 Tritium Process Systems

Tritium process systems include equipment for:

1. removing the D-T mixtures from the main vacuum systems
2. purifying the D-T mixture for recycle to feed systems
3. separating hydrogen isotopic impurities from D-T mixtures
4. plasma fueling and injector feed systems
5. tritium storage systems
6. tritium recovery from blanket modules
7. preparation of tritium-containing wastes for disposal.

A schematic flow chart of the reference design tritium processing system is shown in Fig. 7.1.

The purification technique chosen for the EPR reference design involves uranium beds, perhaps with additional palladium membrane purification on the exit stream. Uranium beds are frequently used for tritium storage and purification and can be considered "current technology". Other hydrides will need to be considered, since they have different affinities for hydrogen isotopes as well as for oxygen and nitrogen. Pd membranes can be used to purify hydrogen isotopes, but they would require compressors to achieve reasonable rates. Compressors are likely to require more maintenance than uranium beds and perhaps present more opportunity for small tritium leaks to secondary containment.

One or more isotope separation methods will be required to prepare deuterium for the injectors, and remove the trace of hydrogen produced by D-D reactions. The first system will be the larger, but the two operations could be carried out in the same or separate equipment. Because the requirements are so different, separate equipment seems more likely; different separation methods are possible. It is too early to prepare conceptual designs for EPR since the purity requirements are not yet known. However, designs should begin as soon as estimates of these requirements become available. We must know if current plans call for unreasonably large isotope separation equipment. Sufficient data on separation methods are available for our immediate needs.

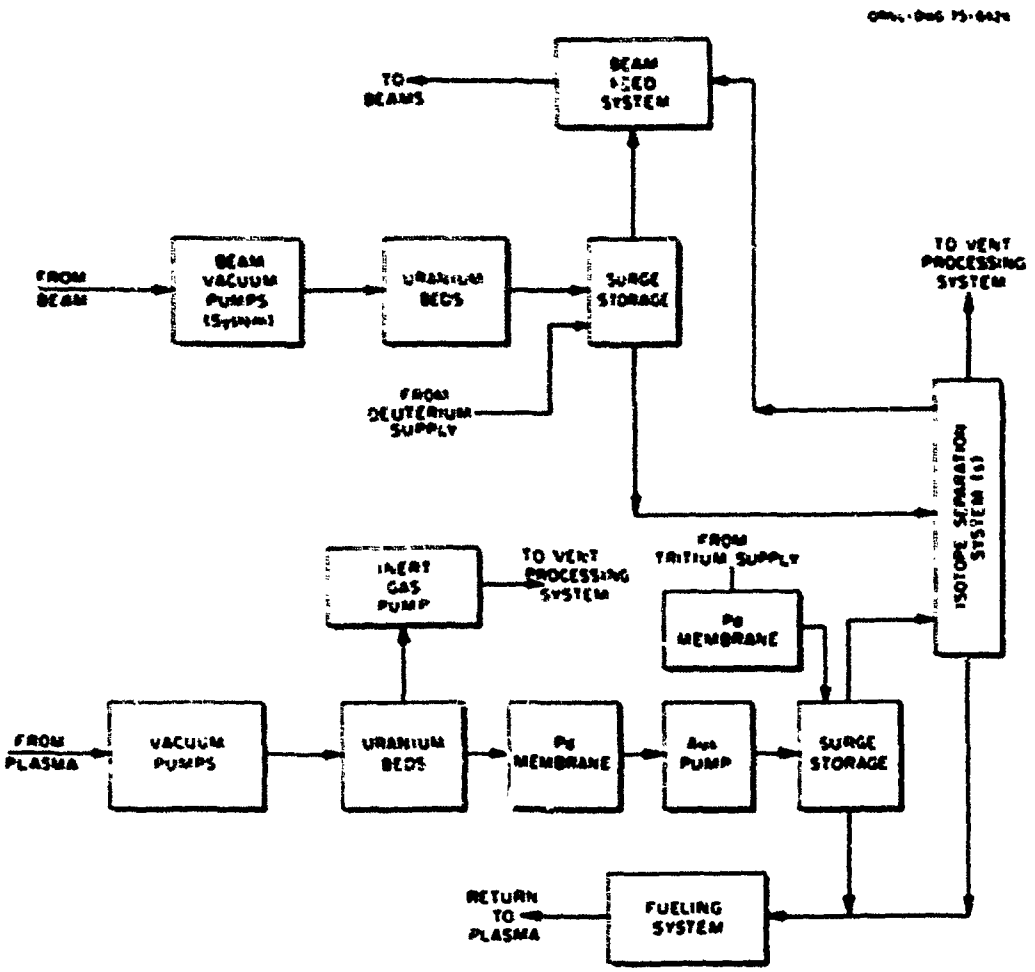

Fig. 7.1 Schematic flow chart of EPR reference design tritium processing system.

Storage of tritium as either a gas or a solid tritide (probably uranium tritide) is considered feasible and safe. There is considerable experience with both methods, and there appears to be little reason for choosing one over the other. However, since solid storage is usually considered to be less susceptible to accidental release, that method will probably be used for most large-scale storage needs of EPR. Small surge storage may be in the form of a low-pressure gas.

No new method for disposal of tritium wastes has been considered for EPR since several forms of double- or triply-sealed containers appear to be adequate.

The blanket recovery system is one of the least well understood items in the tritium processing area, and considerable experimental work will be required to determine the most promising system and to provide the necessary design data. Lithium is currently considered the most promising breeding material. A small side stream can be removed for processing; we are currently considering extraction, permeation, and sorption processes for tritium recovery. To promote further advances in this area, a major effort is needed.

Requirements for plasma fueling and neutral beam injector feed are not yet sufficiently well defined to allow conclusions concerning tritium processing. We think that gas blanket feed systems would involve little special tritium handling equipment, whereas a solid pellet feed system could require complex handling equipment.

7.3 Tritium Containment

Because of the huge quantities of tritium which will be handled in the fuel cycle and the low permissible release values, it will be necessary that all components containing significant quantities of tritium be doubly contained. Techniques to achieve double containment will include glovebox-type enclosures over components which may require periodic maintenance (e.g., pumps), and double-walled pipes. The atmospheres of enclosures and the annuli in the double-wall pipes will be maintained at a slight vacuum with respect to the reactor building, and must be processed through

atmosphere cleanup systems to remove tritium and thus reduce release to the reactor building. The atmosphere cleanup systems will consist of heaters, recombiners using palladium or copper oxide, chillers and regenerable molecular-sieve drier beds.

Many of the enclosures and pipe annuli will contain inert gas to eliminate potential fire hazards stemming from the presence of hydrogen isotopes and pyrophoric metals. Thus, it will be necessary to provide either a controlled amount of air inleakage, or, if the reactor building itself is filled with an inert gas, an oxygen feed to allow proper operation of the cleanup systems. Hydrogen will also be fed to the recombiner inlet to provide isotopic dilution of the tritium.

The reactor building will contain all of the major tritium-handling components. Provision will be made for the building to be filled with inert gas if required to eliminate fire hazards, particularly those associated with liquid metals in the blanket modules. In any case a system will be provided for controlling the building pressure and removing tritium from the building atmosphere. It is proposed that the reactor building be maintained at a slight vacuum (0.25-in. H_2O) which will prevent exfiltration, except during high-speed wind conditions, when dispersion tends to be excellent. The building will be designed for an inleakage of no more than one-half building volume per day under normal wind conditions. This is similar to existing BWR secondary containment buildings which have inleakage rates of one building volume per day under similar conditions. An amount equal to the inleakage will be exhausted from the outlet of the atmosphere cleanup system through a stack which will be approximately 2.5 times the height of the reactor building. The reactor building volume is expected to be about 4,000,000 ft^3. A recirculating building-atmosphere cleanup system with a flow rate of 16,700 scfm and a decontamination factor of 10^2 for tritium was determined to be adequate for that volume. If the stack height is 100 m and the site boundary distance is 200 m, the whole body dose at the site boundary during two hours of fumigation conditions following a release of 5×10^7 Ci of tritium to the reactor building would be approximately 0.62 rem, which is appreciably lower than the reference limit of 25 rem set forth in 10 CFR 100 (Ref. 1).

If normal activated air releases from a stack will be unacceptable, the building will probably be similar to a PWR containment building. Such a structure will be designed to leak at a rate of no more than 0.1 building volume per day under design-basis accident conditions. Because any leakage from such a building will be released at ground level and disperse more gradually than an elevated release, and will contain tritium at the ambient concentration in the building, a larger capacity for atmosphere cleanup will be needed. A system with a flow rate of 67,000 scfm and a decontamination factor of 10^2 would result in a two-hour site boundary dose of 4.9 rem, assuming a 5×10^7 Ci release into the building and a 200-m site boundary radius; again, this is within the exclusion area boundary guidelines of 10 CFR 100.

In either case the basic design of the reactor building atmosphere-cleanup system will be similar to, but larger than, the small enclosure atmosphere-cleanup systems.

REFERENCES

1. "Reactor Site Criteria", *Code of Federal Regulations*, Title 10, Part 100 (10 CFR 100), U. S. Office of Federal Registry (April 1975).

8. SYSTEM INTEGRATION

A guiding principle in the mechanical arrangement and choice of design features has been to ensure that the machine could be assembled, disassembled and maintained by totally remote handling methods. The design of the blanket segments, for example, provides a flange which will permit the clamping of adjoining segments by a jig and fixture operated remotely. A vacuum tight seal weld can then be made remotely.

The following paragraph describes the assembly and key design interfaces and features.

The toroidal field coils are mounted on a cylindrical center column. This column has vertical key-ways around the periphery. A key on each coil fits into a key-way providing positive circumferential location of the coils and also providing additional resistance to bending throughout the inner half of the coil. This center column also supports the centering force of the coil which is about 250×10^6 newtons per coil. The coil, the center column, and plate frame work between coils all operate at 4.2°K. Gravitational loads are transmitted to the support foundation through pipe columns enclosed with dewars to reduce heat loss.

After the center column has been erected, each toroidal field coil is moved radially into the key-way on the column. Individual metal gaskets are affixed around the key in the key-way. After the coil is in place, this gasket is filled with epoxy under pressure to effect the required fit between coil key and column key-way. A quarter section plan view of the machine is shown in Fig. 2.2. On this small scale, details such as the gasket arrangement are not shown.

Inside the toroidal field coils are the segments of the shield, and inside the shield are the segments of the blanket. There is one shield segment under each TF coil. There are two 90° segments and one semicircular (180°) segment between each coil. These are put in place after the blanket segments have been inserted. The shield, being at room temperature, is supported from the foundation. The shield segments are autonomous, each with its own cooling connections and support structure. The individual shield segments are not clamped together but are held in place by the bolted support structure.

Since the blanket segments have to be inserted through the shield, these segments are thin enough to be moved radially into the torus and then rotated under the TF coil. This assembly procedure requires that the blanket be divided into 60 segments. Each blanket segment is hung from a track structure in the center of the shield. When two blanket segments have been put in place, the joint between them is made by clamping and seal welding. This joined blanket segment pair is then rotated into position under a TF coil. The loading of pairs of blanket segments is continued under each of the twenty coils for a total of 40 segments. The remaining 20 segments are then moved into the slots between coils and connected to the other segments to complete the torus by making up the two joints on each side of the segment.

In Fig. 2.1, a set of poloidal field windings is shown mounted inside the inner wall of the shield. The eight windings on the inner side must be installed before the blanket segments are installed, while the outer side windings must be installed after the blanket segment installation is completed.

The poloidal field Shielding-VF coil located on the shield is enclosed in concentric stainless steel pipes. The inner pipe contains the conductor. The annulus between the inner and outer pipes carries the liquid nitrogen coolant. Along its length, an individual turn of the double pipe is made up of curved segments or arcs of concentric pipes, the inner one of which is filled with bare copper conductor. When two segments are in place, the inner pipe ends are welded and a sleeve is welded in place across the gap of the outer pipe. Insulation is provided between the outer pipe and the shield structure. Prefabricated crossover pipes are installed at one place around the circumference and the return lead is brought out over these crossovers to cancel the out-of-plane flux.

An all-welded piping system is used to make up the coils. The mechanical joints and support must provide satisfactory performance with respect to potential cyclic fatigue arising from the pulsed conditions. To effect the electrical joints between the copper filler in the individual segments, the interstitial spaces in the coils are filled with sodium so that there is no mechanical-electrical joint that is subject

to loosening in operation. The coolant should not be water because of the risk of chemical activity between sodium and water in case a leak occurs. Dowtherm E, Mobiltherm or liquid nitrogen are acceptable as coolants. With the former two materials, the coil temperature would be approximately 40°C. An entire sodium conductor is a possible alternative; eliminating the copper would be in the interest of economy.

The poloidal field shielding coil on the outer side of the torus is of the same design as the coil on the inner side, but is installed after the blanket segment. Segments of the coil are installed in the shield segments, and connecting segments are welded into place between the TF coils. The two 180° closure segments of the shield are then slipped into place, the outer segment sliding over the shielding coil joints. The closure shield segment has a larger diameter than the shield segments under the TF coils.

The final part of the poloidal coil system is the main ohmic heating air core solenoid located in the inner support column of the machine. The flux-guiding turns are electrically in series, but located outside the TF coils. This center coil can be fabricated as a unit so that complex in-place construction is not required. Installation and removal is performed from the top of the machine. This solenoid consists of two concentric coils, one of which is the primary of the air core transformer. The other is a decoupling coil used to counter the induced voltage in the inner shield and vertical field coil located on the inside of the nuclear shield. There are small vertical field trim coils also located outside the TF coils and inside the solenoid.

The 30-cm annular clearance between the blanket and shield is determined by the present requirements for tools used between the blanket and shield (e.g. the blanket clamping and welding fixture, impact hammers and wrenches, etc.). Furthermore, this clearance is adequate for the helium coolant headers coming from the blanket segments. Also, thermal insulation over the blanket requires space, since the blanket is running at 550°C and escape of heat from this large surface must be prevented.

It is planned to use air pads to transport the large components and to maneuver them into position. Remotely operated cranes, special handling

tools and modified manipulators will be required. Detailed adaptations of presently available equipment are necessary to make use of this equipment. Versatile remotely-operated welders, cutters, viewing and inspection equipment, all of which are commercially available, will be necessary for work on any of these internal systems of the reactor.

Penetrations into the plasma region must be made through the shield, blanket and wall liner. The major penetrations will be the vacuum pumping ports and the beam injection ports which have been incorporated in the reference design. There will, of course, be various diagnostic penetrations, whose specifications have yet to be determined.

These numerous penetrations require precise positioning of the blanket and shield segments, and each penetration will employ bellows assemblies to allow for differential thermal movement. Because of the inaccessibility of most of these joints and the very limited working space, laser welding will be investigated for making these vacuum-tight welds. Such welding equipment is being developed for other applications and may be adaptable for use in the reactor assembly.

In the event of a fault, the failed component must be removed by going through the remote assembly procedure in reverse order. A replacement component would then be installed by using the remote assembly procedure. Probably the most time-consuming fault would be the failure of a toroidal field coil. We have not attempted to estimate the time required to recover from this fault but, it would probably be a matter of weeks or even months. We will continue to attempt to incorporate design features which will facilitate this very difficult problem of remote maintenance.

9. RESEARCH AND DEVELOPMENT REQUIREMENTS

Because design of an EPR represents a substantial extension of fusion reactor technology in many, if not all of the involved disciplines, considerable understanding and development must occur to establish a firm base from which a successful final design for EPR can be derived. This section highlights some of the needed developments ranging from fundamental research questions to systems applications of known techniques.

Plasma Related

- Neutral beam injection systems capable of 150–200 keV and a power delivery of many tens of megawatts for times up to the burn time.
- Energy storage/supply capability consistent with plasma startup requirements.
- Fueling systems and methods capable of maintaining the desired plasma density during long burn times.
- Plasma skin depth. The factors controlling current penetration must be understood so that the dynamic behavior of a tokamak can be predicted, permitting knowledgeable design of the entire poloidal magnetics system.
- A system to control the plasma/material boundary interaction including suitable first wall materials, configurations, or divertors.
- A plasma shutdown system capable of handling the large stored energies in the plasma.
- An understanding of the source and behavior of impurities and their consequences (impact on power balance) in a large hot plasma.
- Particle and energy transport. Computer simulation may be helpful in this area and experimental studies in next-generation devices should be valuable.

Nuclear

- Refinement of analyses to improve the estimates of neutronic wall loadings, of the neutronic response of candidate first wall materials to the EPR spectrum (including estimates of helium production), and of the stress, stress gradient and stress cycle loading on the first wall.
- Criteria for acceptable radiation damage to the first wall and toroidal field coils.
- Potential for an asymmetric blanket design.
- Impact of penetrations on need for shielding and influence on neutronics and energy deposition.

Electromagnetics

- Reliable superconductors, applicable structure, and cryogenics for combined Nb_3Sn and NbTi toroidal field coils.
- High current density pulsed superconductors with acceptable losses for the poloidal field coils.
- Protection systems capable of handling safely the tens of GJ stored in the magnetic field.
- Analysis of the interrelated plasma and magnetic requirements on shielding systems (STATIC), limiters and divertors.
- Large homopolar generators and high-current, high-voltage switchgear capable of repetitive and reliable operation.

Tritium Handling

- Viable concepts for efficient and acceptable recovery of tritium from the blanket modules.
- Accelerated study of cryosorption pumping and investigation of alternate methods.
- A viable, economic isotope separation system to meet the EPR size requirements and permit recycling.
- Additional work on the behavior of tritium in the environment and the consequences of releases, to aid in establishing final criteria and designs for atmosphere cleanup systems.

Remote Maintenance

- Fabrication and assembly tooling to provide the compatibility of remotely changing any component of the reactor.
- Remote inspection equipment to ascertain that maintenance and assembly operations have been performed satisfactorily.
- Massive precision handling devices for remote assembly/disassembly and transfer of reactor subassemblies.

10. PROJECT ENGINEERING

10.1 Schedule Development

A schedule has been developed for the Experimental Power Reactor with a completion date of 1985 as shown in Fig. 10.1. The schedule was organized using procurement, construction and installation data based on projections for light water reactor (LWR) construction and ERDA's *Appendix 6101 Management of Construction Projects Handbook*. The development of the schedule begins with an assumed 1985 completion date and utilizes the optimistic projection for building light water reactors, principally in terms of facilities and the reactor vessel itself, to determine the required dates for initiation of activities. FY-1979 funding will be required to maintain this schedule. The time from initiation of construction to completion of systems testing is 60 months as in the LWR systems. In comparing this EPR schedule with other comparable projects, it is interesting to note that the TFTR Project, which is considerably less in magnitude than the EPR, is projected to take 75 months from initiation of construction to plasma operation. A greater amount of schedule compression is required of EPR.

Major milestones have been indicated on each schedule. These milestones are based on the specified assumptions for completion and on the premise that these will be Capital Line Item Funding. Major program milestones are indicated to emphasize the interrelationship between the continuing CTR Research and Development Program and the EPR Project.

10.2 Reporting and Funding Requirements

Major funding requirements of *Appendix 6101 Management of Construction Projects Handbook* include Short Form Data Sheets for project identification, Schedule 44 Construction Project Data Sheets and Conceptual Design Reports. The Schedule 44's and the Conceptual Design Reports are required for scope, cost, schedule, performance level, environmental and safety requirements,

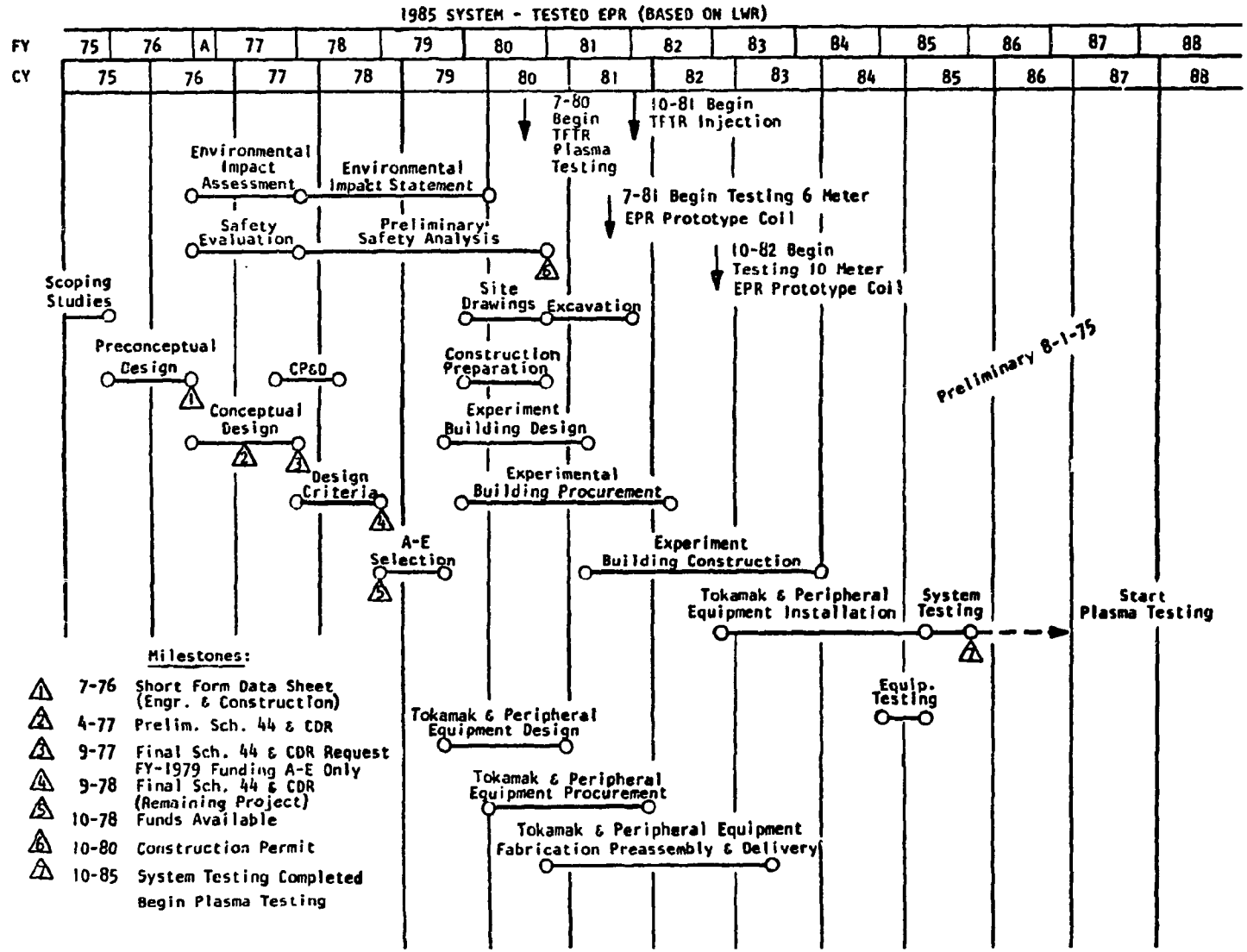

Fig. 10.1 EPR 1985 schedule assuming similarity with current LWR schedule projections.

and methods of accomplishment of the project. Environmental impact assessments and safety evaluations are considered as separate non-critical path activities and are included as part of the Conceptual Design reports. The Environmental Impact Statements (EIS) and the Preliminary Safety Analysis Reports (PSAR) will be completed before Title II design starts, so that hazard and impact prevention measures can be applied and compliance with environmental standards and guidelines will be achieved. It is assumed that a construction permit, which will coincide with the start of excavation, will be issued after the PSAR is approved.

10.3 Construction Schedule

The Construction Schedule was organized from Light Water Reactor (LWR) projections. LWR's in the billion-dollar cost range and producing 800–900 megawatts of electrical (MWE) output have projected schedules based on historical data which required an average of 60 months of construction time (from the start of site work or excavation to criticality or completion of systems testing). Current projections for future LWR's by industry and ERDA of 1100–1150 MWE output plants, which are scheduled for the late 1970's and early 1980's, require 60 to 66 months of construction.

On this schedule the erection or construction of the experiment building will require 2-3/4 years and will begin after 1/2 year of excavation. All building and equipment designs, and approximately 3/4 of the building and equipment procurements, will be completed before the commencement of building erection.

The equipment installation, which requires 1-1/2 years, will begin after approximately 2 years of building erection. All of the equipment and building procurement and most of the equipment fabrication, pre-assembly, and delivery will have been completed before the installation begins.

The systems testing activity of 6-months duration should begin after the completion of the equipment installation. Systems testing is required to check for proper operation, and, if necessary, to correct the integrated systems of the facility before plasma operation begins.

It is important to note that these LWR times (e.g., 6 months of systems testing) arise from the actual experience of the last twenty years, and definitely reflect results far up on the learning curve. Although experience with large tokamak systems in the next six or seven years will be of great help, we find no grounds to believe that these times will be markedly reduced after a detailed analysis of the EPR schedule.

10.4. Comments on Interface of SCMDP and TFTR with the 1985 EPR Schedule

Indicated on the 1985 EPR schedule are four important milestones from the Superconducting Magnet Development Program (SCMDP) at ORNL dated August 1975, and from the Tokamak Fusion Test Reactor (TFTR) schedule at PPL dated April, 1975.

The 1985 EPR schedule requires that:

1. All equipment and building design will be completed before the start in July 1981 of the 6-meter EPR prototypic coil tests and before the start in October 1981 of TFTR injection.
2. Approximately 3/4 of the equipment and building procurement will be completed before the start of these important coil and injection tests.
3. The excavation for the building will be almost completed and about 1/4 of the building erection will be accomplished by the same date.
4. Approximately 3/4 of the equipment fabrication, preassembly and delivery will be completed before the start in October 1982 of the 10-meter EPR prototypic coil tests.

If the development programs demonstrate results appreciably different from those predicted by theory and design, considerable risks in cost and time could result from adherence to the EPR schedule.